Antibiotic Combinations to Tackle Gram-negative Bacterial Pathogens

A thesis presented in partial fulfilment of the requirements

for the degree of Doctor of Philosophy

in

Biochemistry

at Massey University

Manawatu Campus, New Zealand

Van Hung Vuong Le

2019

Abstract

Antimicrobial resistance, especially in Gram-negative bacterial pathogens, is one of the most serious threats with which humans have been confronted. Coordinated efforts from industrial, academic and government sectors have been called and executed to introduce novel antibiotics into the market to meet clinical demand. Despite that, the rate of successful antibiotic development appears to be lagging behind the emergence of antibiotic resistant pathogens in the arms race between humans and super-bugs. In this dire context, alternative approaches are required to tackle Gram-negative bacterial infections.

This thesis reports synergistic interaction between a secondary bile salt, sodium deoxycholate (DOC), and 5-nitrofuran pro-drugs, an old class of synthetic antibiotics, in inhibiting/killing Gram-negative enterobacteria, such as *Escherichia coli*, *Salmonella enterica* and *Citrobacter gillenii*. Using a genetic approach, the underlying mechanism of the synergy between the two drugs was found to involve 5-nitrofuran-mediated inhibition of TolC-associated efflux pumps that otherwise exclude DOC from bacterial cells. This synergistic combination provides a promising tool to combat infections caused by enterobacterial pathogens.

The mechanism of action of individual drugs, DOC and 5-nitrofurans, was also investigated using whole-genome sequence analyses of selected resistant mutants, followed by genetic and biochemical studies. A novel nitrofuran-activating enzyme, AhpF, was identified in *E. coli* that reduces 5-nitrofuran prodrugs in a manner different from that of an established 5-nitrofuran activation enzyme NfsB. This discovery opens new avenues to counteract nitrofuran-resistant clinical isolates by screening for

molecules that upregulate AhpF expression or catalytic activity, or designing nitrofuran analogues activated at high efficiency by the AhpF enzyme.

Also, this thesis identified mutations that cause a low-level resistance to DOC in efflux-pump-deficient genetic background. These all resulted in growth-slowing phenotype, the majority of which were involved in cAMP signaling. Singe mutations conferring high-level DOC-resistance were not identified in the mutant screen, supporting the use of DOC/nitrofuran combinations.

Acknowledgements

The journey to complete the PhD project has truly been a marathon that was full of challenges, struggles and excitements. Over the past few years, I have received enormous help and support from many people. Without them, this thesis could not have been accomplished.

First of all, I would like to thank my supervisor Prof. Jasna Rakonjac for offering a great opportunity with this awesome PhD project and her tremendous guidance and encouragement along the way. To me, calm and stable energy is much needed for long-haul work rather than a constant enthusiasm: when your experiments work, it is good, when your experiments fail, it is fine. That is what I have got from the talk and discussion with her.

I also would like to thank my co-supervisors, Prof. Patrick Biggs and Dr. David Wheeler, especially for training and mentoring bioinformatic skills. Few years ago, if I heard about bioinformatics, my response would be “Nah”, “Ew”, “boring”. Now I can understand, actively search and execute the software for a particular research question. I would like to thank Dr. Ieuan Davies for very useful professional development training and a great tour around New Zealand Pharmaceutical campus.

Secondly, I would like to thank my parents and my brother for continuous support from Vietnam. They have kept calling me to check that I was okay.

Thirdly, I would like to thank all the members of the Rakonjac lab for having great time of working together and learning from each other, especially Sofia Khanum who taught me a lot when I just started the PhD. A big thank to SFS staff (Ann, Paul, Fiona, Cynthia, Debbie) for helping out with different tasks, such as ordering reagents, printing posters, booking flight tickets, registering conference and so on.

Finally, I would like to thank Callaghan Innovation for the PhD scholarship, the School of Fundamental Sciences and New Zealand Pharmaceutical Ltd. for funding the research and conference travel.

Mission accomplished!

List of papers

Paper 1: [Manuscript in press, BMC Microbiology]

In vitro synergy between sodium deoxycholate and furazolidone against enterobacteria

Vuong Van Hung Le, Catrina Olivera, Julian Spagnuolo, Ieuan Davies and Jasna Rakonjac

Paper 2: [Manuscript published, Antimicrobial Agents and Chemotherapy]

Novel 5-nitrofuran-activating reductase in *Escherichia coli*

Vuong Van Hung Le, Ieuan Davies, Christina D. Moon, David Wheeler, Patrick J. Biggs and Jasna Rakonjac 2019. Novel 5-nitrofuran-activating reductase in *Escherichia coli*. Antimicrob Agents Chemother 63:e00868-19.

Paper 3: [Manuscript in revision, Journal of Bacteriology]

Comparative genomic analysis of *Escherichia coli* mutants with decreased bile salt sensitivity

Vuong Van Hung Le, Patrick J. Biggs, David Wheeler, Ieuan Davies and Jasna Rakonjac

Paper not included in the thesis:

Le VVH, Bruce I, Biggs PJ, Rakonjac J. 2019. Draft genome sequence of a canine uropathogenic *Escherichia coli* strain isolated in New Zealand. Microbiol Resour Announc 8:e01665-18

Table of Contents

List of tables

List of figures

Chapter 1

Chapter II

List of abbreviations

AMR	Antimicrobial resistance
cAMP	3’,5’-cylic adenosine monophosphate
CAUTI	Catheter-associated urinary tract infections
CDS	Coding sequence
CFU	Colony forming unit
DMSO	Dimethyl sulfoxide
DOC	Sodium deoxycholate
EPI	Efflux pump inhibitor
ETC	Electron transport chain
FICI	Fractional inhibitory concentration index
FRT	FLP recombinase recognition target
FZ	Furazolidone
IPTG	Isopropyl-β-D-thiogalactopyranoside
LPS	Lipopolysaccharide
MIC	Minimum inhibitory concentration
NFZ	Nitrofurazone
NIT	Nitrofurantoin
NO	Nitric oxide
NTR	Nitroreductase
OD	Optical density
ORF	Open reading frame
PCR	Polymerase chain reaction
PEP	Phosphoenolpyruvate
PTS	Phosphotransferase system
ROS	Reactive oxygen species
Rpm	Rotation per minute
UK	The United Kingdom
US	The United States

UTI	Urinary tract infections
WHO	World Health Organization

Chapter I: Introduction

Antimicrobial resistance in Gram-negative pathogens

Antimicrobial resistance (AMR) is one of the most serious threats with which humans have been confronted. A UK-Prime-Minister-commissioned report in 2014 estimated that AMR, without appropriate interventions, would globally cause 10 million deaths per annum with a cumulative loss of US $100 trillion by 2050 (1). A follow-up report, published one year later, proposed that fifteen novel antibiotics must be introduced for every decade to meet the medical need for treating bacterial infections (2). Taking into consideration the current number of antibiotic candidates in preclinical stages (152 compounds, compiled in the AntibioticDB database) and the attrition rate in antibiotic development, it can be inferred that only three drugs may be approved for clinical uses by 2025, leading to a 12-novel-antibiotic gap during the 10-year period 2015-2025 (3).

Gram-negative bacterial pathogens are more formidable foes than their Gram-positive counterparts, due to three major features in the cell envelope (Fig. 1). First, the outer membrane of Gram-negative bacteria is an asymmetric bilayer, composed of a conventional phospholipid inner leaflet and an outer leaflet made of lipopolysaccharides (LPS), which acts as a barrier to the influx of antimicrobial agents, regardless of the hydrophilic or hydrophobic nature of the drug (4). The second feature is the size/charge selectivity of porins, water-filled β-barrel protein channels, embedded onto the outer membrane (e.g. OmpF and OmpC in *E. coli*), through which antibiotics may internalize into the periplasm. Porins strictly limit the size and charge of the permeating antibiotics due to a small pore size and the charged residues in the pore lining (5). Additionally, sophisticated regulation of porin expression further slows down the influx of the antimicrobial agents upon stress exposure (4). Third, Gram-negative pathogens also possess a wide range of active multidrug efflux pumps, which expel xenobiotics

including antimicrobials out of the cell, preventing access of the drug to intracellular targets (5-7).

Another difficulty in developing antibacterials against Gram-negative pathogens is caused by the differences in the chemical nature of small molecules that can cross the outer membrane *vs.* inner membrane. While antimicrobials that are able to penetrate the outer membrane *via* porins are hydrophilic charged compounds, the cytoplasmic inner membrane favors neutral lipophilic compounds; therefore, an antimicrobial agent that has the necessary properties to traverse the outer membrane may not be capable of penetrating the cytoplasmic membrane to reach a target in the cytoplasm (8). With all the antimicrobial resistance-conferring features of the envelope structure of Gram-negative pathogens described above, it is broadly accepted that successful development of a novel antibiotics for these bacteria is tremendously difficult. It is therefore a monumental task to keep pace with the clinical demand in the face of constant emergence and global spread of novel antibiotic resistant Gram-negative pathogens.

In 2017, the World Health Organization (WHO) issued a list of bacteria for which development of novel antibacterials is urgently needed. Not surprisingly, antibiotic resistant Gram-negative bacteria (carbapenem-resistant and third-generation cephalosporin-resistant Enterobacteriaceae, carbapenem-resistant *Acinetobacter baumannii* and carbapenem-resistant *Pseudomonas aeruginosa*), were ranked at the top of the list, and characterized as a "critical" group of organisms for which the research and development of new antibiotics should be prioritized (9). However, despite this priority classification, there is a bias in antibiotic development against these Gram-negative pathogens due to their properties described above. Data updated until March 2019 from the Pew Charitable Trusts showed that only 16 out of 42 candidate antibiotics in different development phases target the WHO critical priority pathogens.

Only one of these 16 antibiotics, murepavadin, belongs to a novel class that can be used to treat *P. aeruginosa* infections. The rest of the antibacterials under development are improvements to currently existing classes of antibiotics (10). It is not overstated to say that the pace of antibiotic development, in terms of quantity and quality, does and will not match the demand to counteract AMR, especially in Gram-negative pathogens. In this dire context, alternative strategies are warranted to supplement conventional antibiotic research and development, such as antimicrobial combinations, revival of old drugs, capitalization on host innate defense and so on.

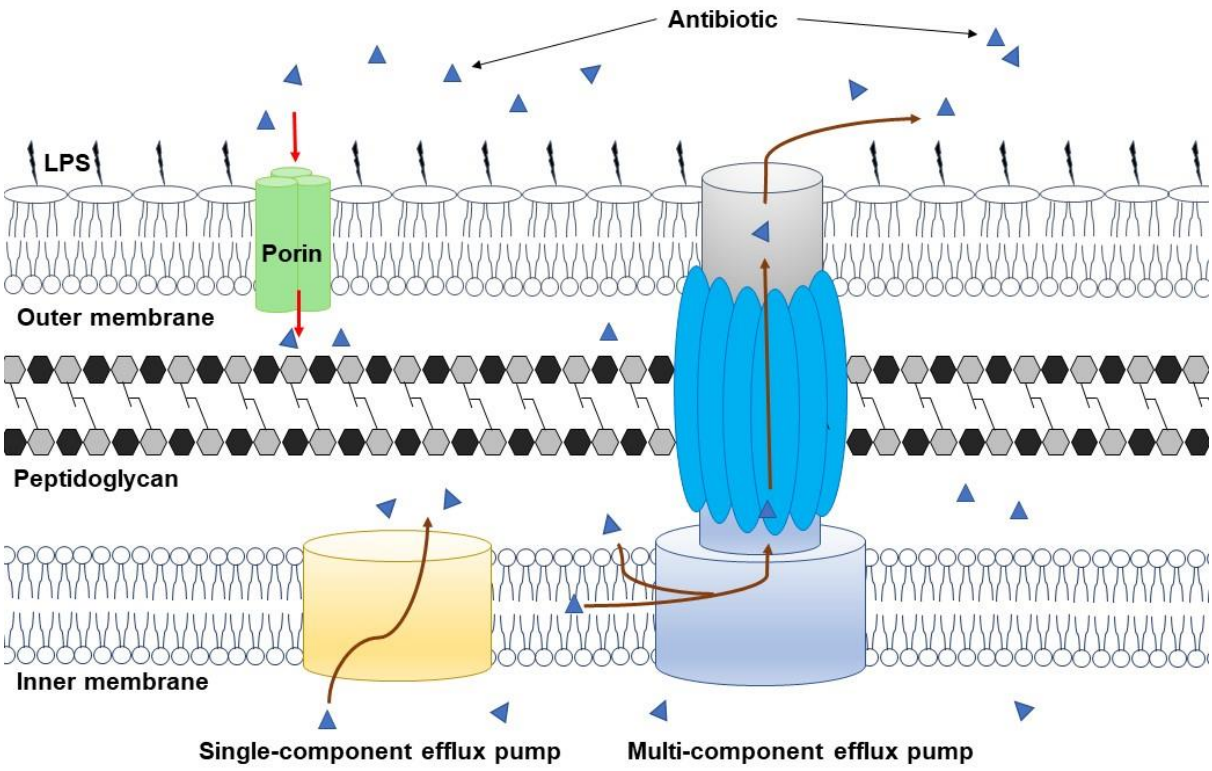

Figure 1: Gram-negative envelope structure and antibiotic resistance. The cell envelope is composed of an outer membrane, a thin peptidoglycan cell wall and an inner membrane. The outer leaflet of the outer membrane made of lipopolysaccharide, making an impermeable barrier to both hydrophilic and hydrophobic compounds. Small hydrophilic compounds penetrate the outer membrane through porins (e.g. OmpF and OmpC in *E. coli*) which restrict the size and charge of the transporting compounds. Multiple-component and single component efflux pumps (*e.g.* AcrAB-TolC and MdtM, respectively) concertedly expel the antibiotic drug out of the cell. LPS, lipopolysaccharide. Adapted from (7) with permission.

Antimicrobial combinations to counteract AMR

Antimicrobial interactions: synergy and antagonism

When two antimicrobial agents are combined, there are interactions between them, leading to an antimicrobial effect exerted by the drug combination that is either stronger or weaker than the expected additive effect of constituent agents. In the former case, the interaction is termed synergy and the latter antagonism. There are two commonly used approaches to define the additivity between two antimicrobial agents, the Bliss independence (11) and Loewe additivity models (12).

The principle of the Bliss independence model is that two additive drugs would act independently in bacterial systems such that the outcome is a probabilistic process (13). For example, when drug A at a particular concentration causes 40 % (or 0.4) growth inhibition and drug B at another particular concentration causes 50 % (or 0.5) growth inhibition, the expected additive effect caused by a combination of drugs A and B at these concentrations would be $0.4 + 0.5 – 0.4 \times 0.5 = 0.7$ or 70 % growth inhibition (Fig. 2A). From this, a drug interaction is synergistic if the combined effect is higher than 70 % and antagonistic if the combined effect is lower than 70 %. While this approach is convenient and rapid for high-throughput characterization of antimicrobial interactions, only a single dose of each drug is used and therefore, an interaction defined by the Bliss independence model does not reflect the interaction across a range of antimicrobial concentrations.

The Loewe additivity model is a dose-effect-based approach, relying on an intuitive principle that a drug does not interact with itself (14). Simply put, combining a concentration of $a \times$ MIC of drug A, given $0 \leq a \leq 1$, with a concentration of $(1 – a) \times$ MIC of drug A is expected to cause an effect equivalent to drug A at its MIC (*i.e.*

complete growth inhibition). Thus, if drugs A and B do not interact with each other, a combination of a × MIC of drug A and $(1 - a)$ × MIC of drug B would cause a growth inhibition effect equivalent to the drug A or B individually at its MIC. If lower concentrations of the two drugs A and B are required to elicit the same effect, the drug interaction is considered as synergy; otherwise, it is considered as antagonism. Capitalizing on the Loewe additivity model, checkerboard assays are commonly employed to characterize the interaction between antimicrobial agents. In this assay, bacterial cultures at a defined inoculum are exposed to serial dilutions of two antimicrobial agents, either alone or in combination, and minimum concentrations that cause bacterial growth inhibition are determined. Drug interaction is categorized using the Fractional Inhibitory Concentration Index (FICI) calculated as follows:

$$\mathbf{FICI = FIC_A + FIC_B,}$$

in which

$$\mathbf{FIC_A = MIC_{A(B)}/MIC_A}$$

$$\mathbf{FIC_B = MIC_{B(A)}/MIC_B}$$

FIC_A & FIC_B: Fractional inhibitory concentration of drug A and B, respectively

$MIC_{A(B)}$ & $MIC_{B(A)}$: Minimum inhibitory concentration of drug A and B, respectively, when used in combination

MIC_A & MIC_B: Minimum inhibitory concentration of drug A and B, respectively, when used alone

The two drugs are additive if the FICI = 1, synergistic if the FICI < 1 and antagonistic if the FICI > 1. However, it is a common practice in antimicrobial interaction studies to use a conservative interpretation in which the drug interaction is synergistic if FICI ≤ 0.5, antagonistic if FICI > 4, and there is no drug interaction if FICI > 0.5 and ≤ 4 (15).

The data obtained from checkerboard assays can also be illustrated using an isobologram in which each data point along the line (also known as isobole) represents minimum inhibitory concentrations of the drugs either alone or in combination (Fig. 2B). Intuitively, a synergistic interaction shows a concave isobole whereas an antagonistic interaction shows a convex isobole. Also using the Loewe additivity model is the Etest in which two strips impregnated with continuous concentration gradients of the two antibiotics are placed on solid agar in a perpendicular direction and bacterial growth inhibition is examined (16). Like the checkerboard assay, FICIs are used to identify drug interactions in the Etest.

Another drug interaction model is the highest single agent approach, also referred to as the Gaddum's non-interaction or cooperative effect (13, 17), in which the resulting effect of the drug combination is compared with the effect of the most active individual agent (Fig. 2C). Although this model is not as commonly applied as the Bliss independence or Loewe additivity, one variant of it, namely the time-kill assay, is widely used in antimicrobial combination studies. In the time-kill assay, bacterial cells are exposed to individual drugs at a desired concentration or the drug combination at those concentrations; the viable cells are enumerated at different time points over 24 h of incubation for fast growing bacteria or 7-10 days for slow-growing bacteria (18). At a defined time point, if the drug combination causes a decrease in the viable cell count by more than 2 $\log_{10}$ CFU/mL in comparison to the single drug agent with higher potency, the drug interaction is defined as synergy (19). Besides providing evidence to classify drug interactions, this assay also determines the rate and phase of bacterial killing, which may be useful in predicting antibacterial efficacy in patients and development of treatment of infections using synergistic drug combinations (18, 19).

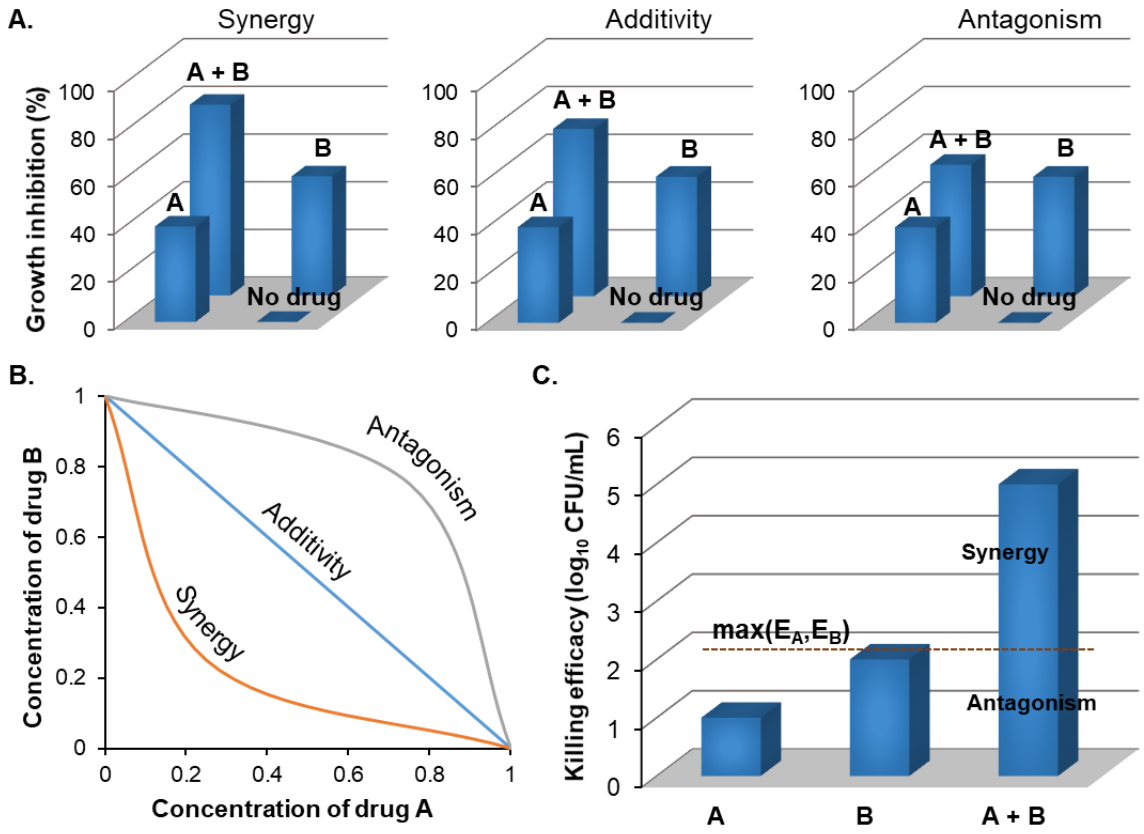

Figure 2: Schematic illustration of pairwise drug interactions using Bliss independence (A), Loewe additivity (B) and highest single agent approaches (C). Drug interactions are classified as synergy or antagonism when the effect exerted by the combination of drugs A and B is greater or lower than the expected additive effect between the two drugs, respectively. (A) In the Bliss independence model, the additive effect is calculated as $E_A + E_B - E_A \times E_B$, where E_A and E_B represent the growth inhibition effect caused by drugs A and B at a particular dose. (B) In the Loewe additivity model, an isobologram is used to describe the drug interaction. Each data point along the line (termed as isobole) represents the minimum concentration of the drug, alone or in combination, that causes a defined cut-off effect (e.g. 90 % or 50 % growth inhibition). (C) In the highest single agent, the effect caused by the drug combination is compared with the effect caused by the most active agent. Each approach has its own method to calculate the cut-off deviation value from the additive effect to which combined effects are compared to categorize the type of drug interaction.

Antimicrobial combinations: advantages and challenges

A major focus of antimicrobial interaction studies is on discovery and development of drug synergistic pairs which provide potential clinical applications, especially against

the multi-drug resistant Gram-negative pathogens. Such combinatorial therapies are expected to possess enhanced antimicrobial efficacy, deceleration of the resistance development rate and alleviation of side effects by lowering the doses of each drug (20, 21). Based on synergistic interactions, a drug that is ineffective due to acquired or inherent resistance mechanisms can be employed to fight these pathogens when combined with another active antimicrobial agent.

From the view of the pharmaceutical industry, drug combinations expand the space of possible anti-infective treatments for drug development. The advent of any novel antimicrobial agent brings about numerous possible double combinations with existing antibiotics to be evaluated, let alone higher-order combinations. Also, a drug combination showing improved antimicrobial efficacy is patentable, even when the combination constituents are not *de novo*-developed compounds, such as off-patent drugs or drugs repurposed from other clinical uses. Such a protection of intellectual properties may attract interest from established pharmaceutical companies and/or create opportunities for start-ups to advance the combination therapy further along clinical development stages. This feature of drug combinations is crucially important because without engagement of dedicated pharmaceutical companies (big or start-up), a huge cost of clinical trials from phase I to III (~ 132.7 million US dollars) (2) and access to multidisciplinary drug development expertise are almost prohibitive to scientists from academic institutions, who rely majorly on public funding and are often specialized in antimicrobial research rather than development.

Besides facing intrinsic challenges associated with development of conventional single antibiotic molecules, a tremendously difficult task in evaluating antimicrobial combinations is translation of *in vitro* synergy into *in vivo* models, given differential pharmacokinetics of the drug partners, which prevents them from reaching the site of

infection at desirable doses. Either one of the drug pair might not reach the target site or the two drugs might reach the target site at different times (18). Apart from the folate pathway inhibitors, trimethoprim-sulfamethoxazole duo, that was introduced in 1968, successful development of antimicrobial combinatorial therapies appears to be limited to β-lactam-β-lactamase inhibitor combinations, despite a plethora of reports describing *in vitro* synergism of drug pairs (22, 23).

Synthetic 5-nitrofuran antimicrobials

Clinical applications

Synthetic 5-nitrofurans are an old antimicrobial class, characterized by a nitro group attached in the C-5 of the aromatic furan ring with varying side chain attached in the C-2 of the ring. Commercially available examples of this group include furazolidone, nitrofurantoin and nitrofurazone (Chapter 2, Fig. 1). Furazolidone (FZ) is currently used as a component in several combinatorial therapies for *Helicobacter pylori* infections, especially in China and Iran (24-27), and is used on its own to treat giardiasis (28), *Trichomonas vaginalis* infections (29) and paediatric diarrhoea in some Latin American countries (cited in 30, 31). In veterinary therapeutics, a recent trial showed that FZ was efficient in treatment of canine cutaneous leishmaniasis when used in combination with domperidone (32).

Nitrofurantoin (NIT) is currently recommended as a first-line antibiotic therapy for uncomplicated urinary tract infections (UTIs) by the European Association of Urology and the Infectious Diseases Society of America, due to the increasing prevalence of resistance to third-generation cephalosporins and carbapenems amongst uropathogenic isolates (33). These recommendations are further supported by high efficiency in clinical and microbiological outcomes reported in a recent review and meta-analysis of controlled trials of the NIT use in UTI therapy (34) and a clinical trial for a 5-day NIT

regime in treating uncomplicated lower UTIs in women (35). Additionally, prophylactic uses of NIT against UTIs have been systematically reviewed and meta-analyzed by two independent groups (36, 37). They both came to a similar conclusion, that NIT has an efficacy equivalent to other antibiotics such as norfloxacin, trimethoprim, sulfamethoxazole/trimethoprim and cefaclor; however, there was a higher risk of adverse effects, majorly gastrointestinal symptoms, associated with long-term use of NIT, than that of other antibiotics. NIT for UTIs are therefore of limited use in prophylaxis.

Nitrofurazone (or nitrofural, NFZ) is used for wound and burn treatments (38-40) and preparation of nasal solution/spay (41). While the current state of NFZ topical applications is not known, recent reports explore novel approaches to enhance NFZ topical drug delivery including microencapsulation (42), hydrogel (43) and nanogel (44, 45), which warrant improved antimicrobial efficacy in next-generation NFZ topical products in years to come. In addition, this drug is employed to produce NFZ-coated urinary catheters aiming to prevent catheter-associated urinary tract infections (CAUTIs). Though the NFZ-coated catheters performed efficiently to eradicate uropathogens in *in vitro* assays (46-50), their clinical efficacy in decreasing CAUTIs was challenged in two clinical trials that reported no beneficial effects and a higher discomfort rate of the NFZ-impregnated urinary catheters as compared to the standard ones (51, 52).

Mechanism of action

The three nitrofuran drugs (NFZ, NIT and FZ) were clinically introduced in 1944, 1953 and 1954, respectively (38), during the golden era of antibiotic discovery when most of the currently existing antibiotic scaffolds were reported. Whereas antimicrobial resistance has become increasingly widespread, threatening the effectiveness of

antibiotics of all classes, recent epidemiological data illustrated a very low prevalence of resistance to 5-nitrofurans amongst *Escherichia coli* clinical isolates around the world, including Peru (30, 53), Mexico (54) , the United Kingdom (55), Denmark (56), Germany (57), France (58), Iran (59) and China (60) to name a few, signifying the increasing importance of 5-nitrofurans to combat antibiotic resistant enterobacteria in the future.

Though the 5-nitrofuran agents have had a long history of clinical use, the knowledge about their mode of action is far from complete. Taking *E. coli* as a model organism, they are prodrugs that require reductive activation mediated by two type I oxygen-insensitive nitroreductases, NfsA and NfsB in a redundant manner, to exert their antibacterial effects (31, 61-63). Type I (oxygen-insensitive) nitroreductase enzymes catalyze the stepwise 2-electron reduction of nitroaromatic compounds (of which 5-nitrofurans are a subfamily) into nitroso and hydroxylamino-derivatives and a final amino product (Fig. 3) (64-67). It has also been reported that type I trypanosomal nitroreductase metabolizes nifurtimox (an anti-trypanosomal 5-nitrofuran) to an unsaturated open-chain nitrile that was found to be responsible for the toxicity toward trypanosomal cells (68). While diverse antibacterial effects of 5-nitrofurans have been described, including triggering DNA lesions, inducing oxidative stress and inhibiting RNA and protein biosynthesis (69-73), it is still uncertain what the reactive intermediates of 5-nitrofuran activation by NfsA/NfsB are responsible for antibacterial effects and what their cellular targets are.

Oxygen-sensitive nitroreductase activity (or type II) were also detected in *E. coli* extracts using biochemical assays in 1979 (74). This activity involves the one-electron reduction of the 5-nitrofuran drug intro a nitro anion free radical, which is oxidized back into the initial prodrug by oxygen, with the resulting generation of superoxide (Fig. 3).

However, the gene(s) responsible for this activity and the extent of the contribution by this pathway to 5-nitrofuran activation have not been identified.

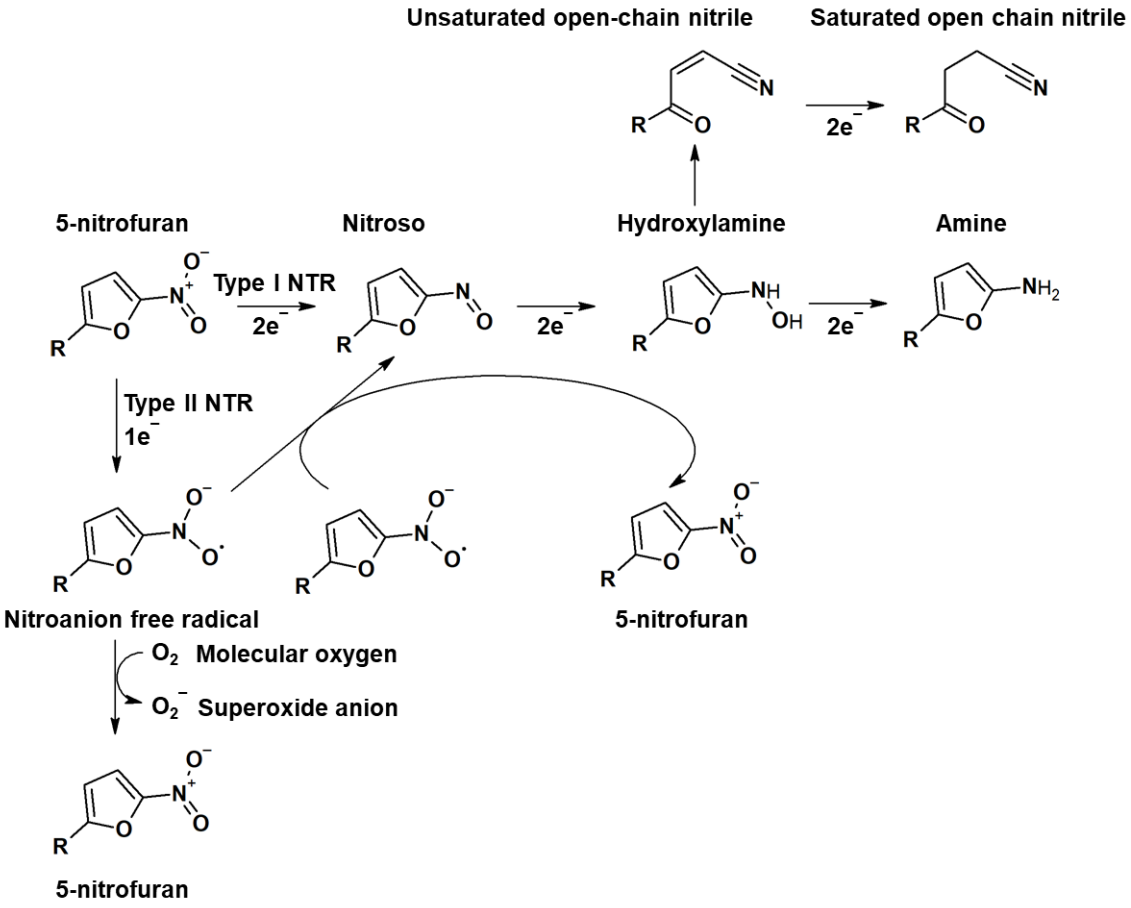

Figure 3: Proposed mechanism of 5-nitrofuran reduction by type I and type II nitroreductase enzymes. NTR, nitroreductase. Adapted from (75) with permission.

Sodium deoxycholate

Bile salts are natural products of the mammalian digestive system, that are synthesized in the liver, stored in the gall bladder and secreted into the intestine following meals, to facilitate fat solubilization and absorption (Fig. 4 and Chapter 4, Figure S1). They are composed of primary and secondary bile salts. In addition, they are present as unconjugated or glycine- or taurine-conjugated form. Primary bile salts (glyco-/tauro-cholate or chenodeoxycholate) are synthesized from cholesterol in the liver (76). The

newly synthesized conjugated bile salts plus the reabsorbed ones are then transported to and stored in the gallbladder. Once secreted into the intestine, they are modified by bacterial enzymes. The conjugated bile salts are deconjugated by the bile salt hydrolases of various intestinal bacterial genera such as *Clostridium*, *Bacteroides*, *Lactobacillus*, *Bifidobacterium*, *Enterococcus*, and even a pathogenic species *Listeria monocytogenes* (76). The unconjugated primary bile salts, cholate and chenodeoxycholate, are further metabolized by 7α-dehydroxylation to secondary bile salts, deoxycholate (DOC) and lithocholate, respectively. This chemical transformation can be performed by bacteria belonging to the genera *Clostridium* (clusters XIVa and XI) and *Eubacterium* (76, 77). Another secondary bile salt in humans, called ursodeoxycholate, is synthesized from chenodeoxycholate by 7α/β-hydroxysteroid dehydrogenase of *Clostridium absonum* (78). While metabolized by intestinal bacterial microflora, the majority of the bile salts (~95 %) are reabsorbed along the intestinal tract and recirculated *via* the portal bloodstream to the liver where they are re-conjugated, completing a process called an enterohepatic circulation (77).

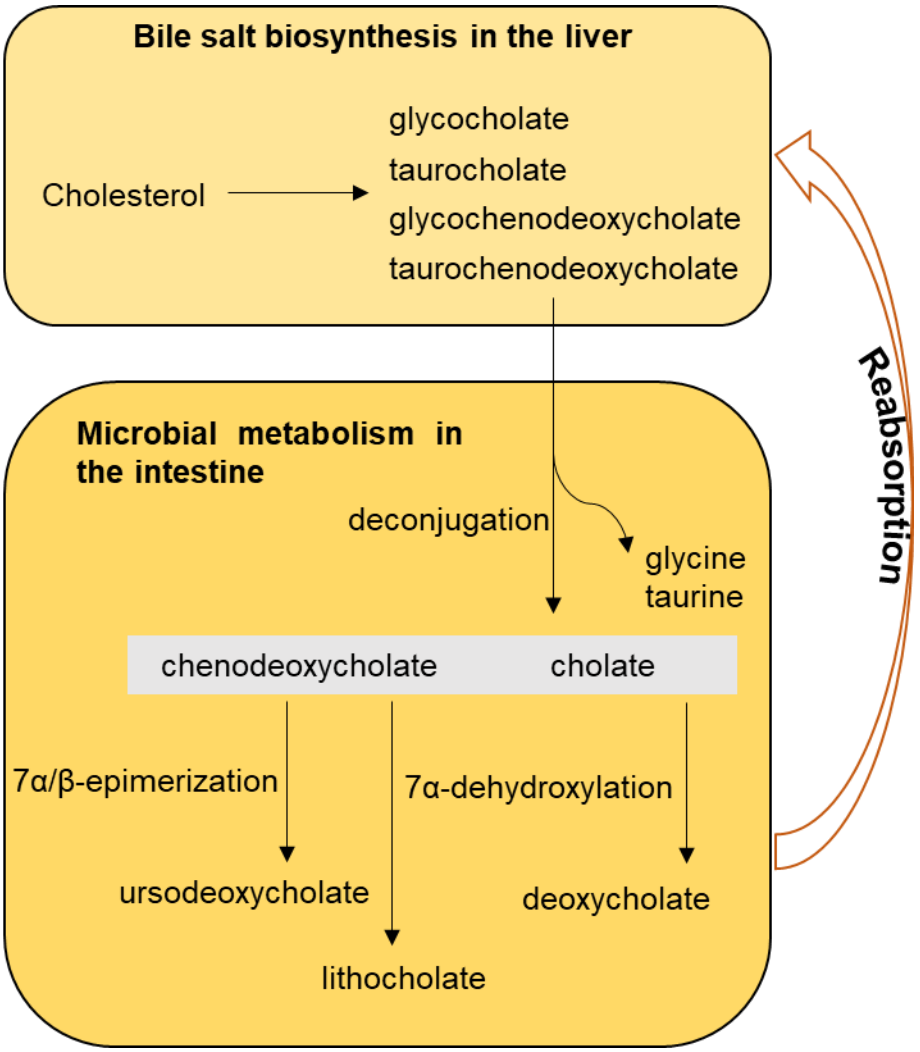

Figure 4: Schematic diagram for biosynthesis in the liver and intestinal microbial metabolism of bile salts. Primary bile salts: cholate, chenodeoxycholate; secondary bile salts: deoxycholate, lithocholate and ursodeoxycholate.

Apart from the supportive role for fat digestion, DOC plays a complex role in the interaction between the host and microbes and amongst microbes in the intestinal ecosystem. On the one hand, DOC participates in the maintenance of the gut microbiome balance, based on its antimicrobial activity, and therefore, contributes to a healthy state of the animal gut, by preventing growth of bacteria such as *Clostridium difficile* (79, 80). On the other hand, multiple bacterial pathogens capitalize on DOC as a signaling molecule to adapt their physiology to the site of infection, for example,

virulence expression, switch on genes involved in degradation pathways for nutrient availability (*e.g.* ethanolamine) and biofilm formation (81-85).

Gram-negative enteric bacterial pathogens, such as *E. coli*, *Salmonella enterica*, *Vibrio cholerae* and *Campylobacter jejuni*, are highly resistant to DOC, primarily as the result of the multiple active efflux pumps that restrict intracellular DOC accumulation (81, 86-89). Additional resistance mechanisms have been described, such as DOC-uptake by the MqsR/MqsA toxin-antitoxin system, DNA repair systems, mutations in genes related to the cell envelope and cell division factors, decreased expression of outer membrane porins, cell wall remodeling and the participation of various stress responses (81, 90-96).

The antimicrobial mechanism of DOC action, though limited in enterobacteria, appears to be promiscuous with multiple targets involved. It was proposed that DOC causes oxidative DNA damage, triggers protein aggregation and compromises cellular membrane integrity (91, 97, 98). Recent studies in other pathogens provide further clues about DOC's action. Sannasiddappa *et al.* (99) reported that DOC lowers the intracellular pH, dissipates the proton motive force and increases membrane permeability even at sub-inhibitory concentrations and kills *Staphylococcus aureus* through membrane disruption, resulting in the leakage of cellular contents. In *C. jejuni*, DOC was found to induce generation of reactive oxygen species (ROS) and DNA damage including 8-oxo-dG lesions and double-strand breaks (100). Overall, it appears that cytoplasmic membrane, DNA and proteins are damaged upon DOC exposure. However, it remains unknown whether these effects are due to direct interactions of these molecules with DOC or consequences of DOC attack on unknown cognate target(s). The involvement of ROS has been reported in causing DNA and protein damage (98, 100), supporting the secondary consequence of DOC action. Exploration of

the DOC targets is important to better understand the mechanism of action and resistance, that may allow a prudent consideration of DOC in antimicrobial therapies.

Thesis aims

The overall aims of the research described in this thesis were to *in vitro* characterize interactions between DOC and 5-nitrofuran drugs in inhibiting/killing enterobacteria from which a therapeutic potential can be evaluated. The mechanisms of action of each of constituent drugs were also separately investigated, by selection of drug-resistant mutants and using next-generation whole genome sequencing to analyze the mutants, followed by genetic and biochemical approaches. The findings from each drug were expected to provide a better understanding of the underlying mechanisms of DOC-5-nitrofurans interactions.

The structure of the thesis

Chapter 1 summarizes the current state of antimicrobial resistance in Gram-negative bacteria, describes the methodology used to classify drug interactions and discusses the pros and cons of antimicrobial combinations. A literature review on DOC and 5-nitrofurans was also included in this chapter.

Chapter 2 reports a synergistic interaction between DOC and 5-nitrofurans in inhibiting the growth of and/or killing enterobacteria, such as *E. coli*, *S. enterica* and *Citrobacter gillenii*. The result shows that the synergy is caused by nitrofuran-mediated inhibition of TolC-dependent efflux pumps that otherwise prevent intracellular DOC accumulation.

Chapter 3 describes the discovery of a novel nitrofuran-activating enzyme, AhpF. This finding paves the way to counteract nitrofuran-resistant isolates by screening for molecules to enhance *ahpF* expression/activity or designing nitrofuran analogues with higher affinity for the AhpF enzyme.

Chapter 4 illustrates novel mutations that cause a low-level DOC resistance in *E. coli* strains deficient in TolC-associated efflux pumps. This chapter also describes the important findings that single-step high-level DOC causing mutations were not identified in the absence of efflux pumps.

Chapter 5 provides a general discussion to correlate the findings in previous chapters and suggests future work that advances the development of the DOC/nitrofuran combination for therapeutic uses.

Chapter II:

In vitro synergy between sodium deoxycholate and furazolidone against enterobacteria

Vuong Van Hung Le[a], Catrina Olivera[a], Julian Spagnuolo[a1], Ieuan Davies[b] and Jasna Rakonjac[a]*

[a]School of Fundamental Sciences, Massey University, Palmerston North, New Zealand

[b]New Zealand Pharmaceuticals Ltd., Palmerston North, New Zealand

[1]Present address: Department of Biomedicine, University Hospital Basel, 4031 Basel, Switzerland

Email address:

Vuong Van Hung Le: v.le@massey.ac.nz

Catrina Olivera: c.olivera@massey.ac.nz

Julian Spagnuolo: julianspagnuolo@gmail.com

Ieuan Davies: ieuan.davies@nzp.co.nz

*Corresponding author: Jasna Rakonjac: j.rakonjac@massey.ac.nz

Abstract

Background

Antimicrobial combinations have been proven as a promising approach in the confrontation with multi-drug resistant bacterial pathogens. In the present study, we identify and characterize a synergistic interaction of broad-spectrum nitroreductase-activated prodrugs 5-nitrofurans, with a secondary bile salt, sodium deoxycholate (DOC) in growth inhibition and killing of enterobacteria.

Results

Using checkerboard assay, we show that the combination of nitrofuran furazolidone (FZ) and DOC has a profound synergistic effect on growth inhibition of several enterobacterial species including *Escherichia coli*, *Salmonella enterica*, *Citrobacter gillenii* and *Klebsiella pneumoniae*. The Fractional Inhibitory Concentration Index (FICI) for DOC-FZ synergy ranges from 0.125 to 0.35 and remains unchanged in an ampicillin-resistant *E. coli* strain containing a β-lactamase-producing plasmid. Findings from the time-kill assay further highlight the synergy between these two compounds with respect to bacterial killing in *E. coli* and *Salmonella*.

We further characterize the mechanism of synergy in *E. coli* K12, showing that disruption of the *tolC* or *acrA* genes that encode components of multidrug efflux pumps causes a complete or partial loss, respectively, of the DOC-FZ synergy. This finding indicates the key role of TolC-associated efflux pumps in the DOC-FZ synergy. Overexpression of the nitric oxide-detoxifying enzyme Hmp results in a three-fold increase in FICI for the DOC-FZ interaction, suggesting a role for nitric oxide in the synergy. We further demonstrate that DOC-FZ synergy is largely independent of NfsA and NfsB, the two major activation enzymes of the nitrofuran prodrugs.

Conclusions

This study is to our knowledge the first report of nitrofuran-deoxycholate synergy against Gram-negative bacteria, offering potential applications in antimicrobial therapeutics. The mechanism of DOC-FZ synergy involves FZ-mediated inhibition of TolC-associated efflux pumps that normally remove DOC from bacterial cells. One possible contribution to this effect is *via* FZ-mediated nitric oxide production.

Keywords

Furazolidone; Nitrofurans; Sodium Deoxycholate; Antimicrobial combination; Synergy; Enterobacteria

Background

Antimicrobial resistance (AMR) is one of the most serious threats with which humans have been confronted. A UK-Prime-Minister-commissioned report in 2014 estimated that AMR, without appropriate interventions, will cause 10 million deaths per annum globally with a cumulative loss of US $100 trillion by 2050 (1). In this dire context, alternative approaches are urgently needed besides the discovery of novel antibiotics. Antimicrobial combinations have proven to be a promising approach with some widely accepted advantages, including enhancement of antimicrobial efficacy, deceleration of the rate of resistance development and the alleviation of side effects by lowering the doses of two drugs (20, 21). Moreover, this approach could amplify the significance of ongoing antimicrobial discovery programs; particularly the advent of any novel antimicrobial compound could bring about a large number of possible double combinations with existing antimicrobial agents to be evaluated, let alone triple and quadruple combinations.

Sodium deoxycholate (DOC) (Additional file 1, Figure S1E) is a facial amphipathic compound in bile, which is secreted into the duodenum to aid lipid digestion and confer some antimicrobial protection (76). Although extensive research has been conducted to elucidate the interaction between DOC, either alone or in the bile mixture, and enteric bacteria, the mode of its antimicrobial action remains elusive. It was suggested that DOC could attack multiple cellular targets, including disturbance of cell membranes, causing DNA damage, triggering oxidative stress and/or inducing protein misfolding (76, 97, 98). Nonetheless, Gram-negative bacteria such as *Escherichia coli* and *Salmonella* are highly resistant to DOC through many mechanisms such as the employment of diverse active efflux pumps, the down-regulation of outer membrane porins and the activation of various stress responses (81, 86, 87, 97).

The 5-nitrofurans are an old class of synthetic antimicrobials, clinically introduced in the 1940s and 1950s (38); several are commercially available, including furazolidone (FZ), nitrofurantoin (NIT) and nitrofurazone (NFZ) (Additional file 1, Figure S1). FZ is used to treat bacterial diarrhea, giardiasis and as a component in combinatorial therapy for *Helicobacter pylori* infections; NIT and NFZ are used to treat urinary tract infections and in topical applications, respectively (40). They are prodrugs which require reductive activation mediated largely by two type-I oxygen-insensitive nitroreductases, NfsA and NfsB. These two enzymes perform stepwise 2-electron reduction of the nitro moiety of the compound into two redox-reactive nitroso and hydroxylamino intermediates and an amino-substituted product (62, 63). A detailed mechanism of how bacterial cells are killed by the reactive intermediate(s) has yet to be clarified. Nevertheless, it has been proposed that the hydroxylamino derivatives could cause DNA lesions, disrupt protein structure and arrest RNA and protein biosynthesis (69-72). Some reports also suggested that nitric oxide could be generated during the activation process, inhibiting the electron transport chain of bacterial cells although clear evidence for this is not so far available (101, 102). It is worth mentioning that nitroreductase-encoding genes are not only commonly present in enterobacteria but also found in other bacterial species such as *Staphylococcus aureus*, *Bacillus subtilis*, *Vibrio fischeri* and parasites (e.g. *Trypanosoma brucei*, *Leishmania major*) (67, 68, 103). The enzymes they encode play different physiological roles in different species; in *E. coli* multiple functions have been proposed for NfsA and NfsB, including dihydropteridine reductase, chromate reductase, quinone-dependent azo reductase, and part of the oxidative stress response (67).

In this study, we have characterized the interaction of DOC with FZ and other three related nitrofurans against a range of enterobacteria. We identified the underlying mechanism of DOC-FZ synergy using *E. coli* K12 as a model organism.

Results

The synergy between DOC and 5-nitrofurans against enterobacteria

To evaluate the synergy between DOC and FZ, the checkerboard growth inhibition assays were performed for a range of enterobacteria, including *Salmonella enterica* serovar Typhimurium LT2, *Citrobacter gillenii*, *Klebsiella pneumoniae* and two *E. coli* antibiotic-resistant laboratory strains (streptomycin-resistant and streptomycin/ampicillin-resistant). DOC and FZ act synergistically in inhibiting growth of the microorganisms listed (Fig. 1), with FICI ranging from 0.125 for a streptomycin-resistant *E. coli* strain (Fig. 1A) to 0.35 for *K. pneumoniae* (Fig. 1E). DOC-FZ synergy was also observed against two *E. coli* pathogenic strains (*E. coli* strain O157 and urinary tract infection strain P50; Additional file 1, Figure S2). It is worth noting that, when used alone, very high DOC concentrations were required to exert an equivalent effect on inhibiting the growth of these Gram-negative enterobacteria, whereas the concentration in combination with FZ at the lowest FICI was within the range of the bile salt concentration in the human intestine (2.5 mg/mL or 6 mM) (104).

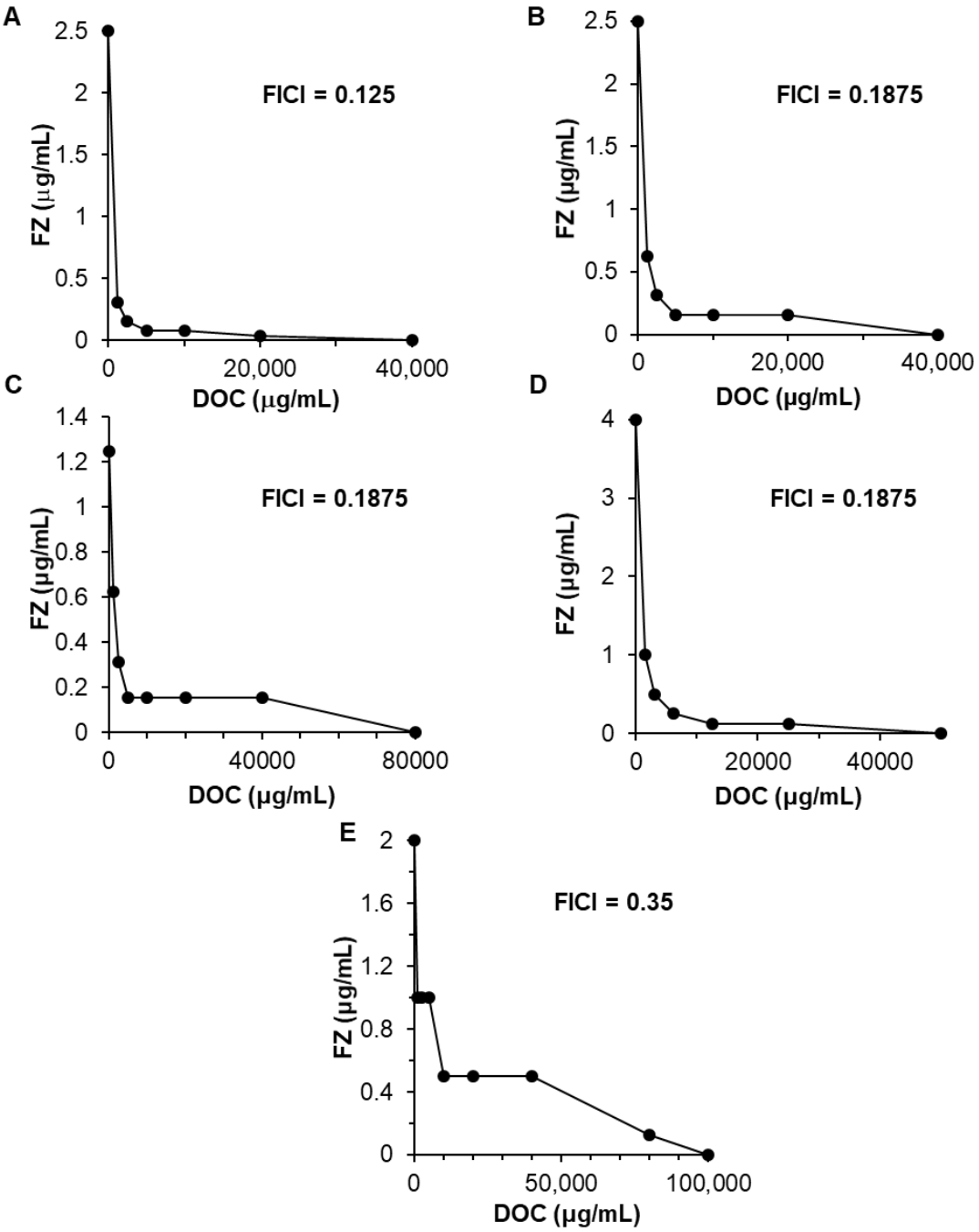

Figure 1: FZ interaction with DOC in growth inhibition of streptomycin- resistant *E. coli* K12 (A), ampicillin- and streptomycin-resistant *E. coli* K12 (B), *Salmonella enterica* serovar Typhimurium LT2 (C), *Citrobacter gillenii* (D) and *Klebsiella pneumoniae* (E). Graphs (isobolograms) were obtained using a checkerboard analysis at multiple concentrations of each molecule. Each data point represents the minimum molecule concentrations alone or in combination causing 90 % inhibition of bacterial growth relative to an unchallenged control culture.

We also examined the interaction between DOC and other nitrofuran compounds, including NIT, NFZ and CM4 (a 5-nitrofuran compound we discovered during an antimicrobial screening campaign against *E. coli*, Additional file 1, Figure S1D) for all bacterial species mentioned above. We found that NIT, NFZ and CM4 were synergistic with DOC against an *E. coli* laboratory strain (Fig. 3), *Citrobacter gillenii* (Additional file 1, Figure S3) and *Salmonella* Typhimurium LT2 (Additional file 1, Figure S4). By contrast, the interaction between NIT or NFZ and DOC was indifferent for a *K. pneumoniae* isolate (Additional file 1, Figure S5). CM4 did not inhibit growth of this *Klebsiella* strain in the range of concentrations used in the experiment (up to 256 μg/ml) so the interaction could not be defined.

To investigate the interaction between DOC and FZ in terms of bactericidal effects, the time-kill assay was employed. Streptomycin-resistant *E. coli* K12 laboratory strain K1508 and *S. enterica* serovar Typhimurium strain LT2 were exposed to sub-inhibitory concentrations of DOC (2500 μg/mL) alone, or FZ (0.5 × MIC) alone, or combination of the two drugs at such sub-inhibitory concentrations, over a 24 h period. The sample was taken at different time points and the surviving bacteria were titrated onto antimicrobial-free plates. Centrifugation and resuspension were applied to each sample before plating to eliminate an antimicrobial carryover. After 24 h, the total cell count in the sample treated with the DOC-FZ combination was about five to six orders of magnitude lower than that in the sample treated with either DOC or FZ alone for both *E. coli* and *Salmonella* (Fig. 2), demonstrating the synergy in bacterial killing between DOC and FZ.

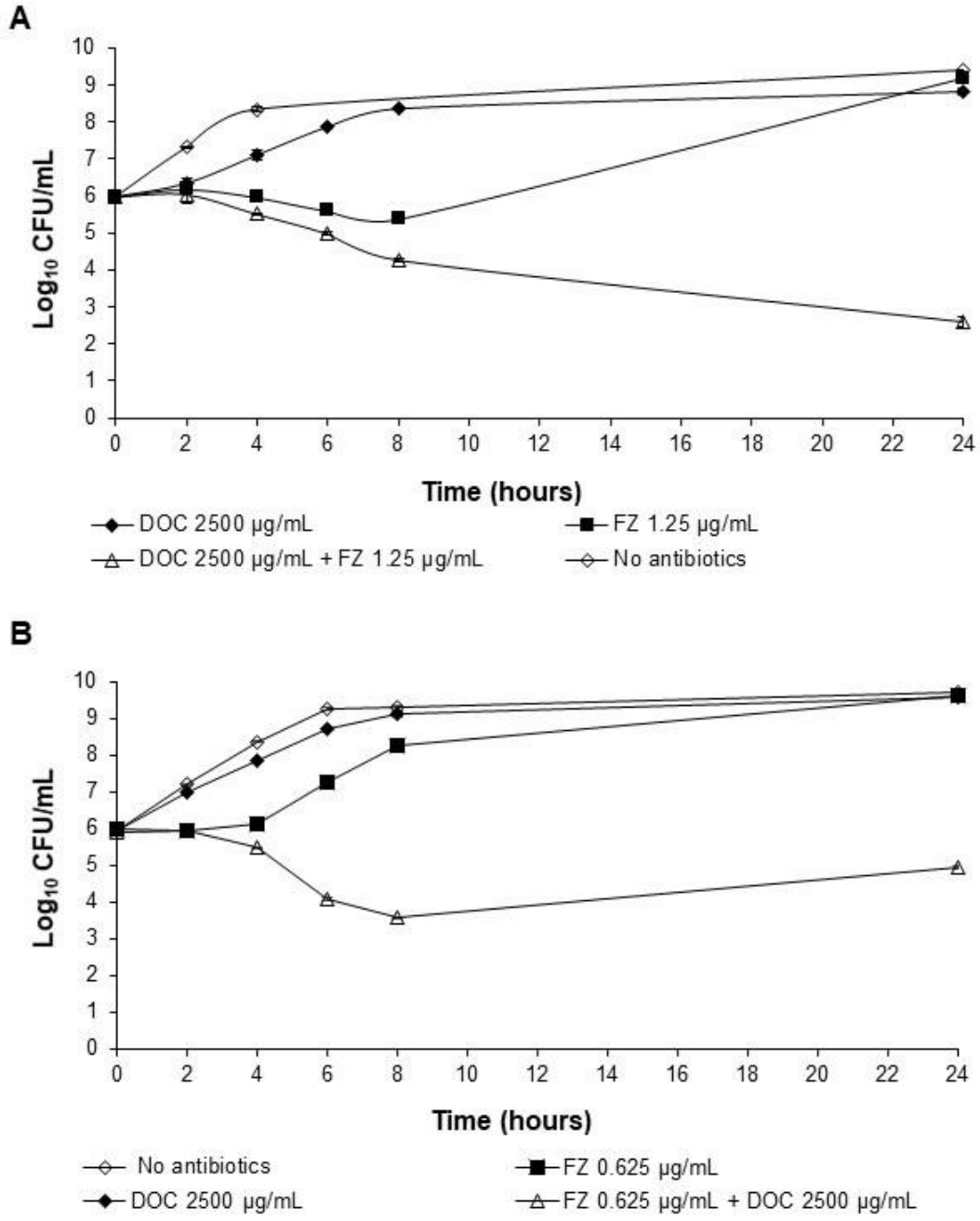

Figure 2: Time-kill analysis of the DOC and FZ combination in killing *E. coli* strain K1508 (A) and *Salmonella enterica* serovar Typhimurium LT2 (B). The data is presented as the mean ± standard error of the mean (SEM) of three independent measurements. The count of the live cells was determined at indicated time points by titration of colony-forming units on agar plates. The lower limit of detection was 60 CFU/mL.

The role of AcrAB-TolC efflux pump in synergistic interaction between DOC and nitrofurans

One commonly accepted principle is that the synergy between two drugs is a consequence of one drug suppressing bacterial physiological pathways that mediate resistance to the other one. It has been reported that DOC can be expelled out of the cell *via* a wide range of efflux pumps, in which the tripartite efflux system AcrAB-TolC plays the major role (86, 87) . This led to the hypothesis that FZ inhibits the activity of efflux pumps, thus allowing intracellular accumulation of DOC to exert its lethal effect. If this scenario were true, disruption of the function of efflux pumps by mutation should make this activity of FZ redundant, thus increasing the interaction index (FICI) in the mutant strains.

To validate this model in *E. coli*, checkerboard assays were performed on strains containing deletions of the individual genes encoding the AcrAB-TolC efflux pump system, Δ*tolC* and Δ*acrA*. Deletion of *tolC* caused a shift from the synergistic interaction between DOC and FZ in the wild type (FICI = 0.125) to indifferent interaction (FICI = 0.75; Fig. 3A). The Δ*acrA* mutant exhibited a 3-fold increase in the FICI relative to the isogenic wild type strain. Such changes were also observed for the interaction between DOC and other nitrofurans, NIT, NFZ or CM4 (Fig. 3B, C and D).

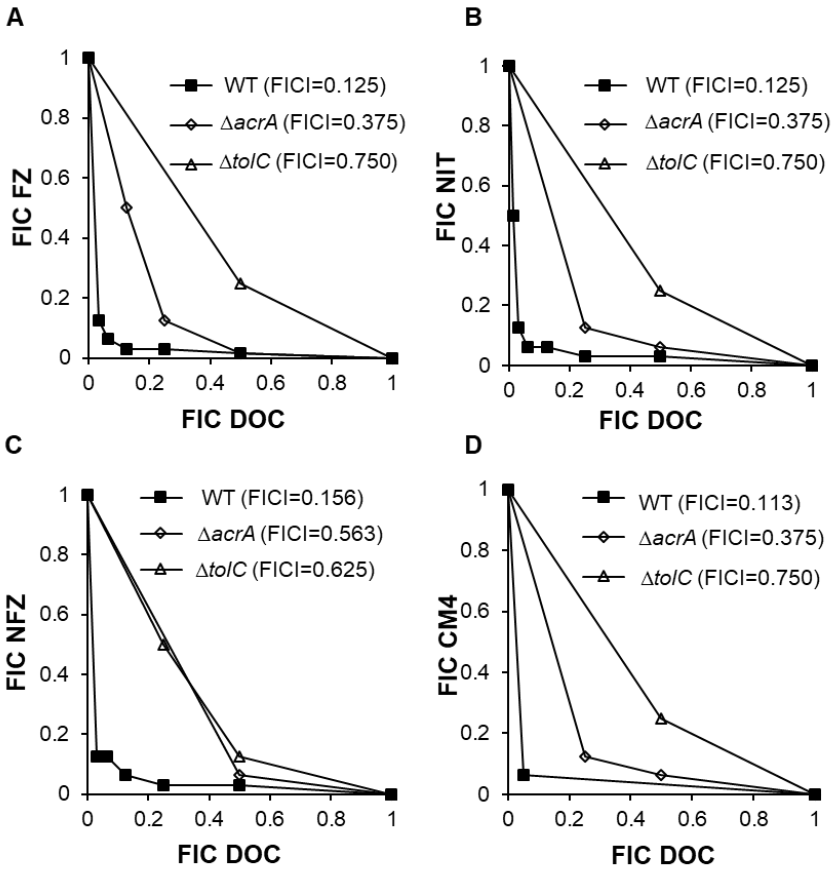

Figure 3: Effect of the Δ*tolC* and Δ*acrA* mutations on DOC synergy with FZ, NIT, NFZ and CM4 in *E. coli*. Isobolograms characterizing interactions of DOC with FZ (A), NIT (B), NFZ (C) and CM4 (D) in growth inhibition assays of the *E. coli* K12 strain K1508 (WT or wild-type and two isogenic deletion mutants, Δ*acrA* and Δ*tolC*). Each data point corresponds to the FIC (ratios of the 90% growth inhibition concentrations in combination *vs.* alone) for one of the four nitrofurans (y axis) and DOC (x axis). The Δ*tolC* strain (K2403) had the MICs for FZ, NIT, NFZ, CM4 at 1.25, 4, 8 and 4 µg/mL, respectively. The Δ*acrA* strain (K2424) had the MICs for FZ, NIT, NFZ, CM4 at 2.5, 8, 8 and 8 µg/mL, respectively. The WT strain K1508 had the MICs for FZ, NIT, NFZ, CM4 at 2.5, 32, 16 and 32 µg/mL, respectively.

To confirm that these observations were conferred by direct effect of the *tolC* and *acrA* deletion, rather than indirect effects of other genes or proteins, complementation of the corresponding deletion mutations by plasmid-encoded *tolC* and *acrA* was performed. To compensate for the multiple copies of plasmid-containing genes, complementation was carried out at a low level of expression, nevertheless it completely restored the strong

synergy between DOC and FZ in these complemented strains (Fig. 4). These findings collectively support the model that the efflux pumps act as the interacting point for the synergy between DOC and FZ.

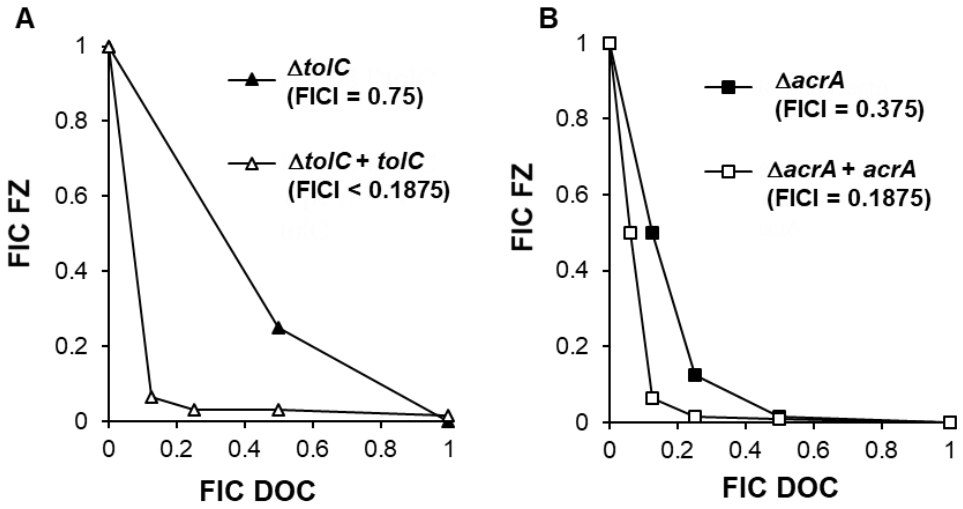

Figure 4: Recovery of FZ-DOC synergy in complemented Δ*tolC* and Δ*acrA* mutants. Isobolograms of FZ-DOC interactions in growth inhibition of: A. Δ*tolC* mutant (Δ*tolC*) and a derived strain containing a plasmid expressing *tolC* gene (Δ*tolC* + *tolC*); B. Δ*acrA* mutant (Δ*acrA*) and a derived strain containing a plasmid expressing *acrA* gene and (Δ*acrA* + *acrA*). Each data point corresponds to the FIC (ratios of the 90% growth inhibition concentrations in combination *vs.* alone) for FZ (y axis) and DOC (x axis).

An intriguing question to be unraveled is how FZ could negatively influence the action of efflux pumps. We hypothesized that FZ could lower the energy supply to efflux pumps by mediating an increase in concentration of nitric oxide (NO). To verify the proposed model, the interaction between DOC and FZ in an *E. coli* strain with increased expression of the protein Hmp (the *E. coli* nitric oxide dioxygenase) was investigated. The rationale for this is that overexpression of the Hmp protein would result in increased conversion of NO into benign NO_3^- ions, thus relieving the effect exerted by NO (105). If NO was involved in the mechanism of the interaction between the two drugs, the synergy degree between them was expected to decrease with an increased abundance of Hmp proteins. In agreement with this hypothesis, overexpression of *hmp*

was found to suppress the synergy between DOC and FZ by a factor of 3 (Fig. 5). This finding supports the model that NO generated during FZ metabolism participates in the inhibition of electron transport chain (106), with the secondary effect of inhibiting the function of efflux pumps which are dependent on the electron transport chain for their activity.

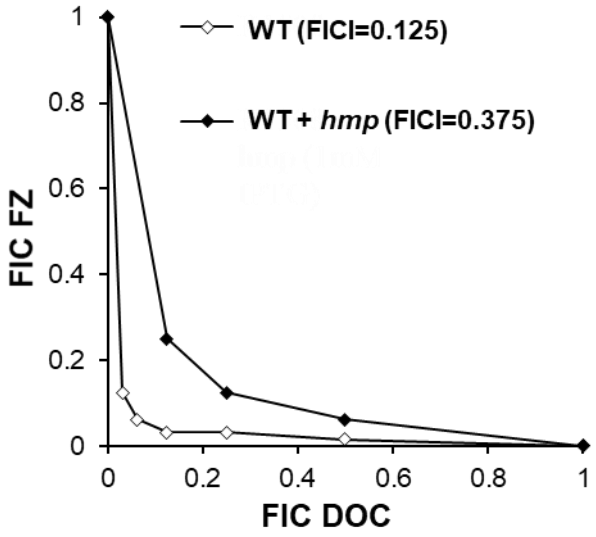

Figure 5: Effect of the *hmp* gene overexpression on FZ-DOC synergy. The isobologram of DOC and FZ interaction in *E. coli* having differential expression of NO-detoxifying protein Hmp. WT, *E. coli* laboratory strain K1508; WT + *hmp*, K1508 containing a plasmid expressing Hmp under the control of a T5-lac hybrid promoter. Expression of *hmp* gene was induced by IPTG (1 mM). Each data point corresponds to the FIC (ratios of the 90% growth inhibition concentrations in combination *vs.* alone) for FZ (y axis) and DOC (x axis).

DOC-FZ synergy is largely independent of NfsA/NfsB-mediated FZ activation

It has long been known that nitrofuran drugs need to be activated by nitroreductases NfsA and NfsB to exert its antibacterial activity (62, 63). As a result, the DOC-FZ synergy is expected to be dependent on the activity of NfsA and NfsB enzymes. To justify that inference, we examined the interaction between DOC and FZ in the Δ*nfsA*

Δ*nfsB E. coli* strain lacking both of these enzymes. In agreement with the FZ activation role of NfsA/NfsB, disruption of these two genes led to an increase in the MIC causing 50% growth inhibition by a factor of 8 (Fig. 6A). Nonetheless, the synergy between DOC and FZ still remained significant in the Δ*nfsA* Δ*nfsB* genetic background, with the FICI at 50 % growth inhibition as low as 0.3125 (Fig. 6B); this FICI value is only slightly higher than that of the wild type strain (0.25). In other words, the contribution of NfsA/NfsB-mediated activation of FZ in the DOC-FZ synergy is very minimal, indicating the presence of an unexplored, but important, mechanism of FZ action or activation.

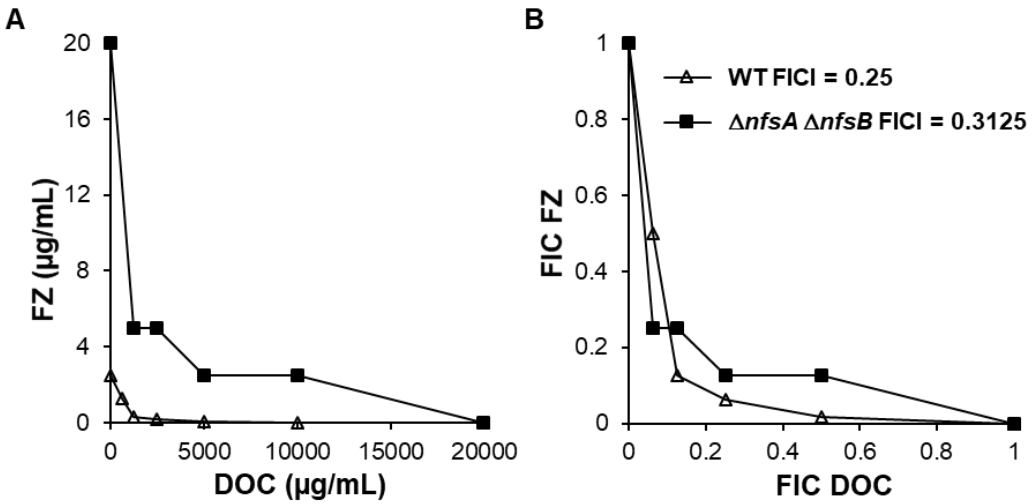

Figure 6: Effect of *nfsA*/*nfsB* deletion on FZ-DOC synergy. Isobologram of FZ-DOC interactions in growth inhibition of wild type strain (K1508) and Δ*nfsA* Δ*nfsB* mutant. A) Each data point represents the minimum molecule concentrations alone or in combination causing 50 % inhibition of bacterial growth relative to an unchallenged control culture. B) Each data point corresponds to the FIC (ratios of the 50 % growth inhibition concentrations in combination *vs.* alone) for FZ (y axis) and DOC (x axis).

Discussion

Capitalization on existing drugs by combining them with other drugs is one of the promising approaches to design novel therapies that will allow the use of antimicrobials which have heretofore been ineffective against Gram-negative bacteria at concentrations that are acceptable for medical treatment. The synergistic interaction between DOC and FZ or other nitrofurans against a range of enterobacteria is of this kind. Decrease in the effective inhibitory concentrations of nitrofurans, when combined with DOC, demonstrated here, is advantageous because of the potential for lowering or removing the reported nitrofuran mutagenic and carcinogenic side-effects (69-72). Gram-negative bacteria, such as *E. coli* and *Salmonella* have evolved high resistance to DOC and other bile salts using various mechanisms, such as multi-drug efflux pumps, a highly impermeable outer membrane, DNA damage repair machines, the MqsR/MqsA toxin-antitoxin system and employment of multiple stress responses (81, 89-91, 107). Inclusion of an active agent, such as FZ or other 5-nitrofurans, could reintroduce the use of DOC in the battle against such formidable pathogens. These findings suggest two potential applications.

Firstly, DOC-nitrofuran combinations could be developed for topical applications, such as wound and burn dressings. In 2015, ATX-101, in which deoxycholic acid is the active ingredient, was approved by the Food and Drug Administrations for reduction of submental fat at a subcutaneous injection dose as high as 10 mg/mL and a volume of up to 10 mL (108). This concentration is much higher than that of DOC (2.5 mg/mL) required for observing the synergy with nitrofurans, indicating that DOC concentrations less than 10 mg/mL could be used in the combination without concern for toxicity. In addition to its antibacterial properties, the hydrogel-forming capability of DOC for transdermal drug delivery in DOC-nitrofuran combination could be exploited. Such uses

of DOC have been described in a rat model (109, 110); no irritant effects on rat skins upon DOC-hydrogel application were observed in histology studies (110).

Secondly, DOC and other bile salts are inherently present in the 2-10 mM concentration range along the gastrointestinal tract, depending on nutritional state and microbiome composition (80, 104). The efficacy of any drug dedicated to treat intestinal infections will depend on the physicochemical properties of the local environment in which an interaction with bile salts is an important factor. For instance, it has been reported that rifaximin, an RNA synthesis inhibitor, worked more efficiently in treating diarrhea-producing *E. coli* in the intestine than in the colon due to the difference in the bile salt concentrations (111). We now provide evidence that FZ, an antibiotic prescribed for bacterial diarrhea (31, 40), acts synergistically with DOC in inhibiting the growth of enterobacteria, reducing the MIC of DOC from > 48 mM to 6 mM, which is within the range of bile salt concentrations in the intestine. It is possible that such synergy *in situ* may contribute to the treatment. Co-administration of FZ and DOC provides a promising tool to treat bacterial diarrhea, especially for patients with conditions such as malnourishment or disorders in enterohepatic circulation and intestinal absorption, all of which may result in low levels of intestinal bile salts (76). It should be noted that DOC alone does not represent the intestinal bile salt mixture and therefore application of DOC together with FZ may be necessary to enhance the synergy. LaRusso *et al.* (112) demonstrated that oral administration of DOC at 750 mg/day in healthy men did not result in any significant side effects even after 2 weeks of application, highlighting the possibility for oral uptake of DOC-FZ combination for bacterial diarrhea.

We have provided insights into the underlying mechanism of the synergy between DOC and FZ in their antibacterial action against *E. coli* as a model Gram-negative bacterium. We showed that disruption of *tolC* or *acrA* gene caused a considerable decrease in the

synergy between DOC and FZ in the corresponding mutants. The TolC protein, whose removal disrupts the synergy more strikingly, appears to be the key determinant of synergy.

The observed difference in the susceptibility to DOC/FZ combination between Δ*tolC* and Δ*acrA* mutants is in agreement with the fact that the TolC protein is shared by at least seven multidrug efflux pumps, while AcrA protein acts as the periplasmic connecting bridge for only two (113). Thus, deletion of *tolC* gene is expected to give rise to a more pronounced effect on the loss of efflux activities than deletion of *acrA* gene.

Of great interest is how FZ could influence the activity of efflux pumps. The findings of this work indicate that more than two efflux pumps (AcrAB-TolC and AcrAD-TolC systems) were affected by FZ. This observation is reminiscent of a common mechanism which could affect a wide range of efflux pumps simultaneously, namely proton motive force. It has been suggested that nitrofuran compounds during reductive activation might generate NO which subsequently inhibits the electron transport chain (ETC), diminishing the proton motive force across the cytoplasmic membrane (101, 102, 106). As a result, many efflux pumps would be de-energized, and become less efficient in extruding toxic compounds. However, NO generation from nitrofurans in bacterial cells remains to be speculative since the trace of NO has yet to be detected using either biochemical or NO-sensing fluorescence methods, possibly due to the detection limit of the used methods or rapid conversion of NO into other compounds (101, 102). In the present work, we provide evidence for the contribution of NO in the interaction between DOC and FZ via the observation that overexpression of NO-detoxifying enzyme Hmp decreased the synergistic interaction between the two agents. Since some DOC-FZ synergy was still retained after NO-detoxification, other mechanisms, including direct

inhibition of the ETC by activated FZ, might be involved in the efflux pump inhibition. Further experiments are warranted to examine the effect of FZ on the electron transport chain by monitoring changes in the two components of the proton motive force using various probes (e.g. tetramethyl rhodamine methyl ester for membrane electric potential and pHluorin for ΔpH) or by monitoring cellular O_2 consumption (114).

Notably, we showed that the DOC-FZ synergy does not depend on the presence of two *E. coli* nitroreductases NfsA and NfsB. This finding raises interesting questions about activation and action of nitrofurans. The retention of synergy in the absence of NfsA and NfsB implies that the inhibitory effect on the TolC-AcrAB efflux pump *via* NO is retained and, therefore, FZ probably undergoes reductive activation by alternative enzymes. The more plausible explanation of retained synergy and increased MIC is a less effective activation rather than the low activity of an unreduced form of FZ. To unearth alternative mechanisms of FZ that are independent of NfsA and NfsB, one possible strategy is to select for FZ-resistant mutants from the Δ*nfsA* Δ*nfsB* strain and employ a whole-genome analysis to identify responsible mutations that may point to alternative activation enzymes.

Conclusion

The current study reports the synergy between FZ and DOC in inhibiting and/or killing several enterobacterial species at concentrations that are demonstrated to be non-toxic in animal and human trials and within the range of intestinal bile salts concentrations. We provide genetic evidence that the efflux pumps play a major role in the FZ-DOC synergy, suggesting that the mechanism of synergy may be a 5-nitrofuran-mediated increase in accumulation of DOC inside the cell. In support of this model, we show that

the key enzyme which detoxifies NO, an FZ-activation product that inhibits ETC, also impairs the FZ-DOC synergy.

Methods

Bacterial strains, growth conditions and antibiotics

All bacterial strains and plasmids used in this study are described in Tables 1 and 2. The introduction of the *kan*^{R} gene deletion mutations into the wild type strain K1508 from the corresponding Keio collection *E. coli* K12 knock-out strains (115) was done using phage P1 transduction, using the standard procedures (116). To eliminate potential polar effects on downstream genes in the operon, the FRT-flanked *kan*^{R} cassette was then removed using FLP-mediated recombination as previously described (117). Plasmids derived from the pCA24N bearing the gene of interest were purified from *E. coli* strains of the ASKA collection containing ORF expression constructs derived from this organism (118) using the ChargeSwitch-Pro Plasmid Miniprep Kit (Thermo Fisher Scientific). The plasmid DNA was then chemically transformed into specific *E. coli* strains for further work (119). Expression from the pCA24N vector is driven from a T5-*lac* chimeric promoter. In the case of membrane protein expression (TolC and AcrA), the basal expression from an uninduced promoter was used in complementation experiments to avoid toxicity of membrane protein overexpression due to Sec system saturation. In contrast, expression of Hmp (a cytosolic NO-detoxifying protein) was induced by 1 mM IPTG.

Table 1: Bacterial strains used in this study

Name	Genotype or description	Source
Escherichia coli* O157 isolate *ERL034336	Human isolate	Dr. Ann Midwinter, School of Veterinary Sciences, Massey University, Palmerston North
***Escherichia coli* UPEC P50 isolate**	Isolate from a canine urinary tract infection	(120)
***Salmonella enterica* LT2**	Type strain, *S. enterica* subsp. *enterica*, serovar Typhimurium	ATCC® 43971™
***Citrobacter gillenii* PMR001**	Isolate from a municipal sewage processing (water purification) plant, Palmerston North, New Zealand (classified by complete 16S rRNA sequencing, 99% identity over 1405 nt to the 16S rRNA sequence of *Citrobacter gillenii* ATCC 51117).	Rakonjac laboratory, Massey University, unpublished.
***Klebsiella pneumoniae* PMR001**	Isolate from a municipal sewage processing (water purification) plant, Palmerston North, New Zealand (classified by complete 16S rRNA sequencing; 99% identity over 1404 nt to the 16S rRNA sequence of *Klebsiella pneumoniae* strain ATCC 13883).	Rakonjac laboratory, Massey University, unpublished
	***Escherichia coli* K12 laboratory strains**	
K1508	MC4100 [F^- *araD*$^-$ Δ*lac* U169 *relA*$^-$ *thiA rpsL* (Str^R)] Δ*lamB106*	(121)

K2403	K1508 Δ*tolC*	This study
K2424	K1508 Δ*acrA*	This study
K2425	K1508 Δ*acrA* pCA24N*::acrA* Δ*gfp*	This study
K2426	K1508 Δ*tolC* pCA24N*::tolC* Δ*gfp*	This study
K2483	K1508 Δ*nfsA* Δ*nfsB*	This study
K2524	K1508 pUC118 (Amp^R)	This study

Table 2: List of plasmids used in this study

Name	**Genotype or description**	**Source**
pCP20	Amp^R, Cm^R, FLP^+, 8 $cI857^+$, 8 p_R Rep^{ts} For removal of an *frt*-flanked *kan* marker from *E. coli* K12 strains by FLP-mediated site-specific recombination	(122)
pUC118	Amp^R, f1 *ori*, P_{lacUV5}, *lacZα*	Creative Biogene, Shirley, NY, USA
pCA24N -*tolC*	Cm^R; $lacI^q$, pCA24N $P_{T5\text{-}lac}$::*tolC* Δ*gfp*	(118)
pCA24N -*acrA*	Cm^R; $lacI^q$, pCA24N $P_{T5\text{-}lac}$::*acrA* Δ*gfp*	(118)
pCA24N -*hmp*	Cm^R; $lacI^q$, pCA24N $P_{T5\text{-}lac}$::*hmp* Δ*gfp*	(118)

Bacterial cultures were grown in 2xYT medium (BD Difco) at 37 °C with shaking at 200 rpm. For preparation of exponential phase cells, fresh overnight culture was diluted 100-fold and incubated to reach an OD_{600nm} of about 0.1-0.3. This cell suspension was then diluted to the desirable concentration depending on the specific purpose of the

experiment. Sodium deoxycholate was a kind gift from New Zealand Pharmaceuticals Ltd. Antibiotics used in this study were purchased from GoldBio. CM4 was purchased from Enamine (catalog number Z49681516).

Checkerboard assay

The checkerboard assay for DOC and FZ was carried out in Corning 384-well microtiter plates with a DOC concentration ranging from 0 to 20000 µg/mL and a FZ concentration ranging from 0 to 10 µg/mL, prepared by 2-fold serial dilution. The concentrations were adjusted depending on the sensitivity of different bacterial strains and the types of nitrofurans to cover at least 2 × MIC to 0.06 × MIC for each drug. Each well contained the starting inoculum of approximately 10^6 CFU/mL, 2 % DMSO and a predefined concentration of each drug in the total volume of 50 µL. The wells containing no drugs and 10 µg/mL tetracycline were used as negative and positive controls, respectively. After dispensing the reagents, the plate was pulse centrifuged at 1000 × g to eliminate any bubbles before being incubated at 30 °C and the OD_{600nm} of the sample was monitored hourly for 24 h using a Multiskan™ GO Microplate Spectrophotometer (Thermo Scientific). Each combination was performed in triplicate. The mean growth inhibition of the triplicate experiments with the cut-off value of 90 % at the time point 24 h was used to define the MIC of the drug used either alone or in combination (123). The fractional inhibitory concentration index (FICI) for the two drugs was calculated as follows:

$$\mathrm{FICI} = \frac{\mathrm{MIC_{DOCcom}}}{\mathrm{MIC_{DOCalone}}} + \frac{\mathrm{MIC_{FZcom}}}{\mathrm{MIC_{FZalone}}}$$

MIC_{DOCcom} and MIC_{FZcom} :MIC of DOC and FZ when tested in combination

$MIC_{DOCalone}$ and $MIC_{FZalone}$: MIC of DOC and FZ when tested individually

The interaction between two drugs was interpreted as synergistic if FICI was ≤ 0.5, indifferent if it was > 0.5 and ≤ 4, and antagonistic if it was > 4 (15). The 50 % growth inhibition was used as the cut-off value to calculate FICI in some cases when stated.

Time-kill assay

Exponential phase bacterial culture at about 10^6 CFU/mL was prepared in the final volume of 10 mL containing 2 % DMSO plus DOC at 2500 µg/mL alone or FZ at 0.5 × MIC µg/mL alone or both drugs. The treatments containing no drug were used as negative controls. The samples were incubated at 30°C with shaking at 200 rpm. At the time points of 0 h, 2 h, 4 h, 6 h, 8 h and 24 h, 500 µL were taken from each treatment and centrifuged at 10000 × g for 15 min before being re-suspended in 100 µL maximum recovery diluent (0.1 % peptone, 0.85 % NaCl). 10 µL of 10-fold serial dilutions was plated on 2xYT agar followed by overnight incubation at 37 °C to determine the cell count. Each treatment was performed in triplicate. The antimicrobial interaction was interpreted as synergistic if the combinatorial treatment caused a killing efficiency ≥2 log higher than the most active agent (19).

Declarations

Ethics approval and consent to participate

Not applicable

Consent for publication

Not applicable

Availability of data and materials

All data generated or analyzed during this study are included in this published article and its supplementary information file. The 16S rDNA sequences of the isolates

Citrobacter gillenni PMR001 and *Klebsiella pneumoniae* PMR001 have been deposited at GenBank under the accession numbers MN515064 and MN515061, respectively.

Competing interest

The authors declare that they have no competing interests.

Funding

Vuong Van Hung Le has received funding from Callaghan Innovation PhD Scholarship. This work was supported by Massey University, the New Zealand Ministry of Business, Innovation and Employment and New Zealand Pharmaceuticals Ltd.

Authors' contributions

JR and VL conceived the study; ID and CO participated in the experimental design. VL and CO acquired and analyzed the study data, JS and JR identified the nitrofuran-DOC synergy and CM4. Manuscript was written by VL with contribution from CO and edited by JR. All authors have read and approved the manuscript.

Acknowledgements

We thank Dr. Anne Midwinter, School of Veterinary Sciences, Massey University, for providing an *E. coli* human O157 isolate and New Zealand Veterinary Pathology Ltd. for an isolate of a canine *E. coli* uropathogenic strain (P50). We are grateful to Fraser Glickman from the Rockefeller University High Throughput and Spectroscopy Resource Center for hosting and advice on the small-molecule drug screen of a synergy screen and to the National BioResource Project (NBRP), Genetics Strains Research Center, National Institute of Genetics, Japan, for providing the ASKA collection. The Keio Collection was purchased from Dharmacon *via* ThermoFisher (Australia). Carel Jobsis is acknowledged for excellent technical assistance.

Supplemental data: Additional file 1

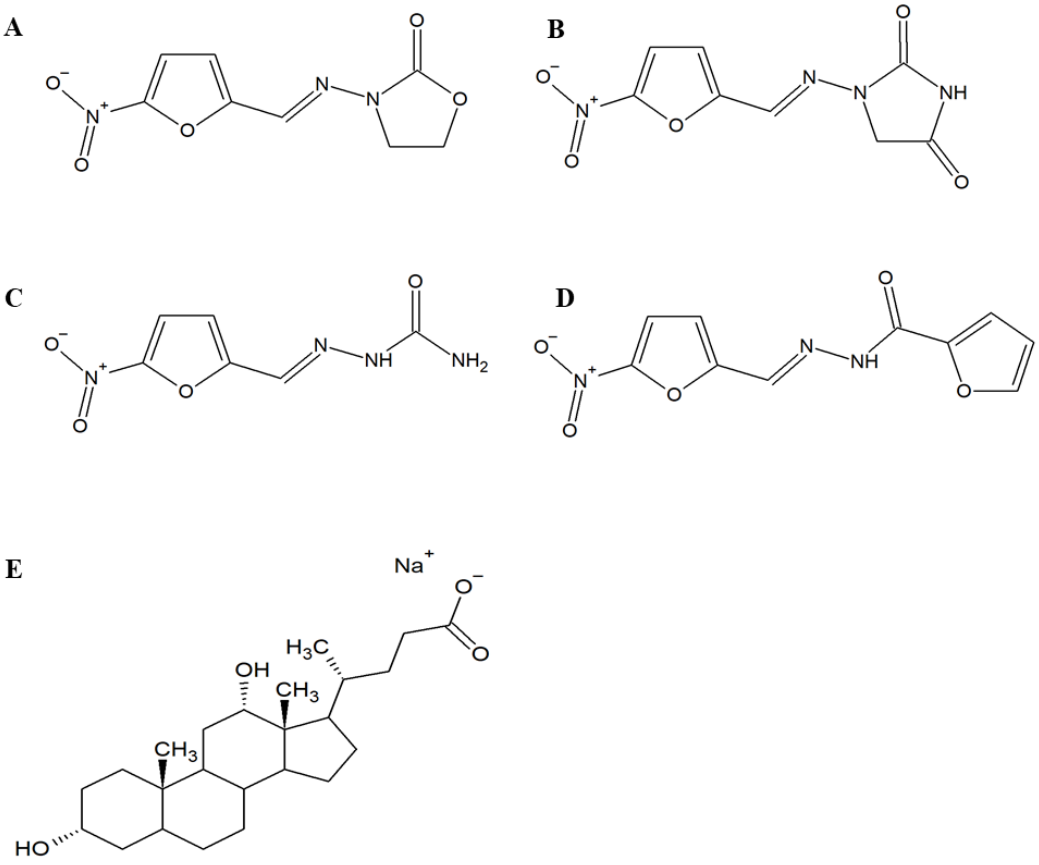

Figure S1: Structural formulae of nitrofurans and sodium deoxycholate (E). A) Furazolidone (FZ); B) Nitrofurantoin (NIT); C) Nitrofurazone (NFZ). D) CM4, Pubchem ID AC1LGLMG (no CAS number). Chemical name: N'-[(5-nitrofuran-2-yl)methylidene]furan-2-carbohydrazide or N-[(5-nitrofuran-2-yl)methylideneamino]furan-2-carboxamide.

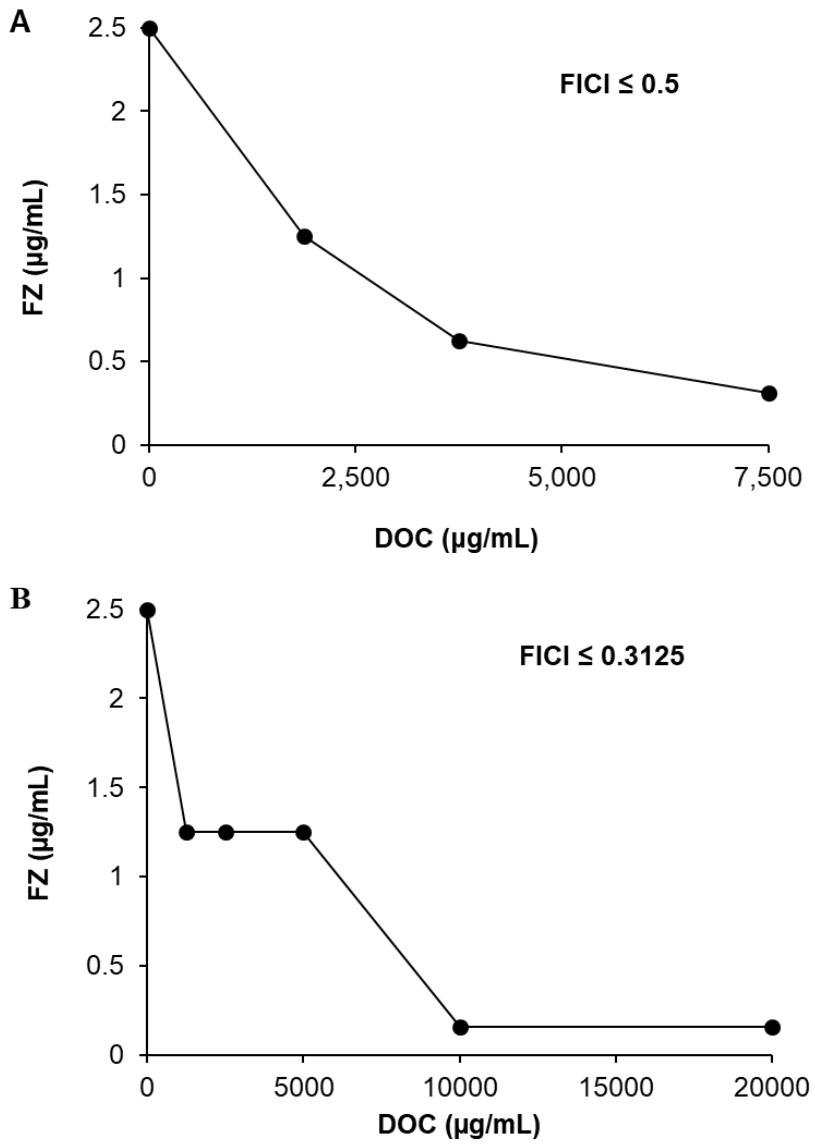

Figure S2: FZ interaction with DOC in growth inhibition of *E. coli* strain O157 (A) and canine uropathogenic *E. coli* P50 (B). Graphs (isobolograms) were obtained using a checkerboard analysis at multiple concentration of molecules. Each data point represents the minimum molecule concentrations alone or in combination causing 90 % inhibition of bacterial growth relative to an unchallenged control culture.

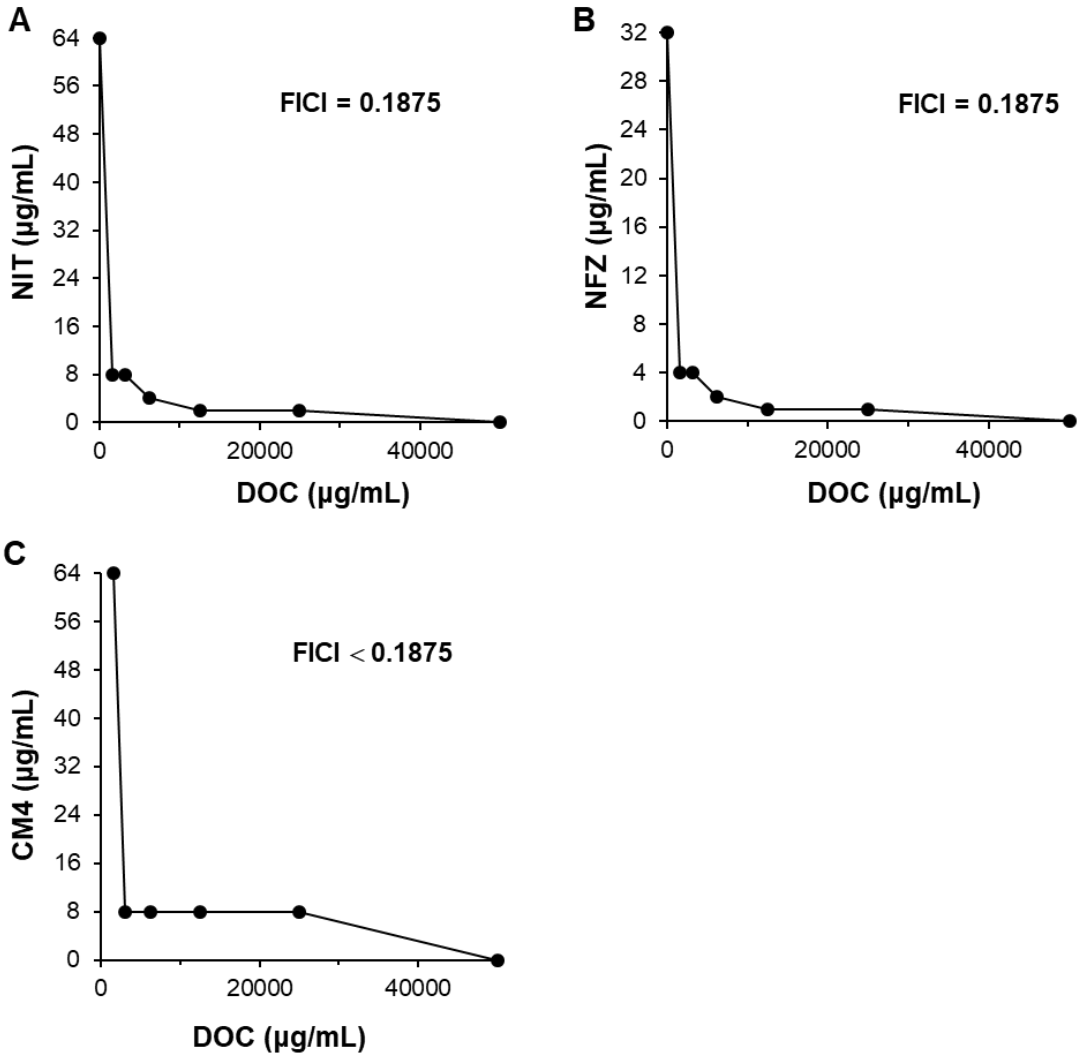

Figure S3: Interactions of three nitrofurans (NIT, NFZ and CM4) with DOC in growth inhibition of *Citrobacter gillenii* PMR001. Graphs (isobolograms) were obtained using a checkerboard analysis at multiple concentration of molecules. Each data point represents the minimum molecule concentrations alone or in combination causing 90 % inhibition of bacterial growth relative to an unchallenged control culture.

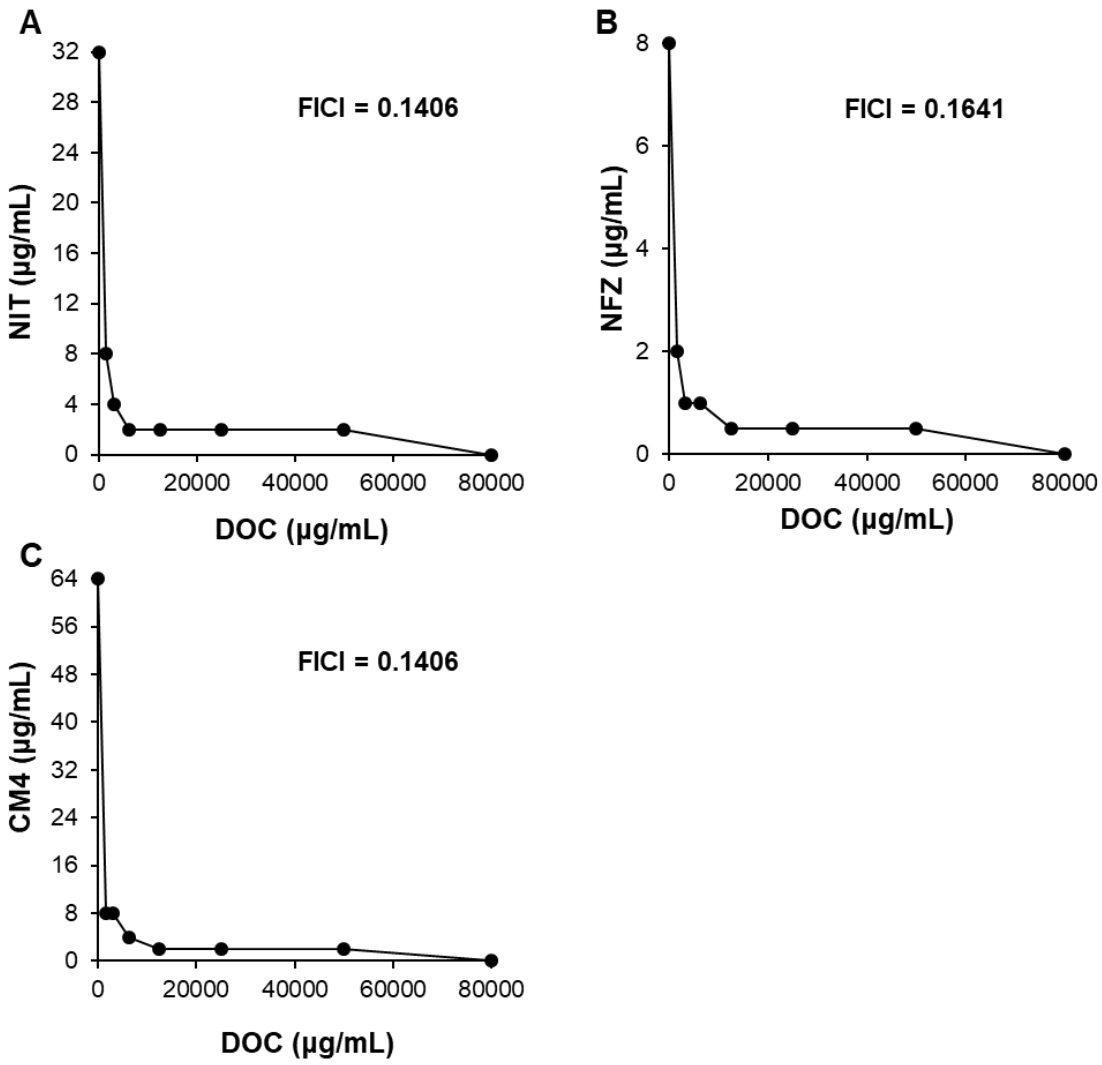

Figure S4: Interactions of three nitrofurans (NIT, NFZ and CM4) with DOC in growth inhibition of *Salmonella enterica* sv. Typhimurium LT2. Graphs (isobolograms) were obtained using a checkerboard analysis at multiple concentration of molecules. Each data point represents the minimum molecule concentrations alone or in combination causing 90 % inhibition of bacterial growth relative to an unchallenged control culture.

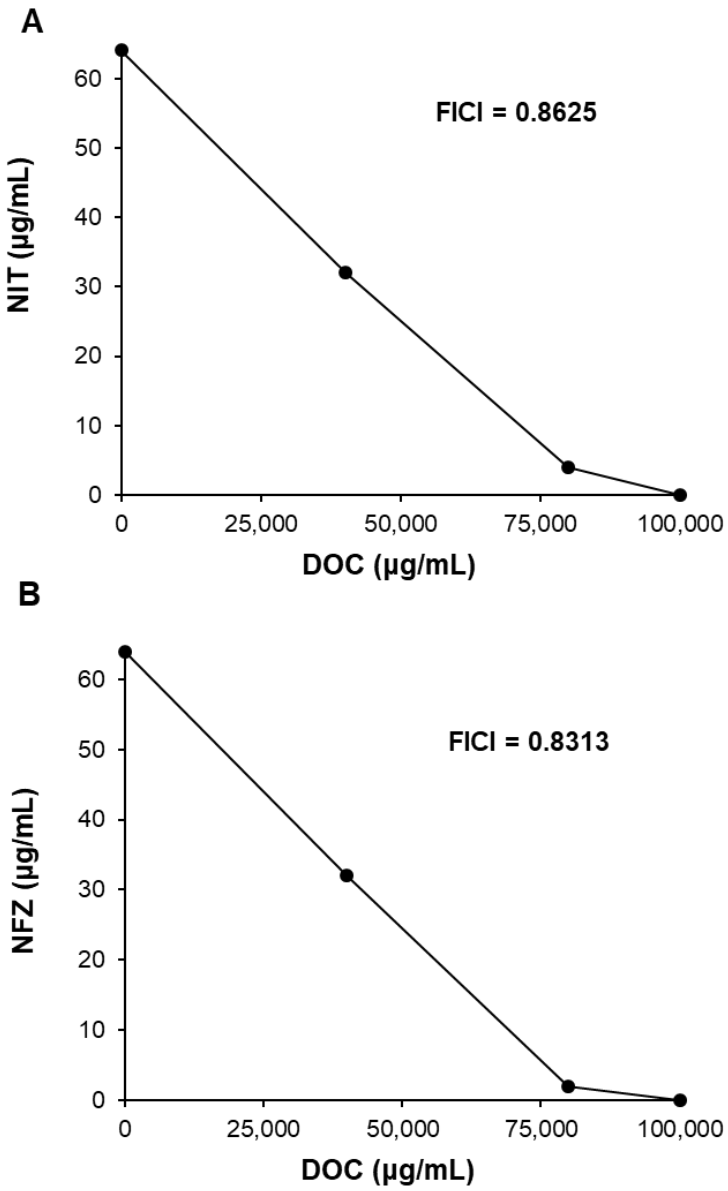

Figure S5: Interactions of two nitrofurans (NIT and NFZ) with DOC in growth inhibition of *Klebsiella pneumoniae* PMR001. Graphs (isobolograms) were obtained using a checkerboard analysis at multiple concentration of molecules. Each data point represents the minimum molecule concentrations alone or in combination causing 90 % inhibition of bacterial growth relative to an unchallenged control culture.

Chapter III:

Novel 5-nitrofuran-activating reductase in *Escherichia coli*

Vuong Van Hung Le[a], Ieuan Davies[b], Christina D. Moon[c], David Wheeler[a]*, Patrick J. Biggs[a,d] and Jasna Rakonjac[a]#

[a] School of Fundamental Sciences, Massey University, Palmerston North, New Zealand

[b] New Zealand Pharmaceuticals Ltd., Palmerston North, New Zealand

[c] AgResearch Limited, Grasslands Research Centre, Palmerston North, New Zealand

[d m]EpiLab, Infectious Disease Research Centre, School of Veterinary Science, Massey University, Palmerston North, New Zealand

*Present address: NSW Department of Primary Industries, Orange, Australia

#Corresponding author:

Jasna Rakonjac, School of Fundamental Sciences, Massey University, Palmerston North, New Zealand

Email**:** **j.rakonjac@massey.ac.nz**

Tel. +64 6 350 5134; Fax +64 6 350 5688

Abstract

The global spread of multidrug resistant enterobacteria warrants new strategies to combat these pathogens. One possible approach is reconsideration of "old" antimicrobials which remain effective after decades of use. Synthetic 5-nitrofurans such as furazolidone, nitrofurantoin and nitrofurazone, are such a class of antimicrobial drugs. Recent epidemiological data reported a very low prevalence of resistance to this antimicrobial class amongst clinical *Escherichia coli* isolates in various parts of the world, forecasting the increasing importance of its uses to battle antibiotic resistant enterobacteria. However, although they have had a long history of clinical use, a detailed understanding of the 5-nitrofurans' mechanisms of action remains limited. Nitrofurans are known as prodrugs that are activated in *E. coli* by reduction catalyzed by two redundant nitroreductases, NfsA and NfsB. Furazolidone, nevertheless, retains relatively significant antibacterial activity in the nitroreductase-deficient Δ*nfsA* Δ*nfsB E. coli* strain, indicating the presence of additional activating enzymes and/or the antibacterial activity of the unreduced form. Using genome sequencing, genetic, biochemical and bioinformatic approaches, we discovered a novel 5-nitrofuran-activating enzyme, AhpF, in *E. coli*. Discovery of a new nitrofuran-reducing enzyme opens new avenues for overcoming 5-nitrofuran resistance, such as designing nitrofuran analogues with higher affinity for AhpF or screening for adjuvants that enhance AhpF expression.

Introduction

Widespread global emergence of multidrug resistant enterobacteria warrants novel strategies to combat these pathogens (124, 125). One of promising approaches is reconsideration of "old" antimicrobials which remain effective after decades of use. Synthetic 5-nitrofurans are such a class of antimicrobial drugs (Fig. 1). Typical examples of this group are furazolidone (FZ) used for treating bacterial diarrhea, giardiasis (40) and as a component in combinatorial therapy for *Helicobacter pylori* infections (26), nitrofurantoin (NIT) for urinary tract infections and nitrofurazone (NFZ) for skin infections (40). Recent epidemiological data illustrated that the prevalence of resistance to 5-nitrofurans amongst clinical *Escherichia coli* isolates is maintained at very low levels in various parts of the world, including Peru (30, 53), Mexico (54) , the United Kingdom (55), Denmark (56), Germany (57), France (58), Iran (59) and China (60) to name a few, heralding the increasing importance of 5-nitrofurans to combat antibiotic resistant enterobacteria.

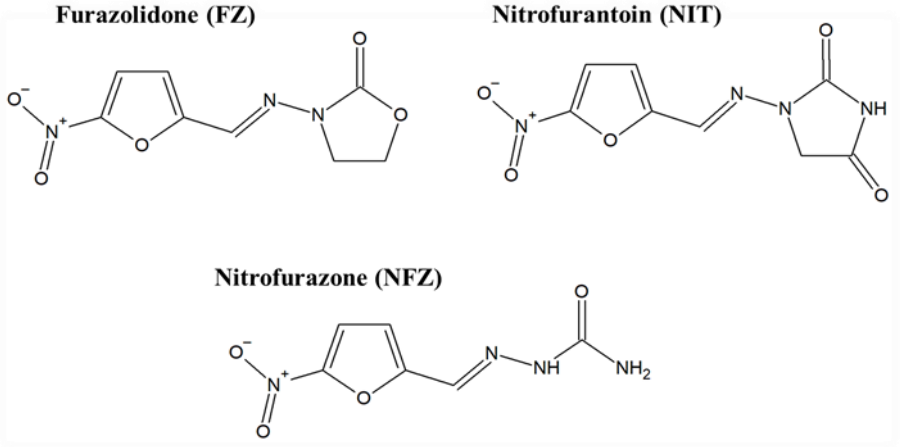

Figure 1: Molecular structure of the 5-nitrofuran antimicrobial agents.

Though the 5-nitrofuran agents have had a long history of clinical use since their introduction in the 1940s and 1950s (38), knowledge about their mode of action is far from complete. Taking *E. coli* as a model organism, 5-nitrofurans are prodrugs that require reductive activation mediated by two type I oxygen-insensitive nitroreductases, NfsA and NfsB, in a redundant manner to exert their antibacterial effects (31, 61-63). The minor nitroreductase NfsB is a 24 kDa flavoprotein which catalyzes reduction of 5-nitrofuran pro-drugs into nitroso and hydroxylamino-substituted products using both NADH and NADPH as reducing equivalents (64, 66). The transfer of electrons from NAD(P)H to 5-nitrofuran catalyzed by NfsB occurs *via* a ping-pong bi-bi mechanism, where the electron donor (NADPH or NADH) reduces the FMN cofactor of the NfsB enzyme (ping) which in turn reduces the 5-nitrofuran substrate (pong). Overall, two reactants, NAD(P)H and 5-nitrofuran, give rise to two products, $NAD(P)^+$ and the nitroso derivative (two-two or bi-bi). The flavoprotein NfsA (27 kDa) is NADPH-dependent and has a dominant role in activating 5-nitrofuran drugs in *E. coli*, sharing the same ping-pong bi-bi mechanism of reduction as NfsB (65). The final product of NfsA-catalyzed reduction, however, remains uncharacterized. It is still uncertain what reactive intermediates of 5-nitrofuran activation by NfsA or NfsB are responsible for the antibacterial effects observed and what their cellular targets are. Diverse effects have been reported, that include triggering DNA lesions, inducing oxidative stress and inhibiting the biosynthesis of RNAs and proteins (69-73). However, it is unknown whether these macromolecules (DNA, RNA and proteins) are directly modified by the reactive intermediates derived from 5-nitrofurans, or whether the cellular machinery that carries out replication, transcription and translation are the primary targets.

Oxygen-sensitive nitroreductase activity (or type II) was also detected in *E. coli* extracts using biochemical assays in 1979 (74). This latter activity involves the one-electron

reduction of the 5-nitrofuran drug intro a nitro anion free radical, which is oxidized back into the initial prodrug by oxygen, with the concomitant generation of superoxide. However, the gene(s) responsible for this activity and the extent of the contribution by this pathway to 5-nitrofuran activation has not been identified.

FZ retains a relatively significant antibacterial activity in the nitroreductase-deficient Δ*nfsA* Δ*nfsB* *E. coli* strain, indicating the presence of additional activating enzymes and/or antibacterial activity of the unreduced FZ. Using genome sequencing, genetic, biochemical and bioinformatic approaches, we identified a new enzyme in *E. coli*, AhpF, that plays a role in activating FZ and two closely related drugs, NIT and NFZ.

Results

Mutations in *ahpF* associated with enhanced FZ resistance

Guided by the observation that FZ retained relatively significant antibacterial activity in the Δ*nfsA* Δ*nfsB* nitroreductase-deficient *E. coli* K-12 strain, we hypothesized that there are alternative activation enzyme(s) present in *E. coli* and/or that the unreduced form of FZ has *E. coli*-inhibitory properties. To examine these hypotheses, fifteen independent *E. coli* spontaneous mutants were selected from the Δ*nfsA* Δ*nfsB* nitroreductase-deficient strain at the FZ concentration (40 µg/mL) that kills the parental strain. It is worth noting that amongst the three FZ concentrations we used for selecting resistant mutants (40, 48 and 56 µg/mL), no colonies were observed on the plates containing 48 or 56 µg/mL even after 48 h of incubation. The mutation rate in the Δ*nfsA* Δ*nfsB* cultures to form colonies on FZ-selective agar plates (40 µg/mL) was calculated to be 8.93×10^{-9} per cell per generation (95 % confidence interval: 6.51×10^{-9} – 1.17×10^{-8}).

All the *E. coli* mutants had the same MIC_{FZ} of 20 µg/mL, which was higher than that of the parental strain (16 µg/mL) in an agar dilution assay. Genomic DNA of the FZ-resistant mutants was extracted and sequenced using the Illumina MiSeq platform as described in the experimental procedures. Comparative genome sequence analyses identified changes in a single gene *ahpF* in all the mutants. The changes in *ahpF* included 13 different mutations (Table 1, Fig. 2). The *ahpF* mutations in these FZ^R mutants were further confirmed by analyzing the size and sequence of *ahpF*-specific PCR products (Fig. S1).

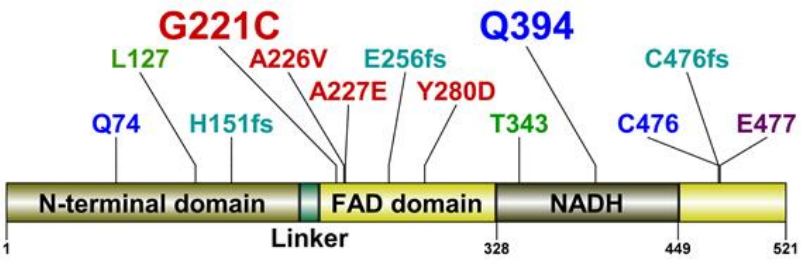

Figure 2: Mutations in the AhpF protein in FZ-resistant mutants. The AhpF protein consists of four regions: The N-terminal domain (1-196), a linker (197-209), the FAD binding domain (210-327 and 450-521) and the NADH binding domain (328-449). The types of mutations are described by colors: red, missense mutation; blue, nonsense mutation; green, IS*1* insertion; aqua, frameshift; purple, in-frame deletion of six codons. The frequency of mutations is described by the size of the annotations: small, 1; large, 2.

Table 1: List of *ahpF* variants found in the *E. coli* mutants having increased FZ resistance

Mutants	Location of the mutation	Predicted mutational change
FZ08[a]	1426_1432delTGCGAAA	Frameshift downstream of Cys476
FZ10[a]	C1180T	Stop gained Gln394 → stop codon
FZ11[a]	IS*1* insertion after the 1029th nucleotide	Loss-of-function
FZ12[a]	C680A	Missense Ala227Glu
FZ13[a]	1430_1447delAAACCAACGTGAAAG GCG	In-frame deletion Glu477_Gly482del
FZ14[a]	451delC	Frameshift downstream of His151
FZ15[a]	766delG	Frameshift downstream of Glu256
FZ16[a]	G661T	Missense Gly221Cys
FZ17[a]	T838G	Missense Tyr280Asp
FZ18[a]	C1428A	Stop gained Cys476 → stop codon
FZ19[b]	IS*1* insertion after the 380th nucleotide	Loss-of-function
FZ20[b]	C220T	Stop gained Gln74 → stop codon
FZ21[b]	C677T	Missense Ala226Val
FZ22[b]	C1180T	Stop gained Gln394 → stop codon
FZ23[b]	G661T	Missense Gly221Cys

[a)] Mutations were determined using the whole genome sequencing and *ahpF*-specific Sanger sequencing.

[b)] Mutations were determined using Sanger sequencing of *ahpF* gene only.

Given that all the mutants had the same MIC_{FZ} and some carried major interruptions to the coding sequence (an IS*1* insertion in mutants FZ11 and FZ19, nonsense mutation in FZ10 and FZ22, and frameshift mutations in FZ14 and FZ15), all the *ahpF* mutations reported in this study were expected to result in a dysfunctional AhpF protein. This inference is also supported by the fact that the mutated residues (Gly221, Ala226, Ala227, Tyr280) are highly conserved among the AhpF homologues according to analyses of evolutionary conservation using two software packages, Consurf (126) and SIFT (127) (Fig. S2). Notably, the SIFT software takes into consideration the physical properties of amino acid residues in homologous sequence analyses, to predict the impact of an amino acid substitution on the protein function, either tolerated or deleterious (128). In this case, all the four mutations (Gly221Cys, Ala226Val, Ala227Glu and Tyr280Asp) were predicted by SIFT to be deleterious to the AhpF function with high confidence.

To confirm that a loss of AhpF function was the cause of increased resistance to FZ, a Δ*ahpF* mutation was introduced into the parental Δ*nfsA* Δ*nfsB* strain by P1 transduction (116), using the Keio strain JW0599 as a donor, followed by removal of the Km cassette as described in the experimental procedures, to obtain a triple Δ*nfsA* Δ*nfsB* Δ*ahpF* mutant. The FZ sensitivity was examined using the broth microdilution and agar dilution assays. In agreement with the findings from the genomic analyses of the spontaneous FZ-resistant mutants, deletion of *ahpF* in the Δ*nfsA* Δ*nfsB* background led to an increase in the FZ MICs in both assays from 16 µg/mL for the parental strain to 28 µg/mL for the Δ*nfsA* Δ*nfsB* Δ*ahpF* strain in the agar plate assay, and from 32 µg/mL to 48 µg/mL in the liquid assay (Fig. 3). Complementation of the Δ*ahpF* mutation by expression of *ahpF* from a high-copy-number plasmid pCA24N::*ahpF* induced by IPTG

in the Δ*nfsA* Δ*nfsB* Δ*ahpF* strain not only restored FZ sensitivity, but also increased it dramatically beyond the level of the Δ*nfsA* Δ*nfsB* strain and close to the level of the FZ sensitive wild-type strain (*nfsA*$^{+}$ *nfsB*$^{+}$) (Fig. 3). Taken together, these findings show that AhpF plays a role in FZ activation in which FZ sensitivity is positively correlated with the amount of *ahpF* in the cell.

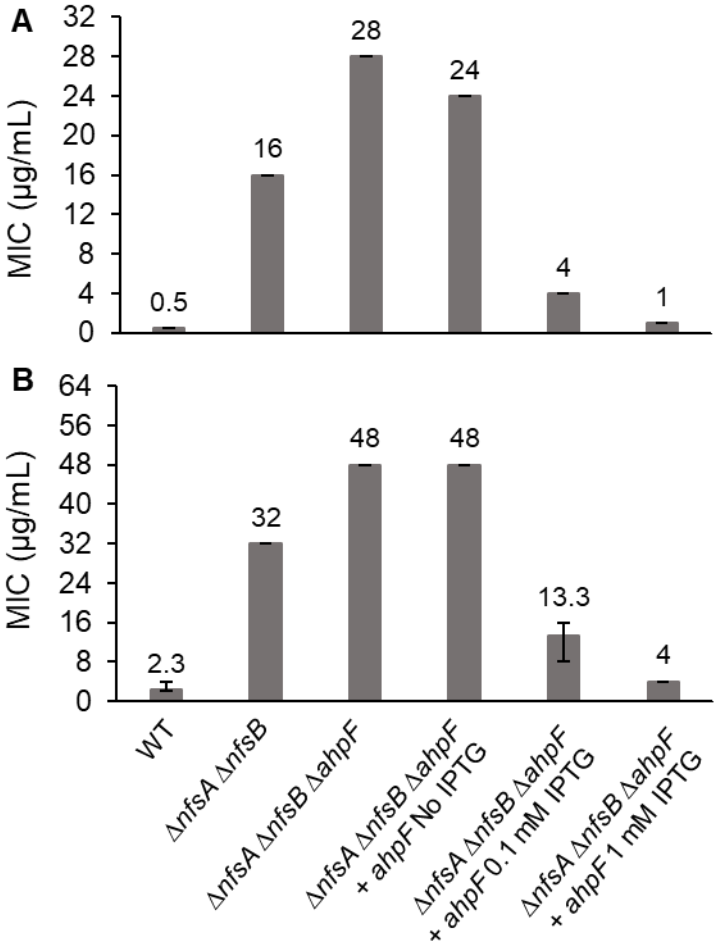

Figure 3: Confirmation of the AhpF role in FZ activation using knock-out mutants and complementation. The FZ susceptibility of Δ*ahpF* mutant in the *nfsAB* null background and AhpF-overexpressing strain using agar dilution assay (A) and broth microdilution assay (B). The *E. coli* K-12 strain BW25113 was used as the wild-type strain. Expression of the *ahpF* gene was induced from a chimeric T5-*lac* promoter of a high-copy-number plasmid pCA24N::*ahpF* by 0.1 mM or 1mM IPTG. MIC was defined as the minimal FZ concentration that inhibited the visible colony formation in an agar dilution assay (A), or that caused 90 % growth inhibition in a broth microdilution assay (B). The MIC values and error bars represent the mean and range of at least three independent experiments.

Effect of *ahpF* on susceptibility of *E. coli* to NIT and NFZ

To examine the cross-resistance of *ahpF* deletion in the nitroreductase-deficient strain (Δ*nfsA* Δ*nfsB*) to NIT and NFZ, a broth microdilution assay was performed for these two 5-nitrofuran antibacterials. It is interesting to note that deletion of *ahpF* conferred a modest increase in sensitivity to NIT and NFZ (Fig. 4). That effect was reverted when the AhpF deficiency in the Δ*nfsA* Δ*nfsB* Δ*ahpF* triple mutant was complemented by a low level of AhpF expression from the pCA24N::*ahpF* plasmid (in the absence of IPTG). Nonetheless, AhpF overexpression upon IPTG induction (0.1 mM or 1 mM) in the Δ*nfsA* Δ*nfsB* Δ*ahpF* triple mutant lowered the MIC_{NIT} and MIC_{NFZ} of the complemented strain to the level of the wild-type (*nfsA*$^+$ *nfsB*$^+$ *ahpF*$^+$) strain where all nitrofuran-activating nitroreductases are present (Fig. 4). Taken together, all these observations strongly suggest that AhpF catalyzes activation of not only FZ, but also NIT and NFZ.

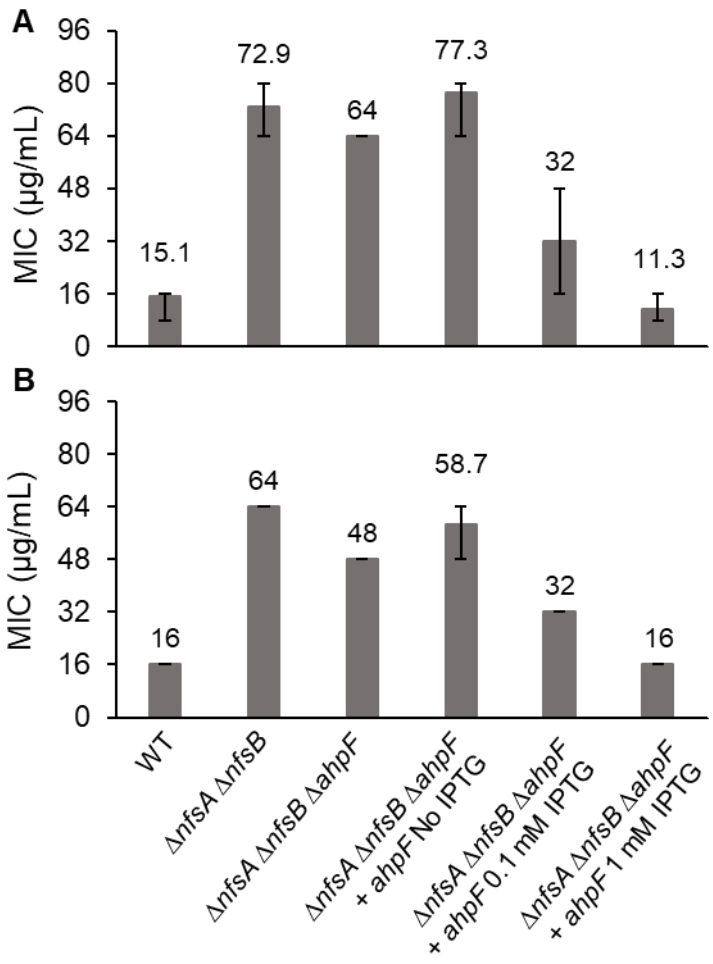

Figure 4: Confirmation of the AhpF role in nitrofurantoin and nitrofurazone activation using knock-out mutants and complementation. Susceptibility to nitrofurantoin (A) and nitrofurazone (B) of Δ*ahpF* mutant in the *nfsAB* null background and AhpF-overexpressing strain using a broth microdilution assay. Expression of the *ahpF* gene was induced from a chimeric T5-*lac* promoter of a high-copy-number plasmid pCA24N::*ahpF* by 0.1 mM or 1mM IPTG. The *E. coli* K-12 strain BW25113 was used as the wild-type strain. MIC was defined as the minimal drug concentration that caused 90 % growth inhibition. The MIC values and error bars represent the mean and range of at least three independent experiments.

We also determined the MICs for the *ahpF* deletion and complemented strains under anaerobic conditions and found a similar pattern in MIC changes for all three 5-nitrofuran drugs (Fig. 5) as under the aerobic conditions. The only exception was NFZ, for which the Δ*nfsA* Δ*nfsB* Δ*ahpF* triple mutant had a mildly increased MIC_{NFZ} in

comparison to the Δ*nfsA* Δ*nfsB* double mutant parent, opposite to the observation under aerobic conditions (Fig. 5C vs. 4B).

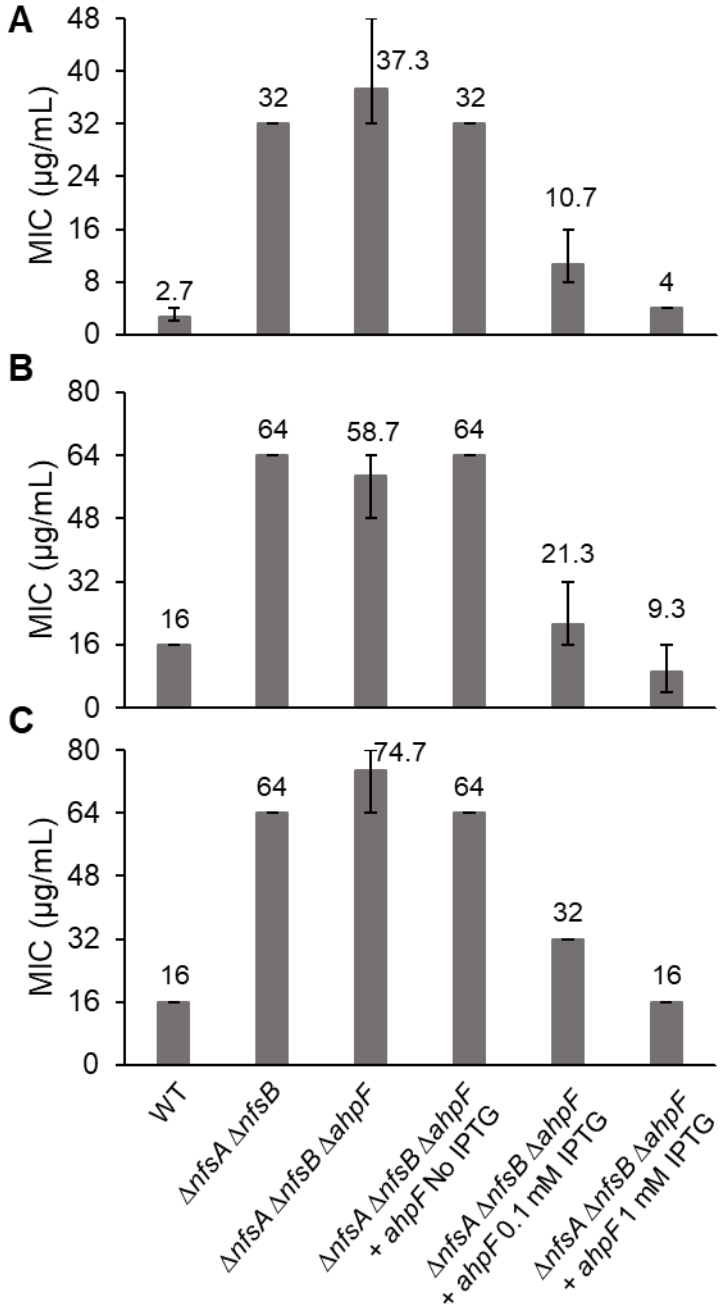

Figure 5: Susceptibility to 5-nitrofurans using a broth microdilution assay under anaerobic conditions. (A) Furazolidone, (B) Nitrofurantoin and (C) Nitrofurazone. Expression of the *ahpF* gene was induced from a chimeric T5-*lac* promoter of a high-copy-number plasmid pCA24N::*ahpF* by 0.1 mM or 1mM IPTG. The *E. coli* K-12 strain BW25113 was used as the wild-type strain. MIC was defined as the minimal drug concentration that caused 90 % growth inhibition. The MIC values and error bars represent the mean and range of at least three independent experiments.

In vitro activity of AhpF

To verify the ability of AhpF protein to catalyze the reduction of 5-nitrofurans (FZ, NIT and NFZ), His-tagged AhpF protein was produced, purified and assayed in a reaction using 5-nitrofuran and NADH as reactants. The protein was expressed in the Δ*ahpC E.*

coli strain from a high-copy number ASKA plasmid, pCA24N::*ahpF* (118). The rationale for *ahpC* deletion in the expression host was to prevent the co-purification of AhpC along with AhpF since these two proteins have been shown to form the multimeric complex $AhpC_{10}AhpF_2$ (129). The presence of AhpC in the protein extract might titer out the AhpF protein, precluding its hypothesized nitrofuran reductase activity.

The nitroreductase assay (Fig. 6) was performed in the presence of 5 µg/mL of Ni-NTA affinity-purified AhpF protein, NADH and one of the three 5-nitrofurans (FZ, NIT, NFZ) at an equal amount (0.1 mM). The absorbance at 400 nm was used to solely monitor the decrease in the concentration of 5-nitrofurans, whereas the absorbance at 340 nm (maximum for NADH) was used to monitor the decrease in the concentration of NADH and 5-nitrofurans simultaneously, given that these two substrates have an overlapping absorbance at this wavelength, and there was no suitable wavelength where NADH could be exclusively detected. It should be noted that oxidation of NADH in the reactions without any 5-nitrofuran drugs was used as a reference to indicate electron transfer from NADH to the three redox centers of AhpF (the FAD cofactor and two disulfide bridge active centers) (130) and ultimately oxygen, due to the oxidase activity of this enzyme (131). In the presence of FZ, NIT or NFZ, the initial reaction velocity monitored *via* the decrease in the absorbance at 340 nm (0.01533, 0.01314, 0.01526 A.U./min, respectively) was significantly higher than that in the sample without 5-nitrofurans (0.00422 A.U./min; $p < 0.001$; Fig. 6A). Continuous monitoring of the reaction over 12 hours showed that the absorbance at 340 nm (measure of NADH oxidation) in nitrofuran-containing samples stopped decreasing after 1.5 hours, whereas the absorbance in nitrofuran-free samples continued to decrease throughout the time period of the assay (Fig. 6A). Spectral analysis at the end-point of the experiment (12 h)

showed that the residual absorbance at 340 nm in all samples was coming exclusively from the 5-nitrofurans (Fig S3A, C, E). This indicates that NADH was used up more rapidly in the presence of 5-nitrofurans. By subtracting contribution of 5-nitrofurans from the absorbance at 340 nm, we calculated that the initial rate of NADH oxidation was 3.64, 2.74 and 2.43 μM/min for the reactions containing FZ, NIT and NFZ respectively, as compared with that of the no-drug reference control that was 1.08 μM/min.

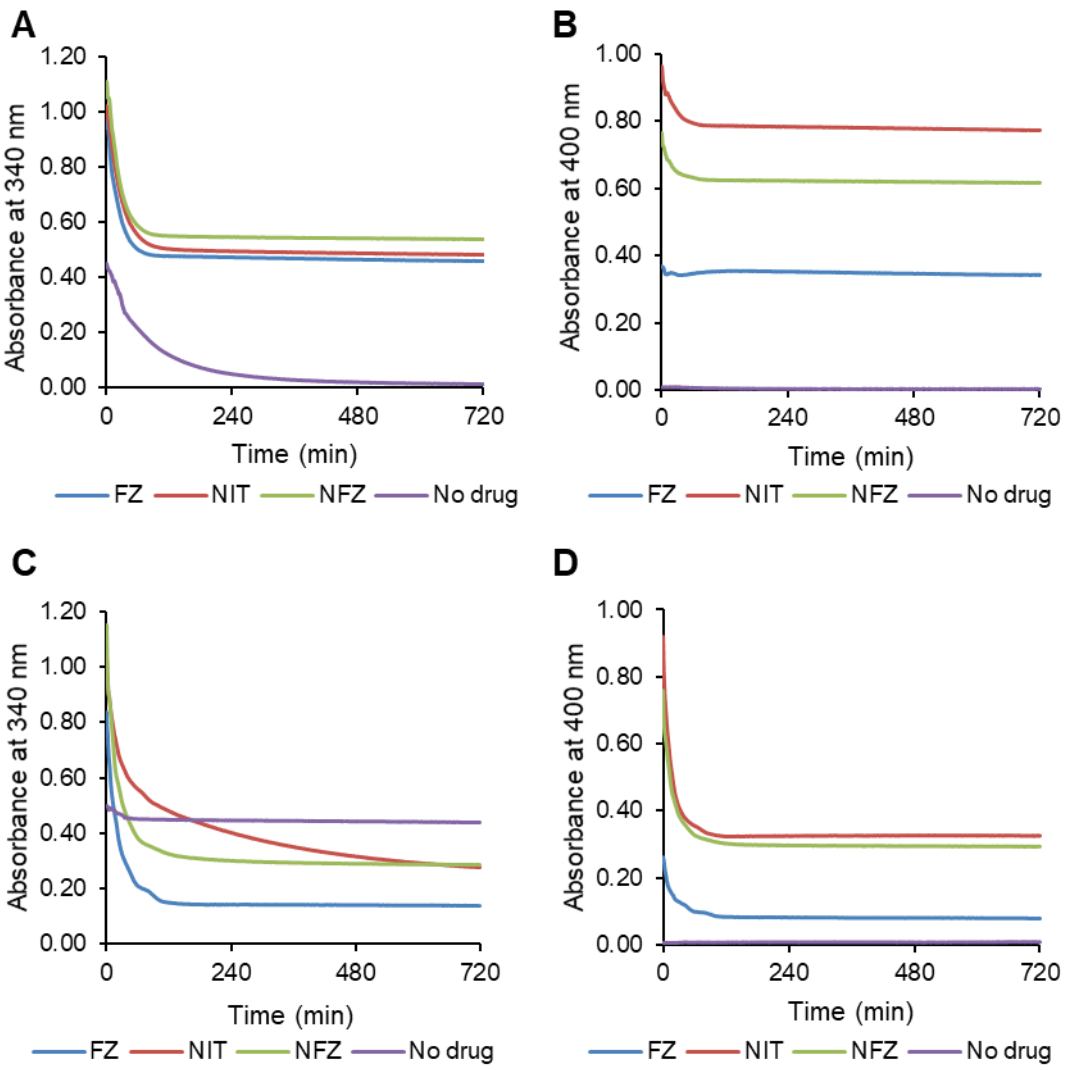

Figure 6: *In vitro* AhpF vs NfsB nitroreductase assay under aerobic conditions. Purified His-tagged AhpF 5 µg/mL (A & B) or NfsB 1 µg/mL (C & D) was combined with furazolidone (FZ), nitrofurantoin (NIT) or nitrofurazone (NFZ) in the presence of NADH as the reducing cofactor. A reaction without 5-nitrofurans was included as a reference (denoted as a no-drug control) to monitor change of the absorbance at 340 nm due to oxidation of the cofactor NADH by the oxidase activity of AhpF. Each data point represents the mean value of the triplicate measurements.

Notably, the absorbance at 400 nm (monitoring 5-nitrofurans) appeared to be unchanged for FZ and decreased modestly for NIT and NFZ (~16 % and 15 %, respectively) even after 12 h (Fig 6B and Figure S3A, C, E). This is in contrast with the 5-nitrofuran reduction reaction catalyzed by the well-established nitroreductase NfsB in which,

under the same conditions and substrate stoichiometry (1:1), more than half of the initial 5-nitrofuran had been reduced (Fig 6D and Figure S3B, D, F).

To eliminate the oxygen that seems to serve as an electron sink in the AhpF-catalyzed reaction, we repeated the nitroreductase assay under strict anaerobic conditions. The absorbance spectrum from 300 to 600 nm of the reaction mixtures and controls was examined at the end of the assay, after 21 h of incubation at 25 °C. Under these conditions, the absorbance between control reactions that contained NADH/AhpF and NADH (in the absence of 5-nitrofurans) over the analyzed spectrum range was identical, showing that no NADH had been oxidized by the AhpF enzyme in the absence of oxygen (Fig. 7) and thus validating the anaerobic condition of the assay. There was an overall decrease in the intensity of the absorbance from 300 to 600 nm between the no-enzyme control (nitrofuran + NADH) to the reaction sample (nitrofuran + NADH + AhpF) for all three drugs, (Fig. 7, red arrows). Given that no molecular oxygen was involved, this difference in the absorbance spectrum can be completely attributed to the reaction between the 5-nitrofuran drug and NADH. In conclusion, this analysis shows that the AhpF indeed catalyzes the reduction of 5-nitrofurans.

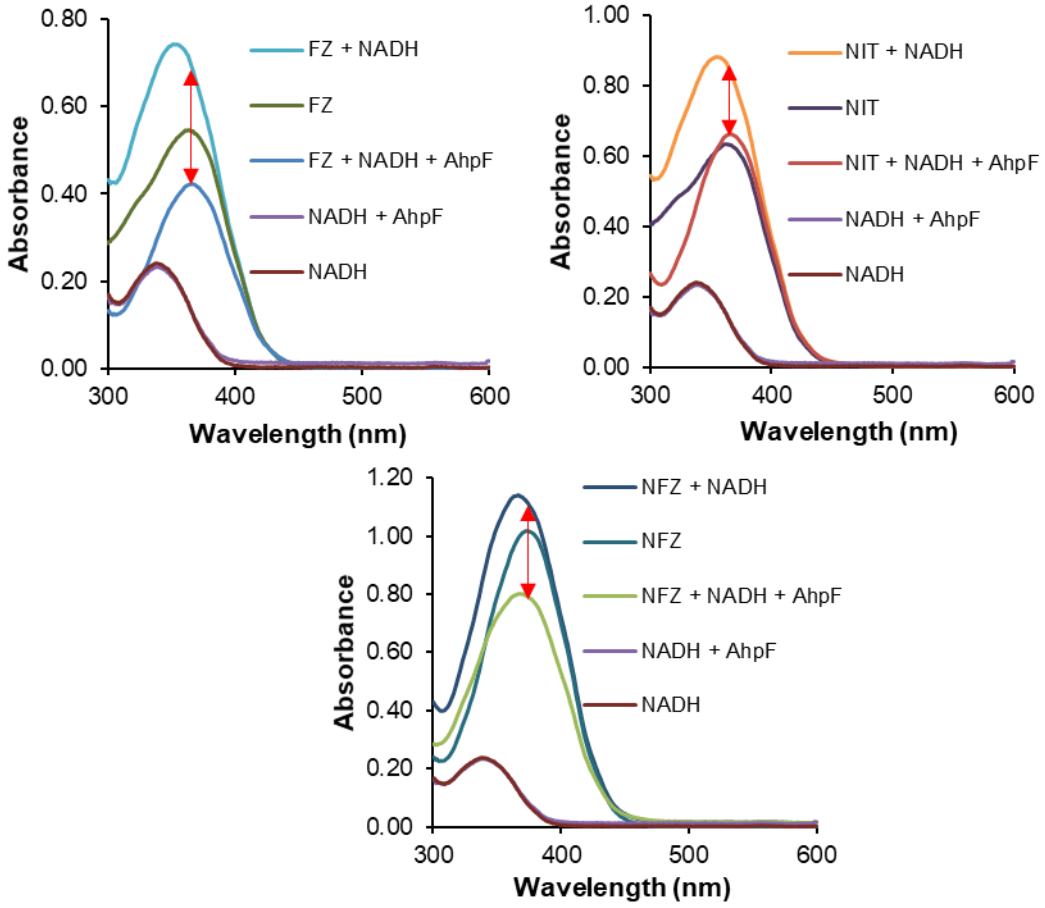

Figure 7: AhpF nitroreductase assay under oxygen-free conditions. The reaction mixture contained purified His-tagged AhpF 5 µg/mL, 5-nitrofuran 0.1 mM (furazolidone (FZ), nitrofurantoin (NIT) or nitrofurazone (NFZ)) and NADH 0.1 mM. The absorbance spectrum was measured after 21 h incubation at 25 °C. Each data point represents the mean value of the triplicate measurements. The red arrows indicate the change in the absorbance caused by AhpF-catalyzed reaction between 5-nitrofuran drugs and NADH.

In silico docking of FZ onto the active site of AhpF protein

To gain a better understanding of the nitrofuran-AhpF interaction, we performed *in silico* docking between FZ and the AhpF enzyme using two different tools, SwissDock (132) and AutoDock Vina (133). According to the SwissDock modelling, the most favorable binding pose of the drug was in a cleft between the FAD and NADH domains, which had the lowest fullfitness (–2728.95 kcal/mol) and binding energy (ΔG = –7.13 kcal/mol; Fig. 8A). Modelling with the AutoDock Vina tool predicted the same binding

site with the free energy as low as −6.9 kcal/mol. The orientations of FZ relative to the protein, however, differed in the predictions by the two modelling approaches (Fig. 8B & C).

Further calculating the inter-atomic interactions between FZ and the AhpF residues using the Arpeggio server (134) predicted that FZ interacts with protein residues more strongly in the AutoDock Vina model than in the SwissDock model (Fig. 8B & C). In the AutoDock Vina model, the furan ring of FZ was predicted to interact with the indole group of Trp326 via a π-π interaction and with the amide group of Gln448 via an amide-π interaction. The binding was further stabilized by three hydrogen bonds between FZ and three protein residues Ile449, Gly450 and Lys495 (Fig. 8C**)**. In the SwissDock model, the indole ring of Trp326 was also predicted to play an important role in the interaction with the furan ring of FZ (Fig. 8B**)**. Of note is the polar interaction between the oxygen of the nitro group of the drug and the thiol group of Cys345. In the AhpF protein, the Cys345XXCys348 motif establishes the redox active center, participating in the transfer of electrons from the cofactor FAD to the redox center in the N-terminal domain (135). Such an interaction predicted in the SwissDock model allows us to propose a molecular basis for the reaction: NADH donates electrons to FAD which then reduces the disulfide bridge of Cys345 and Cys348; after that, the thiol group of Cys345 contacts the nitro moiety of FZ in a manner that permits the transfer of electron(s). We speculate that the FZ binding predicted by AutoDock Vina represents a stable binding mode, while that predicted by SwissDock represents a reactive binding mode once the thiol group of Cys345 is available in its reduced state.

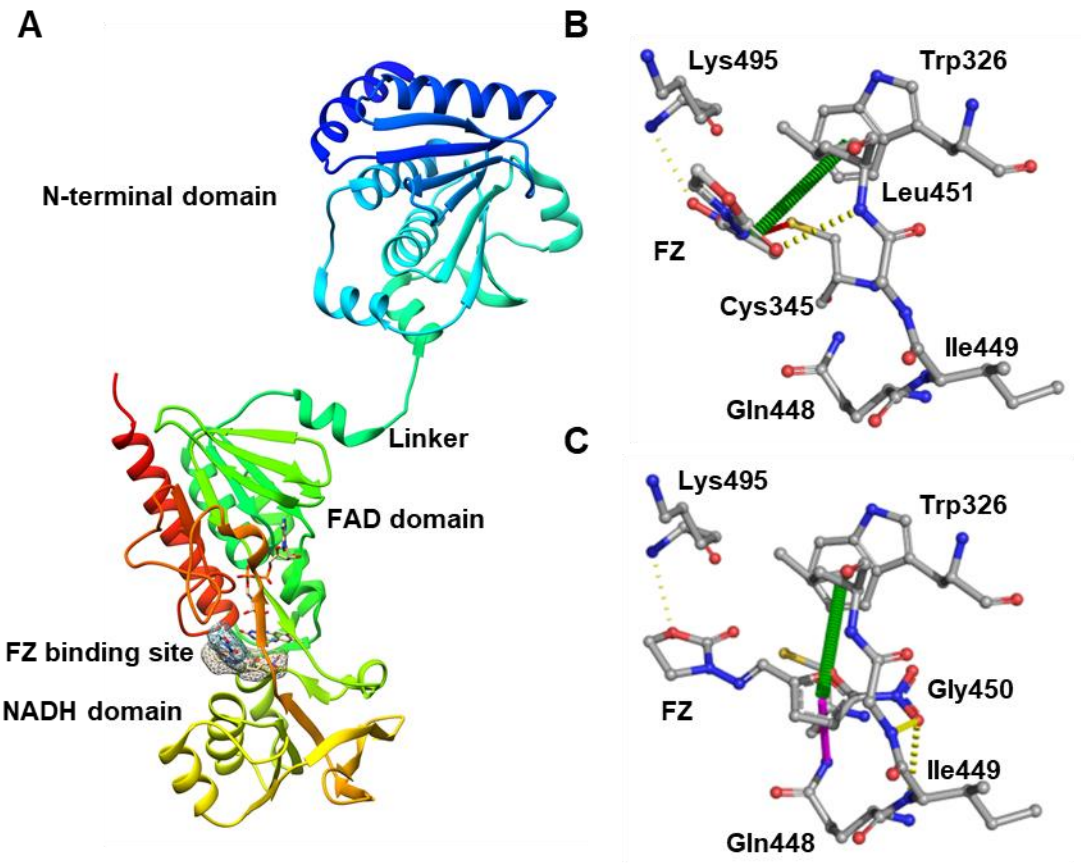

Figure 8: **Docking simulation for AhpF and FZ.** (A) The cartoon 3-D structure of AhpF protein with 3 domains (N-terminal domain, FAD domain, and NADH domain) and the simulated FZ binding site. The surface of FZ in the binding site predicted by SwissDock and AutoDock Vina was highlighted. (B & C) Interaction between FZ and AhpF residues in the binding site. Interactions were calculated and annotated using the Arpeggio server. (B) The binding pose predicted by SwissDock; (C) the binding pose predicted by AutoDock Vina. The interatomic interactions were presented by dashed lines; yellow, hydrogen bonding; red, polar contact; green, π-π interaction; purple, amide-π interaction.

Discussion

Characterization of antibiotic-resistant isolates is an important tool to identify the targets and mechanisms of resistance. All mutants with increased MICs for nitrofurans published prior to our work were isolated from wild-type laboratory K-12 or clinical *E. coli* strains, and most frequently reported to possess mutations in genes encoding the prodrug-activating enzymes NfsA and NfsB (31, 62, 63). Recently, Vervoort and co-

workers (136) incorporated whole genome sequencing to analyze nitrofurantoin-resistant *E. coli* mutants isolated from the wild-type parent, identifying, in addition to *nfsA* and *nfsB* mutations, a 12-nucleotide deletion in the *ribE* gene, encoding lumazine synthase. This is an essential enzyme in the biosynthesis of flavin mononucleotide, which in turn is the cofactor for NfsA and NfsB. Long-term laboratory evolution experiments of *E. coli* laboratory K12 strains under the selective pressure of nitrofurantoin also reported various mutations in *nfsA* and/or *nfsB* in all nitrofurantoin-selected evolved cultures (137, 138). Notably, in these experiments, other mutations have also been detected, such as those in genes *mprA*, *ahpF* and porin-encoding or -expression-regulatory genes (*ompC, ompR*, and *envZ*), although underlying mechanisms and the degree these mutations individually contribute to nitrofurantoin resistance have not been studied further. Overwhelmingly most frequently isolated 5-nitrofuran resistance-causing mutations in the *E. coli* wild-type strains have therefore been those that disrupt the NfsA and NfsB activity. To eliminate these from our genetic screen, we started from the Δ*nfsA* Δ*nfsB E. coli* parental strain and selected 15 independent mutants of increased MIC_{FZ}. We further employed whole-genome sequencing to pinpoint the mutations. Using this strategy, we discovered the involvement of a novel enzyme, AhpF, in activation of FZ. Overexpression of this enzyme decreased MIC for all three tested nitrofurans under aerobic and anaerobic conditions (Fig. 3, 4 & 5). Similar MICs were obtained under both conditions, suggesting that inside the *E. coli* cell 5-nitrofuran activation by AhpF is not affected by general aerobic conditions, possibly due to depletion of oxygen during culture growth. In contrast, in an *in vitro* enzymatic assay combining only the substrates and AhpF, reduction of 5-nitrofurans was oxygen-sensitive, resulting in 5-nitrofuran reduction only in the absence of oxygen (Fig. 6, S3 & 7).

AhpF is a peroxiredoxin reductase, which, together with the peroxiredoxin AhpC, forms the bacterial antioxidant alkyl hydroperoxide reductase AhpCF. The molecular structure of this system and its catalytic mechanism have been solved recently. Briefly, AhpF transfers electrons from the electron donor NADH *via* the redox-active sites of its C-terminal domain and then *via* the disulfide redox-active center within the N-terminal domain to the oxidized AhpC, which subsequently reduces hydrogen peroxide, organic hydroperoxide and peroxynitrite (135, 139, 140). Given its dedicated antioxidant function, it is expected that disruption of *ahpF* would cause an increase in antibiotic susceptibility and its overexpression would confer enhanced antibiotic resistance in general by ameliorating oxidative stress that is generally associated with effect of a number of antibiotics. For example, it has been shown that *ahpF* overexpression protects *E. coli* from aminoglycoside-mediated protein aggregation (141) or from killing by bactericidal antibiotics such as ampicillin, gentamicin, and norfloxacin (142). In contrast to these antibiotics, deletion of *ahpF* gene protects *E. coli* from FZ, while AhpF overexpression majorly increases susceptibility to all three tested 5-nitrofurans, in agreement with a dominant 5-nitrofuran activation role over its protective role under oxidative stress.

Notably, all FZ-resistant mutants isolated from an Δ*nfsA* Δ*nfsB E. coli* strain had an MIC of 20 µg/mL, while complete deletion of *ahpF* in an Δ*nfsA* Δ*nfsB* background resulted in an MIC as high as 28 µg/mL in an agar dilution assay (Fig. 3A). The difference between disruption/point mutants and complete deletion of *ahpF* could be rationalized based on the published findings that *ahpC* mRNA is stabilized by an RNase III-mediated cleavage in the intergenic region of the bi-cistronic *ahpC-ahpF* mRNA (143). Deletion of the *ahpF* ORF sequence is expected to change the RNAse III target and interfere with the processing, resulting in a decrease in the stability of the *ahpC*

transcript and thus in its abundance. Given the antioxidant role of AhpC, lowering its amount in the cell upon the complete deletion of the *ahpF* sequence may confer increased resistance to FZ in addition to the level caused by absence of the nitroreductase AhpF.

Deletion of *ahpF* in the Δ*nfsA* Δ*nfsB* background caused decreased resistance to NFZ and NIT under aerobic conditions (Fig. 4). This phenomenon can be rationalized as follows: AhpF has opposing dual functions, acting alone to activate nitrofurans, and acting in complex with AhpC to counteract the oxidative stress imposed by 5-nitrofurans (73, 135). Integration of these two roles dictates the net effect of *ahpF* deletion on nitrofuran susceptibility. Depending on the degree of oxidative stress induced by 5-nitrofurans, the rate of AhpF-mediated 5-nitrofuran reduction and the toxicity triggered by the reduction product, different effects on resistance to the three drugs (FZ, NIT and NFZ) were observed upon *ahpF* deletion.

The *in vitro* nitroreductase assay of purified AhpF provided a hint of the mechanism of 5-nitrofuran reduction by this enzyme. Monitoring two substrates, 5-nitrofuran and NADH, showed that NADH became oxidized, while the 5-nitrofuran concentration stayed largely unchanged during the time course of the enzymatic experiment when the reaction is carried out under aerobic conditions, i.e. in the presence of oxygen (Fig. 6 and S3). This is a characteristic of the futile reduction cycle catalyzed by the type II oxygen-sensitive nitroreductases as reported by Peterson *et al.* (74). These type II oxygen-sensitive nitroreductases catalyze the one-electron reduction of the nitroaromatic prodrugs to result in a nitro anion free radical which in the presence of oxygen is subsequently oxidized back to the nitro group, while reducing oxygen to generate superoxide. Our AhpF enzymatic assays under aerobic conditions showed that NADH oxidation occurred in the absence of 5-nitrofurans, due to direct reduction of

oxygen, but its rate increased in the presence of 5-nitrofurans. The concentration of 5-nitrofurans, on the other hand, did not change, in agreement with the futile redox cycle of 5-nitrofurans. In contrast, in our oxygen-free assays NADH was oxidized only in the presence of 5-nitrofurans, which in turn remained reduced in the absence of oxygen. This again is in agreement with the observed properties of the type II oxygen-sensitive nitroreductases. Detailed kinetic studies of the AhpF enzyme and determination of the reduced product under aerobic and anaerobic conditions are warranted to shed more light on AhpF-catalyzed 5-nitrofuran reduction mechanism.

In addition to the enzymatic assay, we described *in silico* simulation of FZ-AhpF interaction, using two software packages, AutoDock Vina and SwissDock. Both of these predicted binding of FZ in the cleft near the C-terminal disulfide bridge center between the FAD and NADH binding sites (Fig. 8). However, the predicted FZ orientation within the binding site differs substantially between the two models obtained using these algorithms. Further experimental approaches, such as solving the co-crystal structure of the AhpF enzyme with the drug and/or enzyme structure-function analysis of engineered mutant enzymes are required to improve the interaction model. This is important, since a reliable enzyme/drug interaction model may facilitate the rational design of 5-nitrofuran analogues that are activated by AhpF with a greater efficiency in comparison to the existing commercial 5-nitrofurans. These analogues could potentially be employed effectively against 5-nitrofuran-resistant pathogenic *E. coli* clinical isolates that all have been identified to date to be *nfsA* and/or *nfsB* loss-of-function mutants.

The selection of mutants with increased FZ resistance in the absence of NfsA and NfsB did not result in any mutations of putative 5-nitrofuran targets, reflecting the high probability that once activated, the reactive intermediate(s) of 5-nitrofurans attack multiple cellular components promiscuously rather than having specific targets.

Alternatively, the drug targets are essential in a manner that no resistance-causing mutations are allowed. It is also noteworthy that 5-nitrofurans still have some antibacterial effect in the Δ*nfsA* Δ*nfsB* Δ*ahpF E. coli* triple mutant. It is therefore conceivable that *E. coli* possesses other activation enzymes and/or that the non-reduced forms of 5-nitrofurans have antibacterial properties.

Our discovery of a new 5-nitrofuran-activating enzyme in *E. coli*, AhpF, provides opportunities for development of novel strategies for 5-nitrofuran based antibacterial therapies. Screening for small molecules to upregulate the expression/availability of AhpF and designing 5-nitrofuran analogues with high affinity for AhpF are promising approaches to discover novel antibacterial candidates to counteract pathogenic *E. coli* isolates that are resistant to current commercial 5-nitrofurans (FZ, NIT and NFZ) due to the *nfsA* and *nfsB* mutation.

Materials and methods

E. coli strains, growth condition and antibiotics

All *E. coli* strains and plasmids used in this study are listed in Table 2. Mutations of the Keio single-gene deletion *E. coli* collection containing the FRT-flanked kan^R marker (115) were introduced into *E. coli* recipient strains by P1 transduction according to the standard procedure (116). The FRT-flanked kan^R cassette was then removed using the FLP-mediated recombination as previously described (117). The plasmid pCA24N::*ahpF* was purified from the *E. coli* strain JW0599 of the ASKA collection (118) using the ChargeSwitch-Pro Plasmid Miniprep Kit (ThermoFisher Scientific) and then chemically transformed (119) into the Δ*nfsA* Δ*nfsB* Δ*ahpF* strain for the complementation assay or Δ*ahpC* strain for AhpF production.

E. coli was grown in 2xYT medium (BD Difco) at 37 °C with shaking at 200 rpm. For preparation of exponentially-growing cells, overnight cultures were diluted by 100-fold and incubated until they reached the OD_{600nm} of about 0.1-0.4. This cell suspension was then diluted to a desirable density depending on the specific purpose. Antibacterials used in this study were purchased from Goldbio, apart from nitrofurazone which was purchased from Sigma.

Table 2: *E. coli* strains and plasmids used in this study

Strain	**Genotype**	**Source**
BW25113	*rrnB3* Δ*lacZ4787 hsdR514* Δ*(araBAD)567* Δ*(rhaBAD)568 rph-1*	(115)
K2479	BW25113 Δ*nfsA* Δ*nfsB*	This study
K2506	BW25113 Δ*nfsA* Δ*nfsB* Δ*ahpF*	This study
K2511	BW25113 Δ*nfsA* Δ*nfsB* Δ*ahpF* pCA24N::*ahpF*	This study
K2526	BL21 pCA24N::*nfsB*	This study
K2528	BW25113 Δ*ahpC* pCA24N::*ahpF*	This study
Plasmid	**Notes**	
pCP20	Amp^R, Cm^R, FLP^+, λ $cI857^+$, λ p_R Rep^{ts} For removal of *kan* markers by FLP-mediated site-specific recombination	(122)
pCA24N::*ahpF*	Cm^R; *lacI*^{q}, pCA24N $P_{T5\text{-}lac}$::*ahpF*	(118)
pCA24N::*nfsB*	Cm^R; *lacI*^{q}, pCA24N $P_{T5\text{-}lac}$::*nfsB*	(118)

Isolating FZ resistant mutants

FZ-resistant mutants were isolated from spontaneous mutations in *E. coli* overnight populations. The Δ*nfsA* Δ*nfsB* strain (K2479) was used as the parental strain for

selection. Twenty independent overnight cultures were prepared. Each cell culture (100 µL) was mixed with 2.5 mL of molten soft agar (2xYT 0.5 % agarose) and then poured onto 2xYT plates containing 40 µg/mL, 48 µg/mL or 56 µg/mL of FZ. The agar was allowed to solidify. The plates were examined after 24 h and 48 h incubation at 37 °C. Colonies formed on these plates were sub-cultured onto 2xYT agar and incubated overnight at 37 °C. Only one colony was collected from each culture to minimize the chance of repeatedly isolating the same mutation. Putative resistant mutants were clonally purified and examined for increased MIC_{FZ} by the agar dilution assay, giving rise to 15 true FZ resistant mutants.

Fluctuation assay

Twenty seven parallel cultures, each 100 µL, were prepared in a 96 well plate (Polystyrene, Jet Biofil) at the starting inoculum of 10^5 CFU/mL. The cultures were incubated at 37 °C for 24 h with vigorous shaking. Three cultures were used to determine the bacterial concentration (and thus the number of plated cells per culture) by plating 10-fold serial dilutions on non-selective agar plates. Each of the remaining 24 cultures (100 µL) was mixed with 2.5 ml of molten soft agar (2xYT, 0.5 % agarose) and poured onto selective agar plates containing FZ (40 µg/mL). After 48 h of incubation at 37 °C, the colonies formed on the selective agar were counted. The most probable number of mutations per culture (m) and its 95 % confidence interval were calculated using the newton.LD() and confint.LD() functions, respectively, of the rSalvador package v1.7 (144) in the R environment (v.3.4.4) (145). The mutation rate (μ) was estimated as m/N_t, in which N_t is the number of plated cells per culture (4.93×10^8).

Genomic comparative analysis

The genomic DNA of FZ-resistant mutants and the parental strain (Δ*nfsA* Δ*nfsB E. coli* strain) was purified using the UltraClean Microbial DNA Isolation Kit according to the

manufacturer's instructions (Qiagen). The DNA samples were then submitted to the Massey Genome Service (New Zealand Genomics Limited, Massey University, Palmerston North, New Zealand) for whole genome sequencing using Illumina TruSeq Nano DNA library preparation and 2 x 250 base paired-end v2 sequencing chemistry on the Illumina MiSeq^{TM} sequencing platform. The raw reads were trimmed to a quality cut-off value of Q30 (equivalent to error probability p = 0.001) and any short-length reads (< 25 base by default) were removed using SolexaQA^{++} v3.1.7.1 (146). The DNA sequence data generated resulted in a theoretical genome coverage that was at least 40 × based on the *E. coli* strain BW25113 genome size. The trimmed reads were aligned with the reference *E. coli* strain BW25113 genome (ASM75055v1 from Ensembl (147)) using Bowtie2 v2.3.2 using the --very-sensitive mode (148). The resulting *.sam* files were then converted to *.bam* files using samtools v1.5 (149) and variant calling was carried out using freebayes v1.0.2 (150) using the default parameters, except ploidy was set to 1 (-p 1). The variants were functionally annotated using SnpEff v4.3p (151). The *ahpF* mutations were mapped to the corresponding protein domains using the visualization software DOG v2.0.1 (152).

To identify structural variations in the genomes of FZ-resistant mutants, the unmapped reads were extracted using samtools v1.5 (149) and then assembled to generate contigs using SPAdes v3.9.0 with the --careful option (153). The resulting contigs were compared with the *E. coli* reference genome BW25113 (Accession No. CP009273.1) (154) using the website platform NCBI Nucleotide BLAST 2.7.0+ (155), to determine the boundaries where the structure variations have occurred.

ahpF sequence analysis

Genomic DNA of FZ-resistant isolates was extracted using water boiling as previously described (156). The PCR reactions were performed in 50 µL mixtures containing 10

µL of 5 × Takara PrimeSTAR PCR buffer, 0.2 mM of each dNTP, 0.2 µM of *ahpF* forward primer (5'- AGGTGAAGCAACTCTGGCTC - 3') and 0.2 µM of *ahpF* reverse primer (5'-GCAACCCATCGATTTCGACC - 3'), 0.5 µL of PrimeSTAR^{TM} HS DNA Polymerase (Takara Bio USA) and 5 µL of the DNA extract. The PCR conditions included an initial denaturation at 94 °C for 30 sec, followed by 30 cycles of denaturation at 98 °C for 10 sec, annealing at 55 °C for 5 sec, and extension at 72 °C for 2 min. The PCR products were analyzed using agarose gel electrophoresis as previously described (157).

The *ahpF* amplicons were cleaned up using ChargeSwitch™-Pro PCR Clean-Up Kit (Invitrogen) according to the manufacturer's instructions and submitted to the Massey Genome Service (Massey University, Palmerston North, New Zealand) for DNA Sanger sequencing using Big Dye Terminator v3.1. The primers used for sequencing included *ahpF* forward primer, *ahpF* reverse primer and *ahpF* internal forward primer (5'-GTTCACCTCGCTGGTACTGG - 3'). The low-quality bases of raw sequences were trimmed until the average quality of 20 bases over 30 using Chromas v2.6.4 (Technelysium Pty Ltd). The trimmed sequence of *ahpF* amplicon was then aligned with the *E. coli* reference genome BW25113 (Accession No. CP009273.1) using the website platform NCBI Nucleotide BLAST 2.7.0+ (155) to determine the mutations in the gene *ahpF*.

In silico analysis of missense mutations in *ahpF*

The effect of missense mutations in the gene *ahpF* in FZ-resistant *E. coli* mutants was predicted using the SIFT web server (127) with UniRef 90 database with default parameters and the ConSurf web server with default parameters (126).

Antimicrobial susceptibility assays

The antimicrobial susceptibility of *E. coli* K-12 strains to 5-nitrofurans was examined using the agar dilution and broth microdilution assays as previously described (123, 158). The range of drug concentrations tested included 32, 28, 24, 20, 16, 12, 8, 4, 2, 1, 0.5, 0.25, 0.125 and 0 µg/mL in the agar dilution assay and 80, 64, 48, 32, 16, 8, 4, 2, 1, 0.5 and 0.25 µg/mL in the broth microdilution assay. In *ahpF* complemented strains, expression of *ahpF* was under the control of a chimeric $P_{T5\text{-}lac}$ promoter of a high-copy-number plasmid pCA24N::*ahpF* and induced by 0.1 mM or 1 mM IPTG. For the broth microdilution assay under anaerobic conditions, the plates were incubated in a BBL GasPak^{TM} 150 anaerobic jar (Becton Dickinson) containing three EZ GasPak sachets with an oxygen indicator.

Production and purification of His-tagged AhpF and NfsB proteins

The His-tagged AhpF and NfsB proteins were expressed from a high copy-number plasmid pCA24N::*ahpF* and pCA24N::*nfsB* (118), in the *E. coli* strain K2528 and K2526, respectively. The *E. coli* culture was grown to reach the $OD_{600\ nm}$ of about 0.6 and then induced with 1 mM IPTG at 37 °C for 4 h. The cells were harvested by centrifugation at 4000 × g for 15 min at 4 °C and the pellet was stored at -20 °C until being used for cell lysis and protein purification.

The affinity purification of His-tagged AhpF from cell lysate was carried out using a Ni-NTA Spin Kit according to the manufacturer's instructions, with some modifications (Qiagen). Firstly, the cell pellet harvested from 50 mL of the cell culture was suspended in 3 mL NPI20 lysis buffer (50 mM NaH_2PO_4, 300 mM NaCl, 20 mM imidazole, pH 8.0) containing 1 mg/mL lysozyme (Boehringer Mannheim) and frozen at -80 °C. The suspension was then thawed at room temperature, followed by addition of 2 µL of benzonase endonuclease at 10 units/µL (Sigma) and incubated at 4 °C on a tube roller

for 30 min. The lysis mixture was sonicated two times, each session lasted for 2 min including alternate 1 s on/off pulse at the power 2 using the microtip of a Virsonic 600 Ultrasonic cell disruptor. The cell lysate was then centrifuged at 12000 × g for 30 min at 4 °C.

The Ni-NTA spin column was equilibrated with 600 µL NPI20 buffer and centrifuged at 890 × g for 2 min. Next, 600 µL of cell lysate was loaded into the Ni-NTA spin column and centrifuged at 270 × g for 5 min. Following that, the Ni-NTA spin column was washed four times with 600 µL of NPI50 (50 mM NaH_2PO_4, 300 mM NaCl, 50 mM imidazole, pH 8.0) and centrifuged at 890 × g for 2 min. A His-tagged protein (AhpF or NfsB) was eluted by loading 200 µL of the NPI500 buffer into the Ni-NTA spin column (50 mM NaH_2PO_4, 300 mM NaCl, 500 mM imidazole, pH 8.0) and centrifuging at 890 × g for 2 min. The elution step was performed four times and the eluates were pooled. The exchange to Tris buffer (pH 7,4, 50 mM) and further removal of small unwanted proteins were performed using a Vivaspin ultrafiltration device 2 (GE Healthcare) with the cut-off size of 100 kDa for AhpF eluates and 10 kDa for NfsB eluates, according to the manufacturer's instructions. Purity of the protein extract was analyzed using SDS-PAGE, followed by Coomassie blue staining (159, 160) and densitometric analyses using the ImageJ software v1.51k (161) (Fig. S4).

Protein quantification assay

The quantity of the protein was determined using the Coomassie (Bradford) Protein Assay Kit according to the manufacturer's instructions (Thermo Scientific).

Nitrofuran reductase assay

The enzymatic assay for His-tagged AhpF or NfsB protein extract was performed on 96-well plate (Polystyrene, Jet Biofil) with the total volume of 200 µL containing 0.1 mM 5-nitrofuran (FZ, NIT or NFZ) and 0.1 mM NADH in 50 mM Tris-HCl buffer (pH

7.4). The activity was determined in the presence of 5 µg/mL of the AhpF enzyme or 1 µg/mL of the NfsB enzyme. The wells without 5-nitrofurans were used as references to monitor oxidation of NADH by the oxidase activity of AhpF. The wells containing no protein extract were used as negative controls. Each reaction was performed in triplicate. The reaction was initiated by adding the enzyme. The progress of the reaction was monitored at the absorbance at 340 nm and 400 nm for every 1 min for 12 h at 25 °C using a Multiskan^{TM} GO microplate spectrophotometer (Thermo Scientific). The absorbance spectrum from 300 to 600 nm was recorded at the end of the experiment.

For the nitroreductase assay under anaerobic conditions, the same protocol was applied with some changes. The Tris buffer (7.4) and water was gassed with oxygen-free carbon dioxide and placed in an anaerobic chamber (Coy Laboratory) overnight before the experiment to remove dissolved oxygen (O_2). All the pipetting steps were performed in an anaerobic chamber. The assay plate was then placed in an anaerobic jar and incubated at 25 °C for 21 h. The absorbance spectrum from 300 to 600 nm was recorded at the end of the experiment.

Linear regression and comparison of the initial reaction rate was performed using the emmeans package v.1.3.3 (162) in the R statistical environment (v.3.5.3) (145).

In silico docking of furazolidone to the AhpF protein

For the SwissDock server (132, 163), a blind docking simulation was implemented using ready-to-dock FZ ligand data file from ZINC database (accession number ZINC113418) (164) and the AhpF structural data file from Protein Data Bank (PDB ID 4O5Q) (135). The process was performed using the ACCURATE mode with the flexibility set to 3 Å. The generated docking poses between AhpF and FZ were visualized using UCSF Chimera v1.13 (165). Briefly, the binding poses which had steric clash between FZ and the cofactor FAD were purged. The hydrogen bonds were

then annotated between the ligand and the protein residues; the binding poses with fewer than 1 hydrogen bond were removed. The remaining binding poses were then ranked according to the fullfitness score and the number of hydrogens between FZ and AhpF residues.

For the AutoDock Vina, the PDBQT files for AhpF (from .pdb file 4O5Q) and FZ (from .mol2 file ZINC113418) were generated using AutoDock Tools (ADT) as previously described (166). First, a blind docking protocol was performed for AhpF and FZ using QuickVina-W (167) with the exhaustiveness of 24 and the number of modes of 50 (spacing 1 Å, x = 68, y = 66, z = 124, grid box center -38.786, -27.238, 28.694). This step was performed three times. The resulting poses were used to determine the most likely binding region of the AhpF protein. After that, the docking of FZ into AhpF was executed in a smaller grid box (spacing 1 Å, x = 40, y = 40, z = 40, grid box center -36.936, -33.981, 49.29) with the exhaustiveness of 24 and the number of modes of 50 using AutoDock Vina (133). This local docking was performed 10 times until the most favorable binding pose converged.

The most favorable binding poses obtained from the SwissDock and AutoDock Vina simulation were analyzed using the Arpeggio web server which calculates and visualizes the interaction between the ligand and protein residues (134). The interactions were visualized using PYMOL v1.8.4.0 (168).

Acknowledgements

We thank the Genetics Strains Research Center, National Institute of Genetics, Japan, for providing the ASKA collection and to the Massey University Genome Sequencing facility for the excellent genome sequencing service. We also thank Catrina Olivera for providing the *E. coli* strain K2526 and Pria Soni for technical assistance with anaerobic

chamber experiments. The Keio Collection was purchased from Dharmacon *via* ThermoFisher (Australia). This work was funded by a Callaghan Innovation PhD scholarship, Massey University and New Zealand Pharmaceuticals Ltd.

Supplemental data

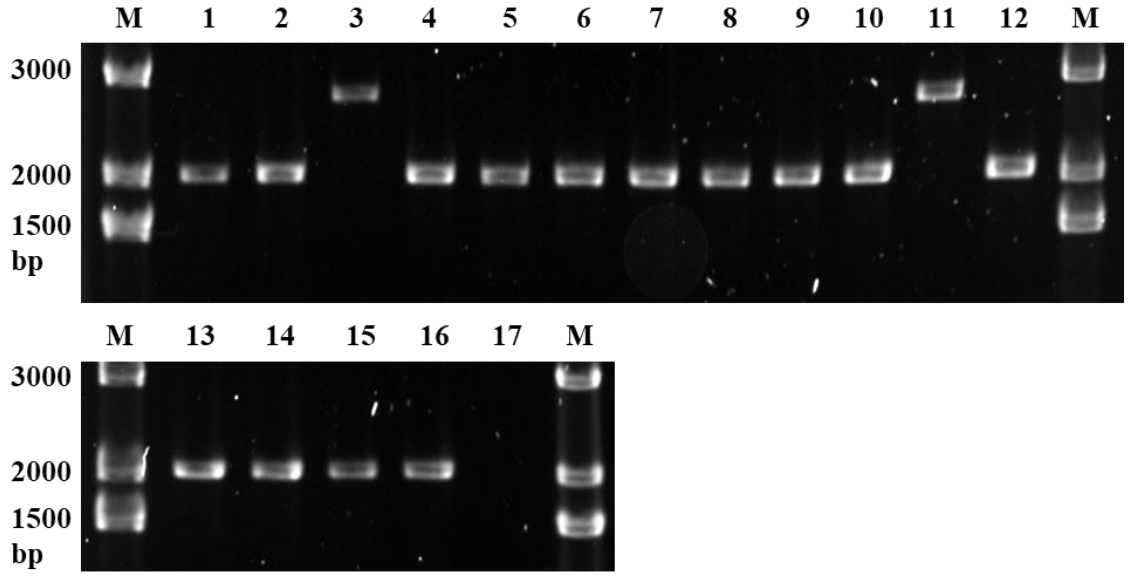

Figure S1: The PCR products of the *ahpF* gene derived from FZ-resistant mutants. Lanes M, 1 kb plus ladder; 1, FZ08; 2, FZ10; 3, FZ11; 4, FZ12; 5, FZ13; 6, FZ14; 7, FZ15; 8, FZ16; 9, FZ17; 10, FZ18; 11, FZ19; 12, FZ20; 13, FZ21; 14, FZ22; 15, FZ23; 16, parental strain K2479; 17, non-template control. The size of *ahpF* amplicon in two mutants FZ11 and FZ19 was larger than that of the parental strain by 800 bp, indicating an 800-nucleotide insertion within the *ahpF* gene in these two FZ-resistant mutants.

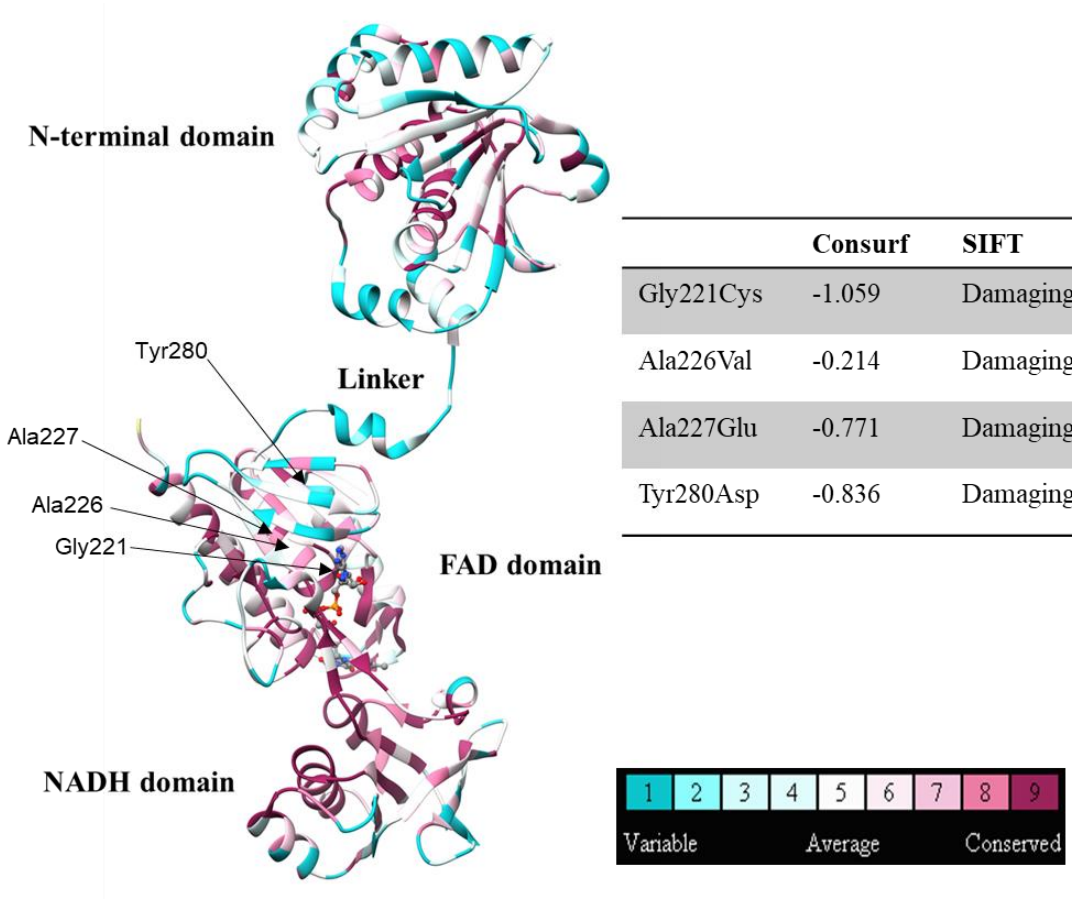

	Consurf	SIFT
Gly221Cys	-1.059	Damaging
Ala226Val	-0.214	Damaging
Ala227Glu	-0.771	Damaging
Tyr280Asp	-0.836	Damaging

Figure S2: Evolutionary conservation analysis of AhpF (PDB ID 4O5Q). The evolutionary conservation of the AhpF amino acid sequence was analyzed using the Consurf web server and the effect of single amino acid substitutions on protein function (damaging or non-damaging) was predicted using the SIFT web server. The table on the right shows the normalized conservation score of protein residues which were mutated in FZ-resistant mutants. The 3D backbone of AhpF was colored according to the color-scaled conservation score of its residues calculated by the Consurf web server. The residues Gly221, Ala226, Ala227 and Tyr280 had negative normalized conservation scores, indicating that these residues are highly conserved during the course of evolution. Mutations in these residues are highly likely to cause a loss of protein structure and function. Similarly, all the four missense mutations, including Gly221Cys, Ala226Val, Ala227Glu and Tyr280Asp were predicted by SIFT to cause the damaging effect to the AhpF protein with high confidence.

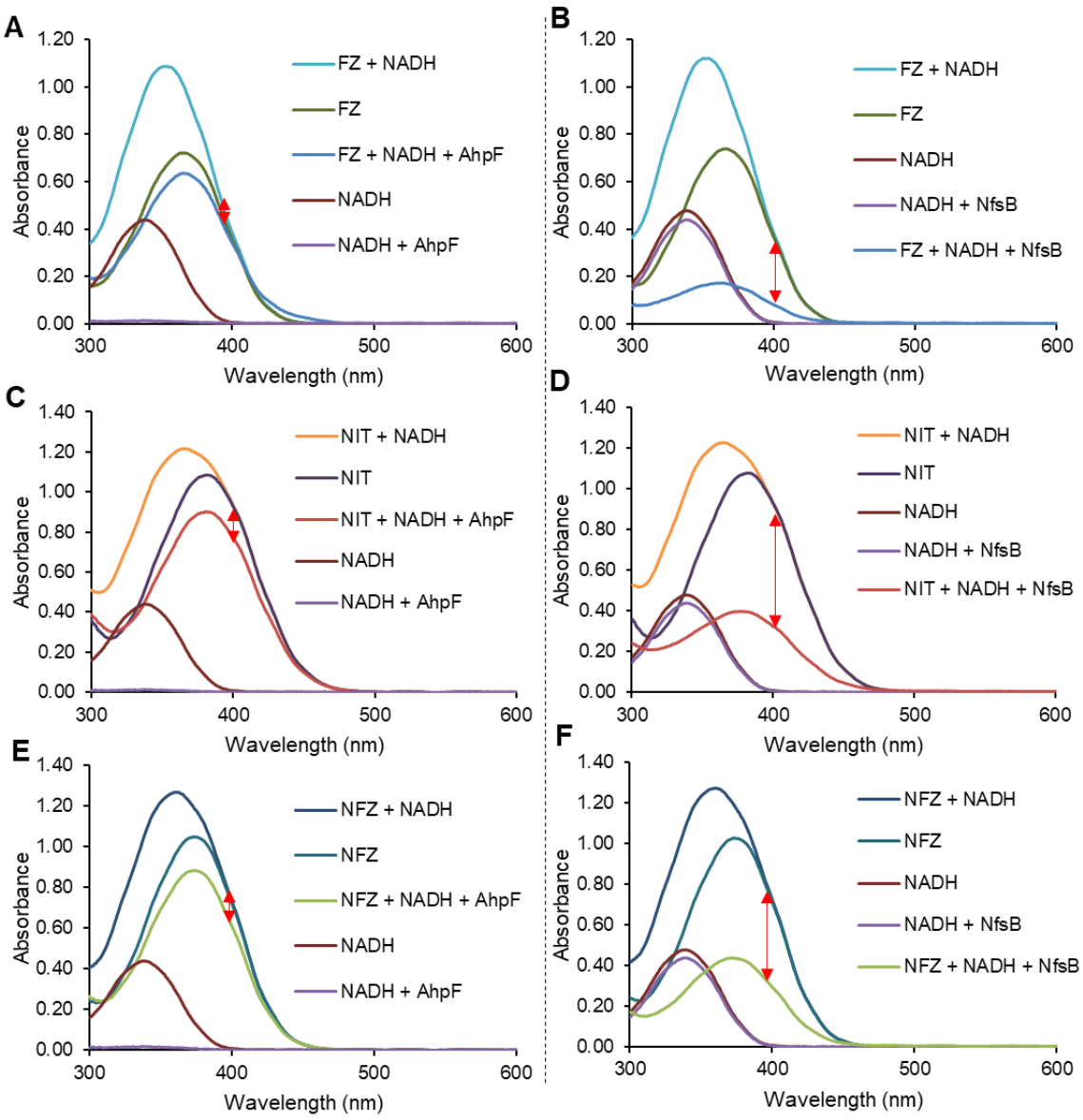

Figure S3: *In vitro* 5-nitrofuran reduction by AhpF and NfsB under aerobic conditions. The absorbance spectrum (300 - 600 nm) of each reaction was measured at the end of the assay (12 h). Purified AhpF 5 µg/mL (A, C, E) or NfsB 1 µg/mL (B, D, F) was mixed with furazolidone (FZ; A, B), nitrofurantoin (NIT; C, D) or nitrofurazone (NFZ; E, F) and NADH at the ratio of 0.1 mM : 0.1 mM. Each data point represents the mean of three replicates. No-enzyme control and the substrates alone were included to allow comparison of the absorbance spectra before and after the reaction. Red arrows indicate the difference in the absorbance due to the nitrofuran reduction.

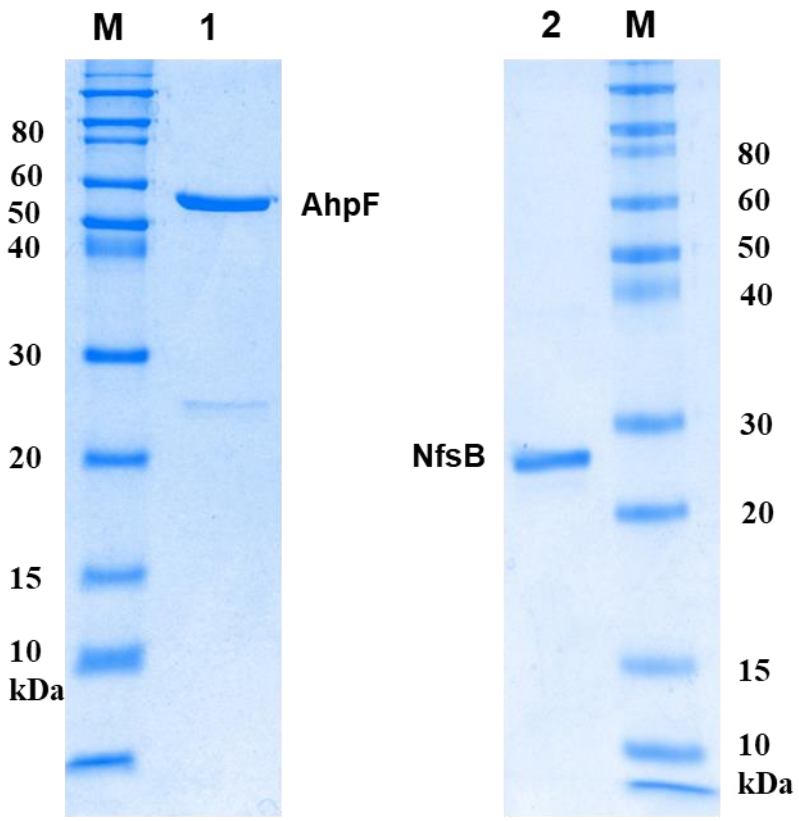

Figure S4: Purification of AhpF and NfsB. SDS-PAGE analysis of the His-tagged AhpF and and the His-tagged NfsB purifcations. Lanes: M, Novex sharp pre-stained protein standard (Invitrogen™); 1, AhpF purified sample; 2, NfsB purified sample. Ni-NTA affinity purification of AhpF (57 kDa) resulted in about 90.3 % purity with one contaminant protein band accounting for the remaining 9.7 %. No non-specific bands were observed in the purified NfsB sample.

Chapter IV:

Comparative genomic analysis of *Escherichia coli* mutants with decreased bile salt sensitivity

Vuong Van Hung Le[1], Patrick J. Biggs[1,2], David Wheeler[1]*, Ieuan Davies[3] and Jasna Rakonjac[1#]

[1] School of Fundamental Sciences, Massey University, Palmerston North, New Zealand

[2] [m]Epilab, Infectious Disease Research Centre, School of Veterinary Science, Massey University, Palmerston North, New Zealand

[3] New Zealand Pharmaceuticals Ltd., Palmerston North, New Zealand

*Present address: NSW Department of Primary Industries, Orange, Australia

[#]Corresponding author:

Jasna Rakonjac, School of Fundamental Sciences, Massey University, Palmerston North, New Zealand

Email: j.rakonjac@massey.ac.nz

Tel. +64 6 350 5134; Fax +64 6 350 5688

Abstract

Bile salts are secreted into the intestine to aid fat digestion and confer antimicrobial protection. Sodium deoxycholate (DOC) is the most potent antimicrobial agent among them. However, Gram-negative pathogens, such as *Escherichia coli*, are highly resistant to DOC, using multiple mechanisms of which the multidrug efflux pump AcrAB-TolC is the dominant one. In this study, we sought to identify targets of DOC by identifying genes involved in DOC sensitivity in the absence of functional efflux pumps (in Δ*tolC* background), using a mutant screen that selected twenty independent spontaneous mutants that had a higher MIC_{DOC} than the *E. coli* parental strain. Whole genome sequencing of these DOC-resistant mutants followed by analysis of knock-out strains showed that proteins encoded by the *ptsI, cyaA, crp, ndh* and *tktA* genes mediate sensitivity of the Δ*tolC E. coli* strain to DOC. In addition, a large deletion of about 15.5 kb, spanning 24 genes and an inversion of almost half of the *E. coli* chromosome via an *insH1*-mediated homologous recombination event were selected based on their increased DOC resistance. Lack of single mutations resulting in high-level DOC resistance points to essential proteins as targets, and/or a broad effect on membranes or DNA. Overall, we show that mutations leading to decreased metabolic rates lead to small increases in DOC resistance, while no high-resistance evolution in the absence of the TolC-dependent multi-drug efflux pumps was identified.

Importance

Sodium deoxycholate (DOC) is a secondary bile salt, naturally present in the gut and involved in the host antimicrobial defence. In this study, we showed possible pathways to gain DOC resistance in an *E. coli* strain which is deficient in TolC-associated efflux

pumps. Disruptive mutations in the genes *cyaA*, *crp*, *ptsI*, *tktA*, *ndh*, a 15.5 kb DNA deletion or a genome inversion conferred low-level DOC resistance. The absence of single-step high-level-DOC-resistance mutants in our mutant screen implies that the emergence of DOC resistance is prevented in the absence of active efflux pumps. This also suggests that this molecule attacks multiple bacterial targets simultaneously and/or that its cognate targets are essential proteins whose mutations are lethal.

Keywords

Sodium Deoxycholate, Bile salts, Adenylate cyclase, PTS system, Efflux pumps, *Escherichia coli*, Antimicrobial resistance, DNA inversion.

Introduction

Bile salts are an important component of bile which is secreted into the intestine to support fat digestion, regulate glucose homeostasis, modulate inflammatory processes and confer antibacterial protection (169), and are sometimes used as signaling molecules for virulence expression of multiple bacterial pathogens (81-83, 170). In humans, these are made up of the primary bile salts, including cholate and chenodeoxycholate and the secondary bile salts, including deoxycholate, lithocholate, and ursodeoxycholate, which are formed from primary bile salts by the 7α/7β-dehydroxylation enzymatic activity of gut commensal bacteria (169, 171). Primary and secondary bile salts, when first secreted into the duodenum, exist in glycine- or taurine-conjugated forms that are then hydrolyzed to unconjugated forms because of the bile salt hydrolase of microbes residing along the intestine (Fig. S1) (171) .

Bile salts have been shown to have varying degrees of inhibitory effects on Gram-positive bacterial pathogens, such as *Staphylococcus aureus* and *Clostridium difficile* (79, 99). Of note is that sodium deoxycholate (DOC) kills *S. aureus* with the highest efficacy among bile salts, followed by cholate and conjugated cholate, by causing membrane disruption and cellular content leakage (99). Regarding *C. difficile*, chenodeoxycholate was found to inhibit spore germination while secondary bile salts, including ursodeoxycholate, lithocholate and DOC inhibited the growth of this pathogen (79).

In contrast to Gram-positive pathogens, Gram-negative counterparts are more resistant to DOC, with enterobacteria being highly resistant. The dominant DOC resistance mechanism in the model enterobacterium *Escherichia coli* is the restriction of intracellular accumulation by employment of diverse active efflux pumps (86, 87). The primary machinery involved is a tripartite multidrug efflux system, called AcrAB-TolC,

whose disruption has been shown to cause a remarkable decrease in the minimum inhibitory concentration (MIC) for DOC (86, 87). This effect upon deletion of the major efflux pump is not only observed in *E. coli*, but also in other gut pathogens such as *Salmonella*, *Vibrio cholerae* and *Campylobacter jejuni* (81, 88).

The antimicrobial mode of action and molecular targets of DOC in *E. coli* are not well understood. It was proposed that DOC could trigger the DNA-damage SOS response, cause protein aggregation via induction of oxidative stress and compromise the cellular membrane integrity (97, 98). It is unclear, however, whether these consequences result from direct attack towards DOC targets (i.e. cytoplasmic membrane, DNA, proteins) or are downstream effects upon the interaction of DOC with its unknown cognate target(s).

In this study, we carried out a mutant screen and employed whole genome sequencing to characterize twenty spontaneous DOC-resistant *E. coli* mutants independently isolated from an efflux-pump-deficient Δ*tolC* parental strain. This approach provided insights into the mechanism of DOC action/resistance in *E. coli* cells other than overexpression of efflux pumps.

Results

Isolating DOC resistant mutants

In order to discover DOC resistance mechanisms outside of efflux pumps, we selected for spontaneous DOC-resistant *E. coli* mutants in a Δ*tolC* genetic background. The selection was performed at three DOC concentrations (100, 125 and 150 µg/mL) that are all inhibitory to the growth of the parental strain. Twenty-six independent overnight cultures were prepared for selection on agar plates. No colonies were observed after 24 h of incubation at any of the three DOC concentrations used and the absence of bacterial growth remained after 48 h of incubation on agar plates containing 125 µg/mL and 150

μg/mL of DOC. Colony formation was observed on plates containing 100 μg/mL of DOC after 48 h of incubation. From these plates, twenty independent *E. coli* mutants showing increased DOC resistance in the Δ*tolC* genetic background were isolated. All mutants had the same MIC_{DOC} of 125 μg/mL, higher than that of the parental strain (100 μg/mL).

Genome sequence analysis

Genomic DNA was extracted from overnight cultures of 20 clonally purified DOC-resistant mutants and the parental strain, and sequenced using the paired-end Illumina Miseq platform. We trimmed low-quality bases from the raw reads and mapped the trimmed reads onto the *E. coli* BW25113 reference genome as described in the method section. For all the DNA samples, the total base number of the resulting trimmed reads was at least 46× the reference genome size, allowing us to confidently identify genetic variants in the DOC-resistant mutants in comparison to the parental strain. Overall, 16 resistant mutants had a mutation in the *ptsI* or *cyaA* gene (Table 1), one had mutations in two genes, *ndh* and *ybhQ*, one had a mutation in *tktA* and one contained a 15.5-kb DNA deletion (Table 2). The size and sequence of the mutated loci were further confirmed by gene-specific high-fidelity PCR and Sanger sequencing, providing evidence in line with the mutations discovered through whole genome sequence analyses (Figs. S2 and S3). One DOC-resistant mutant was found to contain a large DNA inversion that we pinpointed by employing additional genome sequencing and PCR reactions. The details about the mutations involved in DOC resistance are as follows.

Mutations in *cyaA* and *ptsI*

Amongst the twenty DOC^R mutants, eight had a mutation in the *cyaA* gene, whilst eight others contained a mutation in the *ptsI* gene (Table 1). Most mutations occurred at

unique sites within these two genes except for two pairs of mutants, DOC04/12 and DOC01/11, which had identical mutations in the *cyaA* and *ptsI* genes, respectively.

In *E. coli*, the *cyaA* gene encodes a class I adenylate cyclase enzyme which converts ATP into cyclic AMP (cAMP) and inorganic pyrophosphate. The second messenger molecule cAMP interacts with the cAMP receptor protein Crp (Catabolite Repression Protein) to form an active transcriptional regulator cAMP-Crp which regulates the expression of at least 378 promoters that are involved in central metabolism such as transport of carbon sources, carbon metabolism, aerobic respiration, switch control between glycolysis and gluconeogenesis and a number of transcriptional regulators (172). The CyaA protein is composed of a catalytic domain at the N-terminal region and a regulatory domain at the C-terminal region, which inhibits the activity of the catalytic domain (173). The five missense mutations in *cyaA* occurred exclusively within the catalytic domain (Fig. 1). The gene *ptsI* encodes enzyme I (EI or PtsI) of the phosphoenolpyruvate-sugar phosphotransferase (PTS) system which is responsible for importing sugar molecules. This enzyme comprises an Hpr (histidine protein)-binding domain, a His domain and a PEP (phosphoenolpyruvate)-binding domain (174). The mutations in *ptsI* were distributed over all three major functional domains.

Table 1: List of mutations in the *cyaA* and *ptsI* genes found in the mutants having increased DOC resistance (MIC= 125 µg/mL) relative to the parental strain (100 µg/mL)

Locus	Isolate	Location of mutation	Predicted mutational change
cyaA **Adenylate cyclase**	**DOC02**	IS*1* insertion at -1 position with 9-nucleotide duplication	Disruption in expression of the ORF
	DOC04	T900A	Asp300Glu
	DOC05	G563A	Arg188His
	DOC12	T900A	Asp300Glu
	DOC19	T803G	Leu268Arg
	DOC20	A-5C	5' UT sequence; interference with translation
	DOC21	G185T	Cys62Phe
	DOC22	C530A	Thr177Asn
ptsI **phosphoenolpyruvate-sugar phosphotransferase enzyme I**	**DOC01**	G41A	Gly14Asp
	DOC03	G1550A	Gly517Glu
	DOC06	G877A	Gly293Ser
	DOC09	G1067A	Gly356Asp
	DOC11	G41A	Gly14Asp
	DOC15	1332A duplication	Frameshift from Glu445
	DOC16	C103T	Gln35 > stop
	DOC18	G115A	Glu39Lys

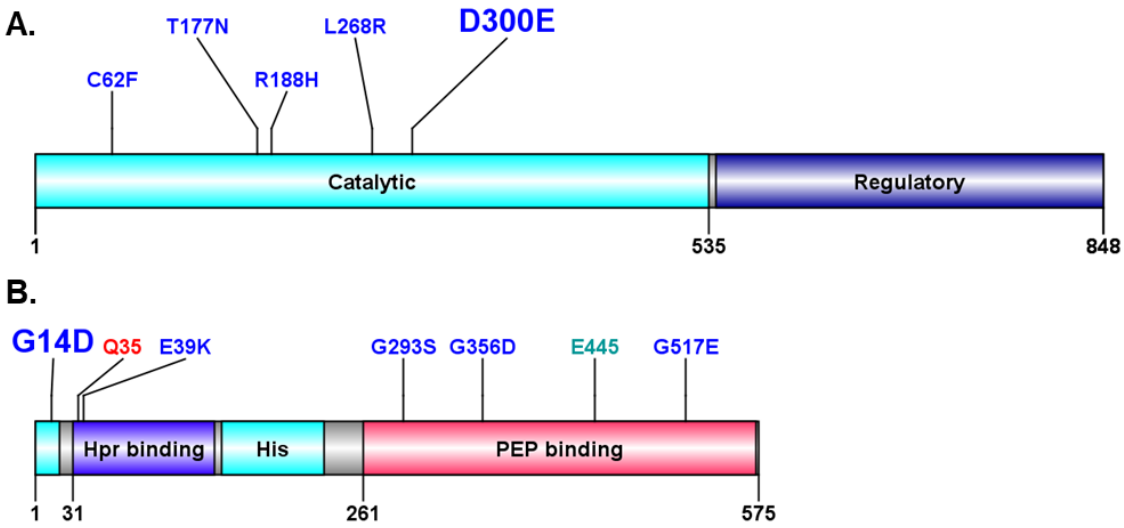

Figure 1: Mutations in the proteins CyaA (A) and PtsI (B) in DOC resistant isolates. A) The CyaA protein consists of two regions, including the adenylate cyclase catalytic domain (residues 1-535) and the regulatory domain (residues 541-848). A single nucleotide substitution and one IS*1* insertion in the 5'-unstranslated regions of *cyaA* mRNA are not shown in this figure. B) The PtsI protein consists of three regions, including the His domain (residues 1-20 and 149-230), the Hpr binding domain (residues 31-143) and the PEP-binding domain (residues 261-573). The types of mutations are illustrated by the color of annotations: blue, missense mutation; cyan, frame-shift mutation; red, nonsense mutation. The frequency of mutations is described by the size of the annotations: small, 1; large, 2.

Effects of *cyaA* or *ptsI* knock-out mutations on DOC resistance

Based on the observations of frequent involvement of different mutations in *cyaA* or *ptsI* in rendering enhanced DOC resistance, we hypothesized that the mutations in these genes (Table 1) are likely to lead to a loss of function. To test this hypothesis, we generated knock-out mutations in *cyaA* or *ptsI* in the Δ*tolC* genetic background and examined the DOC resistance of the corresponding strains using an agar dilution assay. The double knock-out mutants had an increased DOC resistance relative to that of the parental strain (125 µg/mL; Fig. 2) and equivalent to that caused by spontaneous mutations in *cyaA* or *ptsI* listed in Table 1. The identical phenotype of knock-out and spontaneous mutants confirms that the mutations identified in our screen are indeed

loss-of-function mutations in either *cyaA* or *ptsI*, irrespective of the widely different changes they caused in the protein, from a premature translation stop to missense mutations.

To confirm that the increased DOC resistance was solely due to the deficiency of the mutated gene, complementation assays were performed with plasmid-expressed CyaA or PtsI. Basal expression of *cyaA* from the chimeric $P_{T5\text{-}lac}$ promoter of a high-copy number plasmid pCA24N::*cyaA* was found to render the complemented strain more sensitive to DOC in comparison to the same strain bearing an empty plasmid or the parental strain (Fig. 2). The *cyaA* overexpression by promoter induction at 0.1 mM or 1 mM IPTG was found to be lethal. In the *ptsI* complementation assay, expression upon induction by 0.1 mM IPTG conferred a major decrease in the MIC_{DOC} as compared to that of the parent or knock-out containing the empty vector (Fig. 2); the plasmid-selective antibiotic, chloramphenicol, was not included in the DOC-containing agar plates, since we noted that a high *ptsI* expression was completely inhibitory to the growth of the *ptsI* complemented strain in the presence of chloramphenicol.

Given a close functional relationship between CyaA, which catalyzes conversion of ATP to cAMP and Crp, the transcription factor that is active only when complexed with cAMP, we introduced a *crp* knock-out mutation into the parental Δ*tolC* strain and examined the effects of the gene knock-out and complementation on DOC susceptibility. The *crp* knock-out in the Δ*tolC* strain caused the same increase in MIC_{DOC} as the Δ*cyaA* mutant (125 μg/mL). Complementation with Crp expressed at a basal level from the multi-copy plasmid pCA24N::*crp* lowered the MIC_{DOC} to the level of the parental strain (Fig. 2).

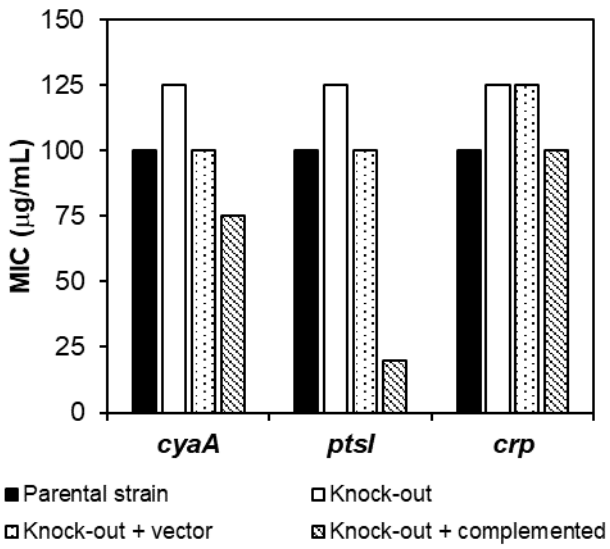

Figure 2: DOC susceptibility in *cyaA*, *ptsI* or *crp* disrupted mutants and corresponding complemented strains. The MICs for DOC were determined using agar dilution assays. Each treatment was performed in triplicate, giving the same MIC. Complementation of *cyaA* and *crp* was conducted at a basal expression level from the chimeric $P_{T5\text{-}lac}$ promoter in the high-copy number plasmid pCA24N. Complementation of *ptsI* expression was performed at 0.1 mM IPTG. Parental strain, BW25113 Δ*tolC*; Knock-out, the gene knock-out strain; Knock-out + vector, the gene knock-out strain transformed with the empty plasmid control pCA24N; Knock-out + complemented, the gene knock-out strain transformed with the plasmid pCA24N carrying the gene to be complemented.

Mutations in other loci conferring increased DOC resistance

Apart from the sixteen DOC^R mutants found to possess *ptsI* or *cyaA* mutations as described above, one mutant, DOC07, was identified to contain mutations in two genes, *ybhQ* (a missense mutation) and a deletion including the *ndh* coding sequence (CDS) and upstream regulatory sequence (a 405-nucleotide deletion; Table 2 and Fig. S3). The *ybhQ* gene encodes a putative inner membrane protein with unknown function, while the gene *ndh* encodes a type II NADH dehydrogenase (also known as NADH:quinone oxidoreductase II) which is part of the bacterial electron transport chain. This enzyme transfers electrons from NADH to quinones and regenerates NAD^+ without generating an electrochemical gradient across the cytoplasmic membrane; thus, its role is thought

to maintain the [NADH]/[NAD^+] ratio (175). The deletion in the *ndh* gene identified in this mutant spans from nucleotide -285 upstream of the CDS to nucleotide 121 of the coding sequence and is predicted to completely disrupt *ndh* expression and function, thus conferring a loss of type II NADH dehydrogenase activity in the DOC07 mutant. Introduction of the precise Δ*ndh* mutation into the Δ*tolC* strain caused an increase in the MIC_{DOC} to 125 µg/mL, the same as that of the isolate DOC07 (Fig. 3), showing that the 405-nucleotide deletion including portion of the *ndh* CDS in this mutant was responsible for the increased DOC resistance rather than the point mutation in *ybhQ*. This was further reinforced by a complementation assay in which basal *ndh* expression from the pCA24N::*ndh* plasmid lowered the MIC_{DOC} in the complemented strain back to the level of the Δ*tolC* parental strain (Fig. 3).

Table 2: Mutations found in other loci conferring enhanced DOC resistance

Isolate	Locus	Location of mutation	Predicted mutational change	Cellular function affected
DOC07	*ybhQ*	C254T	Ala85Val	putative inner membrane protein
	ndh	405-nucleotide deletion from -285 to +120 positions	Loss of function	NADH:quinone oxidoreductase II
DOC13	Part of CP4-6 prophage	15490-nucleotide deletion from 254176 to 269665	Loss of function of multiple genes	Unknown
DOC17	*tktA*	621ΔT	Frameshift from Tyr208	Transketolase 1

Another DOC resistant mutant (DOC17) contained a single nucleotide deletion in the *tktA* gene at the position 621 that causes a frameshift from the residue Tyr208, leading to disruption of the C-terminal two thirds of the protein (Table 2). The *tktA* gene

encodes transketolase 1 whose major role is to catalyze the reversible transfer of a ketol group between different substrates, thus connecting the glycolysis and pentose-phosphate pathway (176). That the TktA loss of function was responsible for the DOC resistance phenotype in DOC17 was confirmed by measuring the MIC_{DOC} in the *tktA*-ORF-deleted strain, which had the same level of DOC resistance as the DOC17 mutant. Complementation showed that overexpression of *tktA* upon 0.1 mM IPTG induction not only compensated for the *tktA* deletion but also further lowered the MIC_{DOC} to 50 µg/mL, below the level of the parental Δ*tolC* strain (Fig. 3).

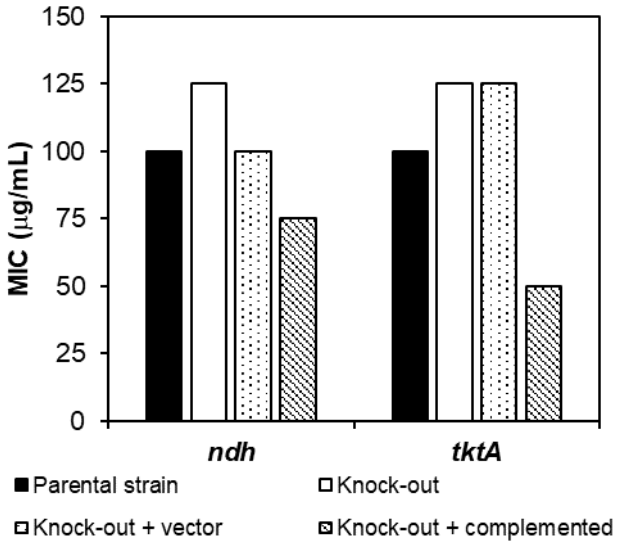

Figure 3: DOC susceptibility in *ndh* or *tktA* disrupted mutants and corresponding complemented strains. The MICs for DOC were determined using agar dilution assays. Each treatment was performed in triplicate, giving the same MIC. Complementation of *ndh* was conducted at a basal expression level from the chimeric $P_{T5\text{-}lac}$ promoter in the high-copy number plasmid pCA24N. Complementation of *tktA* expression was carried out at 0.1 mM IPTG. Parental strain, BW25113 Δ*tolC*; Knock-out, the gene knock-out strain; Knock-out + vector, the gene knock-out strain transformed with the empty plasmid control pCA24N; Knock-out + complemented, the gene knock-out strain transformed with the plasmid pCA24N carrying the gene to be complemented.

The DOC13 mutant was found to have gained enhanced DOC resistance through a 15.5 kb deletion, from the *frsA* gene to the IS*5A* element within the CP4-6 prophage, that

removed 23 genes and 85 nucleotides from the 3'-end of the *frsA* gene (Fig. 4). We confirmed this mutation using primers designed to amplify the sequence flanking the deletion (Fig. S3, lane 7, ~1100 bp). These primers were too far apart to obtain a PCR product in the parental strain (16585 bp).

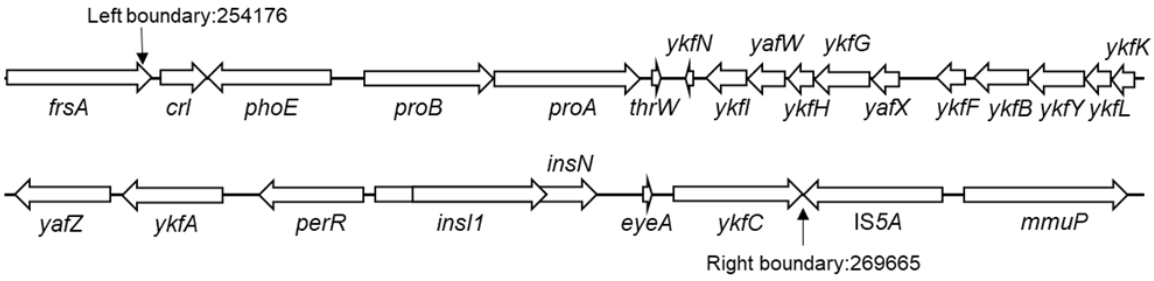

Figure 4: A large deletion in the genome of the DOC13 mutant. The arrows indicate the boundary sites of the deletion (co-ordinates: 254,176-269,665). This affects 24 genes, from *frsA* to *ykfC*, and covers the first 10 kb of the CP4-6 prophage (co-ordinates: 258,669-292,976).

A large genome inversion in the DOC14 mutant

Surprisingly, there were no DNA mutations detected in DOC14, using the whole genome sequence analysis of the DNA extracted from the overnight cultures as described above. A likely explanation for this is that the genome of the DOC14 mutant possessed an inversion, relative to that of the parental strain, due to homologous recombination events mediated by two inverted repeats that are longer than the average length of DNA fragments (~ 550 bp) in the libraries prepared for the Illumina genome sequencing. If this was occurring in DOC14 then it would be very difficult to identify this even using standard Illumina sequencing in combination with reference based short read mapping.

To test the possibility that DOC14 contained an inversion that was responsible for its DOC resistance phenotype, we used a strategy based on the replication-associated gene dosage effect in exponentially growing cultures where the cell cycle is shorter than the chromosome replication. Under these conditions, DNA copy number is greater in the region near the origin of chromosome replication (*oriC*) than in the region closer to the termination region, resulting in genome coverage distribution corresponding to an inverted-V shape, with the origin of replication as the central peak (177). If any inversion occurs in the mutant, this distribution will be skewed in the inverted portion of the genome. We extracted and sequenced the genomic DNA from the exponentially growing cultures of the DOC14 mutant and parental strain. Surprisingly, the genome coverage of both the parental strain and the DOC14 mutant appeared to have irregular peaks throughout the genome (Fig. 5A). Nonetheless, a comparison of both genomes showed that in the DOC14 mutant, a region spanning the coordinates between 1.4-1.6 Mb had higher coverage than expected and a region spanning the coordinates between 1.9-2.4 Mb had lower coverage than expected. This evidence supports the conclusion that there is an inversion spanning the coordinates between 1.4-1.6 Mb and 1.9-2.4 Mb in DOC14.

Using the software for detection of repetitive sequences (repseek) (178), we predicted 87 possible homologous recombination events mediated by two inverted repeats with a size larger than 500 bp, according to the reference genome sequence BW25113 (Table S1). After considering the range estimated from the genome coverage analysis, the number of candidate recombination endpoints was narrowed down to eight *insH1* sites (P1 to P8). The recombination endpoints were identified using diagnostic PCR reactions flanking these eight *insH1* sites (Table 6). Our rationale is that if an *insH1* site participates in the inversion, the forward and reverse primers of that site will be

separated and no PCR product will be observed. This approach resulted in identification of two sites, *insH1* P2 and P7, that were involved in the inversion in the DOC14 mutant (Fig. 5B). It is noteworthy that a low-intensity band corresponding to the wild-type was present in the DOC14 lanes for the *insH1* P2 and P7 sites (~3000 bp and 2000 bp, respectively) in the PCR gel rather than complete absence (Fig. 5B); this could be either the result of the artefact of the PCR, due to overlap extension of products that have hybridized to each other over the identical *insH1* sequences, or due to spontaneous recombination between P2 and P7 that results in reversion (179).

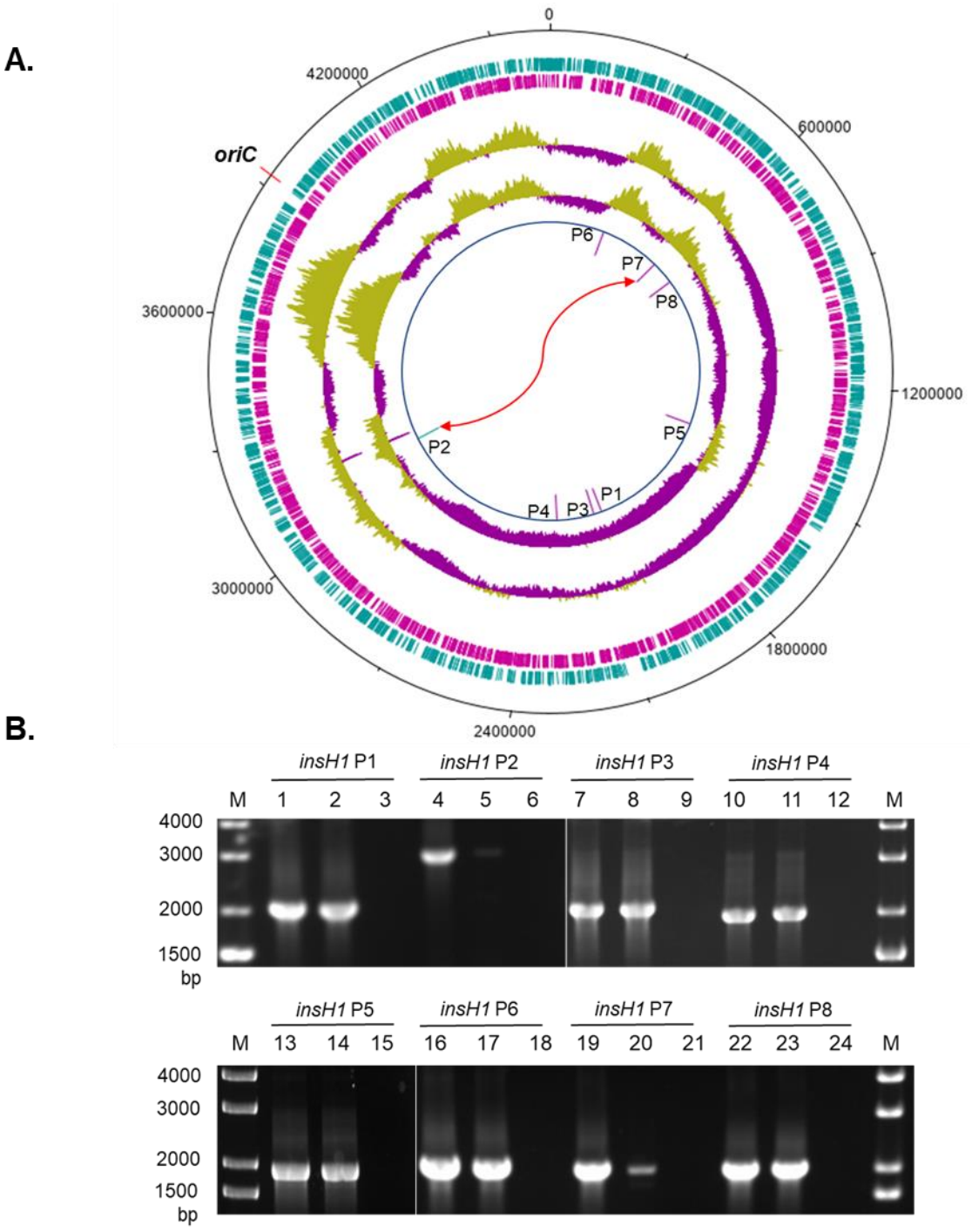

Figure 5: A large inversion in the genome of the DOC14 mutant. A) Structural map of the reference genome BW25113. The features were represented in circular plots counted from the outside to center as follows: the outermost ring 1, coordinates of the reference genome; 2, plus-strand CDS (cyan); 3, minus strand CDS (magenta); 4, genome coverage of the parental strain; 5, genome coverage of the DOC14 mutant, yellow (above average) and purple (below average); 6, *insH1* sites tested for hypothetical inverted-repeated mediated homologous recombination, on plus strand (cyan), on minus strand (magenta).

The red arrow indicates the inversion present in the DOC14 mutant. B) Amplification of the eight *insH1* sites hypothesized to be involved in homologous recombination in the DOC14 mutant. Each set of three lanes includes the parental strain, the DOC14 mutant and a non-template control. M, 1 kb plus DNA ladder (Thermo Scientific).

The primers flanking the *insH1* sites P2 and P7 are expected to give products if the inversion has brought them to proximity. If so, the P2 forward primer and P7 forward primer are relocated to amplify a 2000 bp product, the P2 reverse primer and P7 reverse primer can amplify a 3000 bp product (Fig. 6A). To positively identify this rearrangement, we performed two sets of PCR assays that contained three primers, of which two would enable positive amplification of either the parent or the predicted recombinant, each giving a product of a specific predicted size, as illustrated in Fig. 6A. In the PCR reaction containing the P2 primer pair and P7 forward primer, the parental strain showed a major product at 3000 bp, corresponding to the distance between the P2 forward and reverse primers in the wild-type configuration, whilst the DOC14 mutant showed a 2000 bp band, as expected for the distance between the P2 forward and P7 forward primer after recombination between these two *insH1* sites (Fig. 6B). The product lengths expected from the wild-type and invertant were also obtained in the PCR reaction probing flanking sequences around the P7 *insH1* site (containing the P7 forward and reverse primer pair and P2 reverse primer; Fig. 6B). Taken together, our data supports the conclusion that the genome of the DOC14 mutant possesses a DNA inversion, relative to the parental genome, that arose through a recombination event between the *insH* P2 and *insH* P7 loci. As no other difference was identified between DOC14 and the parent, it appears that the inversion event is responsible for the increased DOC resistance in this mutant.

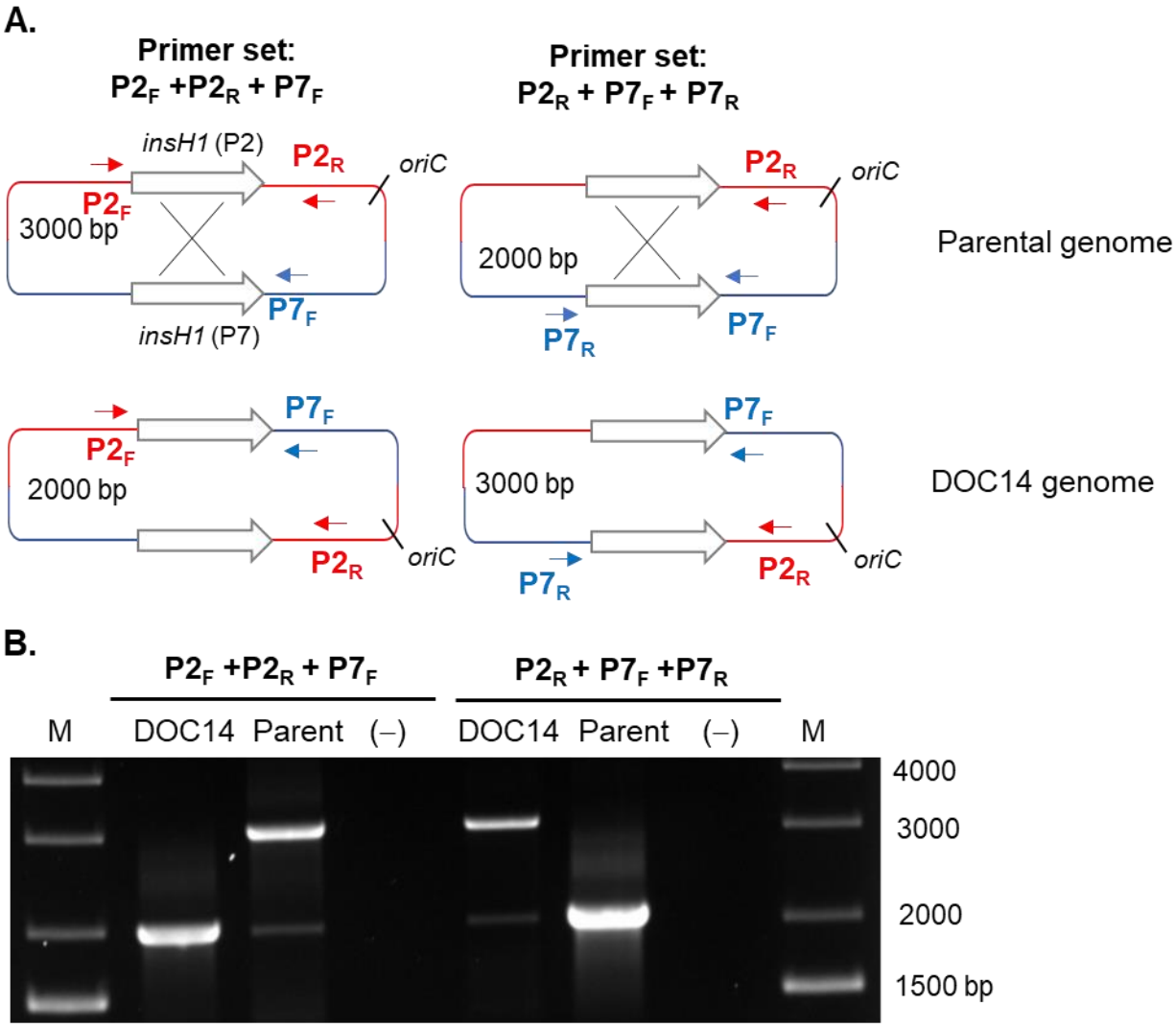

Figure 6: Three-primer PCR to confirm the genome inversion in the DOC14 mutant. A) Schematic illustration of the relative positions of PCR primers on the genomes of the parental strain and the DOC14 mutant. The expected size of PCR amplicons was labelled inside the genome when three primers are combined in the PCR reactions. Genome color: red, the left arm of the chromosome; blue, the right arm of the chromosome. $P2_F$, *insH1* P2 forward primer; $P2_R$, *insH1* P2 reverse primer; $P7_F$, *insH1* P7 forward primer, $P7_R$, *insH1* P7 reverse primer. Red arrows, P2 primers; blue arrows, P7 primers. B) Agarose gel analysis of PCR products amplified by three-primer combinations. Each set of three lanes includes the DOC14 mutant, the parental strain (BW25113 Δ*tolC*), and a non-template control. M, 1kb plus DNA ladder (Thermo Fisher Scientific).

Fitness cost of DOC-resistance-causing mutations

We examined the effect of deletion mutants of genes analyzed in this work, *ptsI*, *cyaA*, *crp*, *ndh* and *tktA*, as well as the spontaneous multi-gene deletion mutant DOC13

(containing a deletion around the CP4-6 prophage) on the cell fitness by monitoring their growth continuously over 24 h (Fig. 7A). We found that disruption of *ptsI*, *crp* or *ndh*, or the large deletion around the CP4-6 prophage in the DOC13 mutant caused a slight increase (by 1 or 2 min) in the doubling time of the corresponding strain in comparison to that of the parental strain (doubling time = 23.6 min) (Fig. 7B). In contrast, a profound burden on the bacterial growth was observed in the Δ*tktA* strain whose doubling time was increased by as much as 10 minutes relative to the parental strain. Changes in the growth fitness upon mutations were also reflected through the optical density at stationary phase cultures. After 24 h of incubation, the optical density at 600 nm of the Δ*cyaA* or Δ*crp* strains was significantly lower than that of the parental strain (Fig. 7A and C).

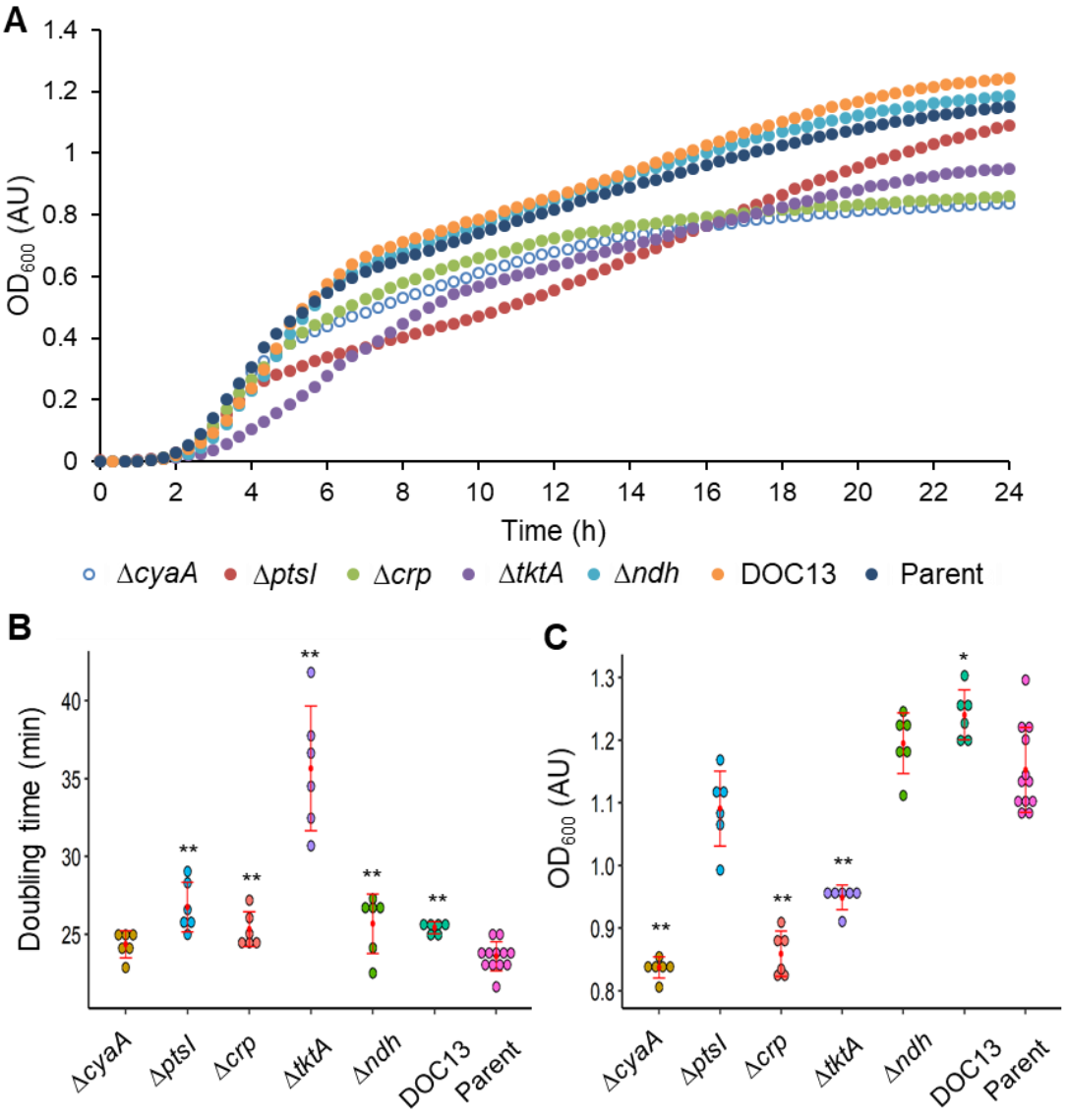

Figure 7: Fitness cost of DOC resistance causing mutations. A) The bacterial growth curve over 24 h of incubation at 37°C. The OD_{600} was measured every 20 minutes. B) Doubling time at the exponentially growing phase of bacterial cultures. C) Absorbance at 600 nm of bacterial cultures after 24 h of incubation at 37 °C. The error bar represents mean ± standard deviation of at least six replicates. Parental strain, BW25113 Δ*tolC*. Statistical significance was determined using Student's t-test (* $p < 0.05$, ** $p < 0.01$).

Discussion

In this study, we have isolated and characterized DOC-resistant mutants from an *E. coli* K-12 strain in which seven efflux pumps, AcrAB-TolC, AcrAD-TolC, AcrEF-TolC,

MdtABC-TolC, MdtEF-TolC, EmrAB-TolC and MacAB-TolC were inactivated by deletion of the gene encoding the common outer membrane component, TolC (113). The deletion of efflux pumps eliminated the chance of isolating resistance mutations associated with overexpression of efflux pumps whose correlation with DOC resistance has been well characterized. Also, this allowed simulation of DOC resistance/action in *E. coli* when DOC is co-administered with a TolC-efflux-pump inhibitor.

Whole genome sequence analyses of twenty independent *E. coli* mutants selected for their enhanced DOC resistance showed frequent mutations in the *cyaA* and *ptsI* genes (Table 1). The former encodes adenylate cyclase and the latter gene encodes Enzyme I (EI) of the PTS system. Proteins encoded by both of these genes are involved in adjustment of the intracellular cAMP level, a universal cell-signaling second messenger. In *E. coli*, adenylate cyclase (CyaA) catalyzes the formation of cAMP from ATP; thus, it is apparent that disruption of the CyaA-encoding gene leads to a drop in the cAMP level. The situation for PtsI is more complex. This enzyme transfers a phosphate group from phosphoenolpyruvate (PEP) to the Hpr protein which then phosphorylates a sugar-specific component of PTS system, including the glucose-specific protein IIA^{Glc}, an adenylate cyclase-activating enzyme when phosphorylated (180). Therefore, we hypothesized that the *ptsI* loss-of-function mutations result in a drop in the amount of phosphorylated IIA^{Glc}, which in turn causes a low adenylate cyclase activity and thus a decline in cAMP levels. This argument is in agreement with the reported considerable drop in cAMP level in an *E. coli* mutant with a defective PTS system (181). Additionally, we showed that the knock-out mutation of the *crp* gene encoding the cAMP-dependent transcription factor caused the same effect as *cyaA* or *ptsI* mutations, further emphasizing the role of cAMP in enhanced DOC resistance. An intriguing question is that of the potential role of the Crp-cAMP level in mediating resistance to

DOC. The Crp-cAMP regulatory complex controls the expression of a large number of genes, covering a wide range of cellular functions, such as sugar transport and metabolism, aerobic respiration and expression of a number of transcriptional regulators which, in turn, control expression of other genes (172). It is highly likely that the enhanced DOC resistance results from the integration of multiple pathways regulated by Crp-cAMP, some of which might have opposing or compensatory effects, that collectively allow resistance-causing mutations to occur with a minimal fitness cost. Analyses of the downstream effect(s) cascaded from the Crp-cAMP regulator might reveal some pathways/proteins that are targets of DOC action or mediate resistance to this antibacterial molecule.

It is also worth mentioning that the majority of *cyaA* and *ptsI* mutations found in the DOC^R mutants were missense mutations that all caused a loss-of-function phenotype of the corresponding protein. This provides a useful source of information about the important residues for the study of the structure and function of CyaA and PtsI, especially for the former protein, a class I adenylate cyclase, whose structure has not yet been solved.

An increased DOC resistance was also caused by a knock-out mutation of *ndh* or *tktA*. Tran *et al.* (182) found that a loss of the *ndh* gene led to a 4.5-fold reduction in the electron transport from NADH to oxygen. Provided that the electron transport chain is a source of reactive oxygen species (ROS) which play important roles in bacterial death caused by bactericidal antibiotics (183, 184), a decrease in the electron transport rate would lower the burden of the oxidative stress imposed by DOC exposure (98, 185). A similar explanation can be applied to the *tktA* mutation. Null mutations in *tktA* led to a lower growth rate (Fig. 7) from two possible causes: intracellular accumulation of the toxic metabolite methylglyoxal (186) and a shortage of glycerol-3-phosphate, an

essential precursor for phospholipid biosynthesis (176). The slowed growth may mitigate the activity of DOC by alleviating generation of ROS from the bacterial electron transport chain.

In the DOC13 mutant, a large deletion was identified that affected the 24 genes from *frsA* to *ykfC* (Fig. 4); Many of the missing genes encode products with poorly understood functions. The gene whose loss was responsible for selective advantage upon DOC exposure remains to be identified.

We described the asymmetrical chromosome inversion in the DOC14 mutant that occurred by homologous recombination between identical and oppositely orientated insertion sequences *insH1* (Fig. 5). This inversion was mapped by combination of sequence analyses of the chromosomal DNA extracted from exponentially growing cultures and a series of diagnostic PCR assays (Figs. 5 and 6). Theoretically, an asymmetric genome inversion would move some genes closer to the origin of replication *oriC* (the genes downstream of the *insH1* P7 gene) and thus increase their copy number and expression during the exponential phase due to a replication-associated gene dosage effect. By contrast, the genes upstream of the *insH1* P2 site were moved away from *oriC* by inversion and therefore have a decreased copy number and expression level during the exponential phase. However, such a simple scheme cannot be applied to the genome inversion in the DOC14 mutant. The gene dosage profile in the DOC14 mutant and the parental strain has more than one peak, and none of them was found to be located at the *oriC* site (Fig. 5A). This phenomenon complicates the prediction of which metabolic changes in the DOC14 mutant lead to DOC enhanced resistance. Also, such a gene dosage pattern is reminiscent of *oriC*-independent chromosome replication initiations. Irregular replication initiations have been reported in *E. coli* mutants deficient in *rnhA*-encoded RNase HI or *recG*-encoded DNA

translocase in which DNA replication initiations were shown to take place from R-loops in the former mutant or replication fork fusion in the latter (187, 188). Nonetheless, the gene dosage profile (or replication profile) upon the *tolC* deletion was significantly different from those seen in the *rnhA* or *recG* deletions, which had a prominent replication initiation at the termination region and a functional *oriC*. By contrast, we found that the *tolC* mutant appeared to have an inactive *oriC*, rather initiating DNA replication at the chromosome coordinates of approximately 0.3, 0.5 3.2, 3.7, 4.3 and 4.5 Mb that are in the 2/3 of the chromosome around *oriC* (Fig. 5A). Perhaps, the *tolC* deletion interferes with the regulation of DNA replication, including *oriC*-firing-related functions and prevention of uncanonical DNA replication initiations. This surprising observation expands the functions of the TolC-associated efflux pumps. Inactivation of *tolC* not only affects the efflux pump activity directly, but also causes a global effect by changing the gene dosage profile in the exponential phase. Further studies are warranted to provide a better insight into the involvement of *tolC* in DNA replication.

Returning to the DOC-resistance selection, it is worth noting that we attempted but failed to identify any single gene responsible for significant DOC resistance in the Δ*tolC* strain. This implies that the emergence of DOC resistance is prevented in the absence of efflux pumps. Possible reasons for the lack of specific mutations responsible for significant resistance could be that DOC affects multiple cellular targets simultaneously, including DNA, cellular membrane and protein structures (97, 98) or that its cognate targets are essential proteins and the mutations in them are lethal. Notably, mutations that resulted in low-level DOC resistance were associated with a decreased growth rate or a lowered stationary phase cell density (Fig. 7). Taken together, these data support the development of slower metabolic rate as a mechanism for increased resistance to DOC in the absence of efflux pumps. A practical outcome of

our work is the finding that there was no evolution of DOC resistance in the absence of TolC-associated efflux pumps, suggesting that combinations of DOC and an efflux pump inhibitor acting through TolC to combat enteric Gram-negative pathogens will be immune from developing resistance outside of the potential the efflux pump target mutations and acquisition of horizontally transferred DNA.

Materials and methods

Bacterial strains, growth conditions and antibiotics

All *E. coli* strains and plasmids used in this study are listed in Table 3 and 4**.** Introduction of the complete CDS-*kan*^{R} replacement alleles from the corresponding Keio collection *E. coli* K12 knock-out strains into the strain JW5503 (BW25113 Δ*tolC*) (115) was performed using the P1 phage transduction, according to the standard procedures (116). To eliminate potential polar effects on downstream genes in the operon, the FRT-flanked *kan*^{R} cassette was then removed using FLP-mediated recombination as previously described (117). Plasmids derived from pCA24N bearing the gene to be tested were purified from *E. coli* strains of the ASKA collection containing ORF expression constructs derived from this organism (118) using the ChargeSwitch-Pro Plasmid Miniprep Kit (Thermo Fisher Scientific). The plasmid DNA was then chemically transformed into specific *E. coli* strains for further work (119). In the case of P1 phage-mediated transduction of the Δ*crp*::*kan* mutation from Keio strain JW5702 to the Δ*tolC* strain, the position of *crp* (3479479-3480111) is close to *tolC* (3171474-3172955), permitting an undesirable reintroduction of the intact *tolC* allele along with Δ*crp::kan* into the Δ*tolC* strain in some transductants. Replica plating of putative transductants on Kan- and DOC-selective agar (50 µg/mL and 1 mg/mL, respectively) was used to screen for the Δ*tolC* Δ*crp::kan* recombinants which grew on Kan-selective agar but did not grow on DOC-selective plates.

E. coli cultures were grown in 2xYT medium (BD Difco) at 37°C with shaking at 200 rpm. To prepare exponential phase cultures, fresh overnight cultures were diluted 100-fold and incubated at 37°C to reach the OD_{600nm} of about 0.1-0.4. This cell suspension was then diluted to the desirable concentration, depending on specific purposes. Antibiotics used in this study were purchased from GoldBio and sodium deoxycholate was provided by New Zealand Pharmaceuticals Ltd.

Table 3: List of *E. coli* strains used in this study

Strain	Genotype	Source
BW25113	*rrnB3* Δ*lacZ4787 hsdR514* Δ*(araBAD)567* Δ*(rhaBAD)568 rph-1*	(115)
JW5503	BW25113 Δ*tolC*	(115)
K2535	BW25113 Δ*tolC* Δ*cyaA*	This study
K2536	BW25113 Δ*tolC* Δ*ptsI*	This study
K2537	BW25113 Δ*tolC* Δ*tktA*	This study
K2538	BW25113 Δ*tolC* Δ*ndh*	This study
K2545	BW25113 Δ*tolC* Δ*cyaA* pCA24N::*cyaA*	This study
K2546	BW25113 Δ*tolC* Δ*cyaA* pCA24N	This study
K2540	BW25113 Δ*tolC* Δ*ptsI* pCA24N::*ptsI*	This study
K2541	BW25113 Δ*tolC* Δ*ptsI* pCA24N	This study
K2542	BW25113 Δ*tolC* Δ*tktA* pCA24N::*tktA*	This study
K2543	BW25113 Δ*tolC* Δ*tktA* pCA24N	This study
K2544	BW25113 Δ*tolC* Δ*ndh* pCA24N::*ndh*	This study
K2547	BW25113 Δ*tolC* Δ*ndh* pCA24N	This study
K2548	BW25113 Δ*tolC* Δ*crp*::*kan*	This study

K2554	BW25113 Δ*tolC* Δ*crp*::*kan* pCA24N::*crp*	This study
K2555	BW25113 Δ*tolC* Δ*crp*::*kan* pCA24N	This study

Table 4: List of plasmids used in this study

Plasmid	Genotype or description	Source
pCP20	Amp^R, Cm^R, FLP^+, λ cI857$^+$, λ p_R Rep^{ts} For removal of an *frt*-flanked *kan* marker from *E. coli* K-12 strains by FLP-mediated site-specific recombination.	(122)
pCA24N	Vector control for ASKA collection plasmids	(118)
pCA24N-*cyaA*	Cm^R; *lacI*^{q}, pCA24N $P_{T5\text{-}lac}$::*cyaA* Δ*gfp*	(118)
pCA24N-*ptsI*	Cm^R; *lacI*^{q}, pCA24N $P_{T5\text{-}lac}$::*ptsI* Δ*gfp*	(118)
pCA24N-*tktA*	Cm^R; *lacI*^{q}, pCA24N $P_{T5\text{-}lac}$::*tktA* Δ*gfp*	(118)
pCA24N-*ndh*	Cm^R; *lacI*^{q}, pCA24N $P_{T5\text{-}lac}$::*ndh* Δ*gfp*	(118)
pCA24N-*crp*	Cm^R; *lacI*^{q}, pCA24N $P_{T5\text{-}lac}$::*crp* Δ*gfp*	(118)

Selection for DOC resistant mutants

E. coli mutants with enhanced DOC resistance were selected from the *E. coli* overnight cultures of the parental strain JW5503 (BW25113Δ*tolC*). Briefly, independently set cell cultures (from separate single colonies) were spread each onto three selective 2xYT plates containing 100 µg/mL, 125 µg/mL and 150 µg/mL of DOC (100 µL per plate). The plates were incubated at 37°C and growth was examined after 24 h and 48 h of incubation. Colonies formed on these plates were sub-cultured onto 2xYT agar and incubated overnight at 37°C. Only one colony was collected from each original culture to minimize the chance of identifying the same mutation. The putative resistant mutants

were examined for increased MIC_{DOC} using an antimicrobial agar dilution assay before further analysis.

Antimicrobial susceptibility assay

DOC susceptibility of the *E. coli* K-12 parental strains and selected progeny DOC^R mutants were examined using agar dilution assays as previously described (158). Briefly, 10 µL of exponential phase cultures at 10^6 CFU/mL was pipetted onto agar plates containing 150, 125, 100, 75, 50 and 25 µg/mL of DOC. Lower DOC concentrations were included in some assays when particular strains did not grow on the lowest DOC concentrations (25 µg/mL). The agar plates without DOC were used as negative controls. Each treatment was performed in triplicate. The plates were incubated at 37°C for 16-20 h before assessing bacterial growth. The MIC was defined as the lowest DOC concentration which completely inhibits bacterial growth.

For complementation assays, the expression of a gene to be tested (*cyaA*, *ptsI*, *tktA*, *ndh* and *crp*) was driven from a T5-*lac* chimeric promoter of the high-copy-number pCA24N expression vector (118). Chloramphenicol at 25 µg/mL was included in the medium to maintain the pCA24N plasmid and its derivatives. For the genes *cyaA*, *ndh* and *crp*, basal expression from the uninduced promoter was used since their higher expression was found to be toxic to the growth of the corresponding complemented strain. Expression of *tktA* was induced by 0.1 mM IPTG. For the *ptsI* complementation assay, chloramphenicol was not included in the antimicrobial agar (see explanation in the results) and expression of *ptsI* was induced by 0.1 mM IPTG.

Comparative genome analysis

The genomic DNA of DOC resistant mutants and the parental strain *(*Δ*tolC E. coli* strain) was extracted from their overnight cultures using the UltraClean Microbial DNA Isolation Kit according to the manufacturer's instructions (Qiagen). Purified

chromosomal DNA samples were then submitted to the Massey Genome Service (Massey University, Palmerston North, New Zealand) for whole genome sequencing using an Illumina TruSeq Nano DNA library preparation and 2 x 300 base paired-end v3 sequencing on the Illumina MiSeq™ platform. The raw reads were trimmed to a quality cut-off value of Q30 (equivalent to error probability p = 0.001) and the short-length reads (< 25 bases by default) were removed using SolexaQA^{++} v3.1.7.1 (146). The remaining reads resulted in a theoretical genome coverage that was at least 46 × based on the *E. coli* strain BW25113 genome size. The trimmed reads were aligned with the *E. coli* BW25113 reference genome (ASM75055v1 from the Ensembl genome database) using Bowtie2 v2.3.2 in the --very-sensitive mode (148). The resulting alignment *.sam* files were then converted to *.bam* files using samtools v1.5 (149) and variant calling was performed with FreeBayes v1.0.2 using the default parameters, except ploidy was set to 1 (-p 1) (150). Subsequently, the variants were annotated using SnpEff v4.3p (151) and examined manually using the Integrative Genomics Viewer v2.5.0 (189). The *cyaA* and *ptsI* mutations were labeled on the corresponding protein domains using the visualization software DOG v2.0.1 (152, 174, 190).

To determine any structural variants in the genome of DOC-resistant mutants, the unmapped reads were extracted using samtools v1.5 (149) and then assembled to generate contigs using the genome assembler software SPAdes v3.9.0 in the --careful mode (153). The resulting contigs was compared with the *E. coli* reference genome BW25113 (Accession No. CP009273.1) using the website platform NCBI Nucleotide BLAST 2.7.0+ (155) to determine the boundaries where the structure variants have occurred.

In another experiment, the genomic DNA of the DOC14 mutant and the parental strain was extracted from exponentially growing cultures using the UltraClean Microbial

DNA Isolation Kit (Qiagen). The exponential-phase cultures were obtained by diluting an overnight culture 100-fold with fresh 2xYT medium and incubating the diluted cultures with shaking for 1.5 hours at 37 °C. The genomic DNA was also sequenced, quality-trimmed and aligned with the reference genome BW25113 as described above. The genome coverage information at individual coordinates was extracted from the *.bam* alignment file using bedtools v2.28.0 (genomecov -d) (191). The genome coverage data of the DOC14 mutant and parental strain was plotted in circular maps using the visualization tool DNAPlotter v18.0.2 (192). Hypothetical homologous recombination events mediated by inverted repeats longer than 500 bp were predicted using the software Repseek v6.6 (-l 500 -c -i) with the BW25113 reference genome sequence (178).

Gene-specific PCR and sequence analysis

Genomic DNA extraction from bacterial colonies for analysis by PCR was carried out using the rapid boiling method as previously described (156). For the genes involved in DOC resistance, the PCR reactions were performed using the PrimeSTAR™ DNA Polymerase (Takara Bio USA), based on the melting temperatures of the primers as directed by the manufacturers; DNA was included at 1/10 reaction volume (5 µL in 50 µL). For the *insH1* loci in the DOC14 mutant and the parental strain, the PCR assays were performed with the DreamTaq™ Hot Start DNA Polymerase (Thermo Fisher Scientific) according to the manufacturer's instructions. The primers used for PCR and Sanger sequencing are listed in Table 5 and 6, and were designed using Primer-Blast (193).

The PCR amplicons were purified using the ChargeSwitch™-Pro PCR Clean-Up Kit (Invitrogen) according to the manufacturer's instructions and analyzed by Sanger sequencing using the Big Dye Terminator v3.1 chemistry at the Massey University

Genome Service (Palmerston North, New Zealand). Low-quality bases of raw sequences were trimmed using Chromas v2.6.4 (Technelysium Pty Ltd.) until the average quality of 20 consecutive bases was over 30. The trimmed sequences were then aligned with the *E. coli* reference genome BW25113 (Accession No. CP009273.1) using the website platform NCBI Nucleotide BLAST 2.7.0+ (155) to determine the presence of mutations in the genes under examination.

Table 5: List of primers used in PCR and Sanger sequencing

Primer name	**Sequence (5' to 3')**	**Expected size of amplicons (bp)**
***cyaA* forward**	TAC GGT CAA TCA GCA AGG TGT	1305
***cyaA* reverse**	TTA GCG CGG TTA TCG AGC AT	
***ptsI* forward**	GAA GGC GAA GAC GAG CAG AA	1781
***ptsI* reverse**	CGT TGT CGG TTG AGC AAG AG	
***tktA* forward**	AAC CAT CAC CTG ACG CTG TT	1258
***tktA* reverse**	CCT GTG GCG TGA TTT CCT GA	
***ndh* forward**	GTA CCT GAT GCG CTC CGA AT	1691
***ndh* reverse**	CCG CCA GTG TAC GTC GAT TA	
CP4-6 forward	CAA CAA AAA GCC TGT GCG GA	16585
CP4-6 reverse	GCC AGA TAC AAG GGG TTG CT	
***ybhQ* forward**	GTT CCG GCA AAA TGA AGC GT	909
***ybhQ* reverse**	TGG TGG GAT TCG GTC TGT TG	

Table 6: *insH1* primers to examine the DNA inversion in the DOC14 mutant

Primer sequence (5' to 3')	Genome coordinates	Expected size
F: AGG ATT TGC GAG GTA GCG AT	***insH1* P1**: 2059139-2061195	2057
R: CCG GGG CTG CAT TTT CTA TTC		
F: AGG GTG GTG TGT CAA AAC CTT	***insH1* P2**: 3123100- 3126146	3047
R: TTA TGA TGG ACC GGG GAT TGG		
F: TAC GCC GAT CTG TTG CTT GG	***insH1* P3**: 2094726- 2096854	2129
R: TCG TTT CCC ACG GAC ATG AA		
F: AAT AGC ACC GCC TGC TTT CT	***insH1* P4**: 2281942- 2283946	2005
R: TGT TTG AGC GTA GCG TTG GT		
F: TTC GTG CTA TGC GGA GTG AG	***insH1* P5**: 1421471- 1423431	1961
R: ATT TTC TGA GGC CAG CGT GT		
F: GGA TCA GTG ACG CAC GTT TC	***insH1* P6**: 269114- 271170	2057
R: CGC TCC AGT GGT GGA AAT GA		
F: TGT CAC TGG CAG GTA AGC AT	***insH1* P7**: 569656- 571670	2015
R: AGG ATT CGG TAT CGG TGC AA		
F: TCG AAA GTG CCG TTT TGC AG	***insH1* P8**: 682881- 684859	1979
R: GCT GAC GGC ATT GTT TGG TT		

F: Forward; **R**, Reverse

Bacterial growth analysis

Bacterial growth measurements were performed in 384-well microtiter plates without shaking. Each 50 µL exponential-phase culture (10^6 CFU/mL) was incubated at 37 °C and the $OD_{600\ nm}$ was monitored every 20 min for 24 h. Six replicates were included for each DOC-resistant mutant and twelve replicates for the parental strain. The doubling time estimation was implemented using the GrowthRates v3.0 software (194). The

differences in the doubling time and stationary phase cell density between the DOC^R mutants and the parental strain were assessed using Student's t-test and visualized using the R package ggplot2 v3.1.0 in the R statistical environment v3.5.3 (145, 195).

Acknowledgements

Vuong Van Hung Le has received funding from Callaghan Innovation PhD Scholarship. This work was supported by Massey University, the New Zealand Ministry of Business, Innovation and Employment and New Zealand Pharmaceuticals Ltd.

We thank New Zealand Pharmaceutical Ltd. for providing sodium deoxycholate, the Genetics Strains Research Center, National Institute of Genetics, Japan, for providing the ASKA collection and to the Massey University Genome Sequencing facility for the excellent genome sequencing service. The Keio Collection was purchased from Dharmacon (ThermoFisher, Australia).

Supplemental data

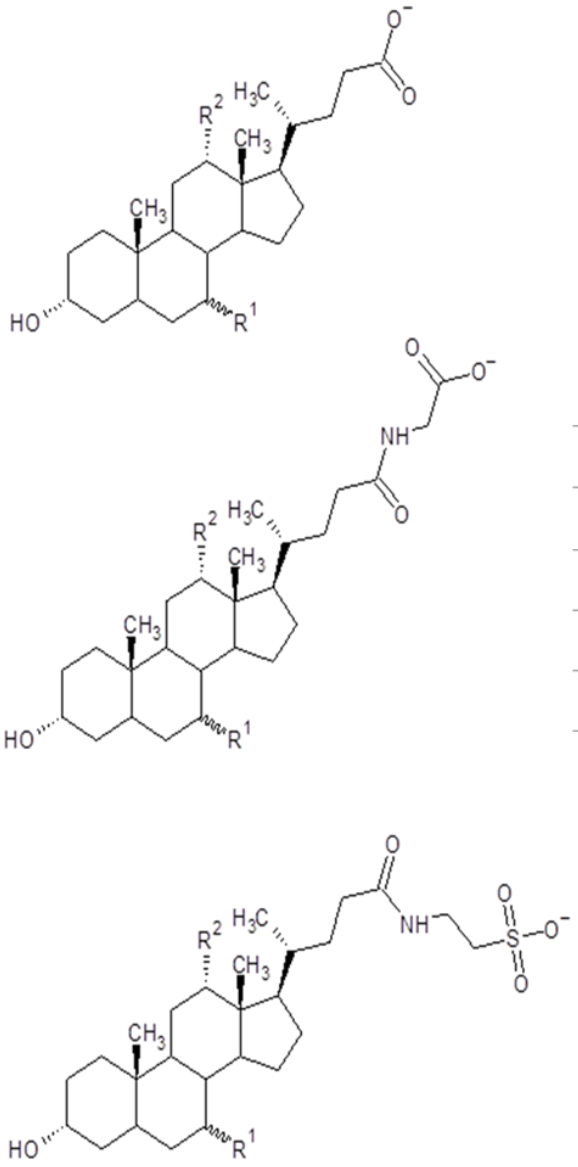

Bile salt	R^1	R^2
Cholate	α-OH	OH
Chenodeoxycholate	α-OH	H
Deoxycholate	H	OH
Ursodeoxycholate	β-OH	H
Lithodeoxcycholate	H	H

Figure S1: Molecular structure of unconjugated bile salts (top), glycine conjugated bile salt (middle) and taurine conjugated bile salt (bottom).

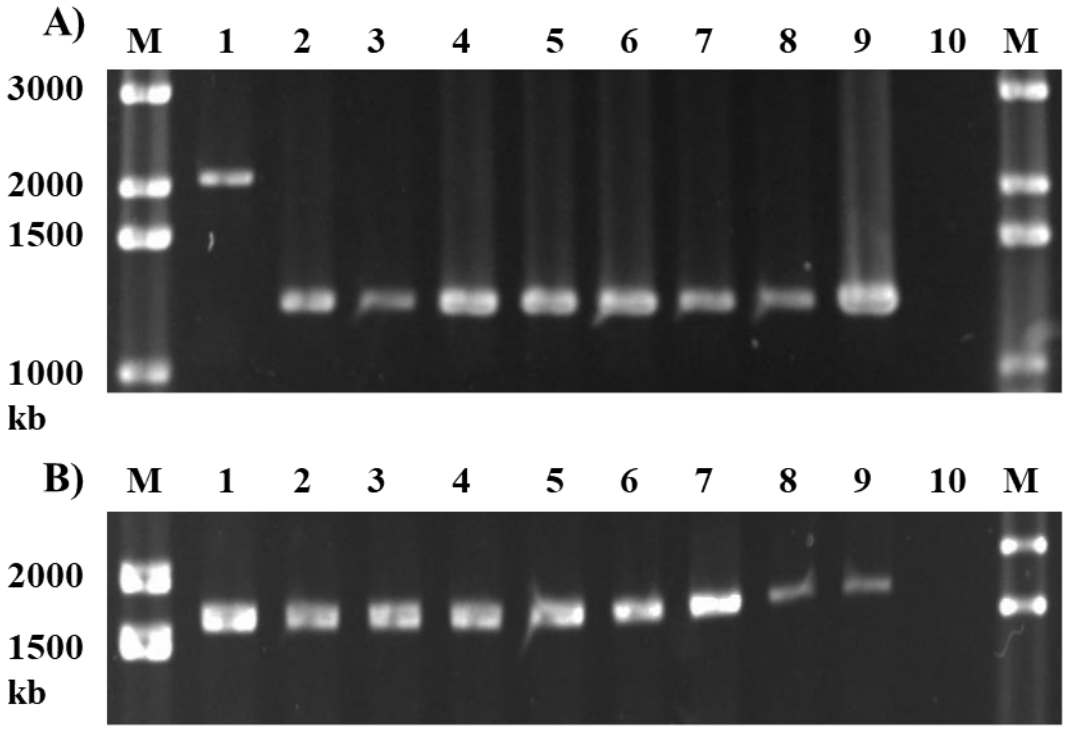

Figure S2: The PCR products of the *cyaA* gene (A) and *ptsI* (B) derived from the *E. coli* mutants with enhanced DOC resistance. Amplicons were analyzed using agarose gel electrophoresis. Gel (A); lanes M, 1 kb plus DNA ladder (Thermo Scientific); 1, DOC02; 2, DOC04; 3, DOC05; 4, DOC12; 5, DOC19; 6, DOC20; 7, DOC21; 8, DOC22; 9, parental strain; 10, non-template negative control. Gel (B); lanes M, 1 kb plus DNA ladder (Thermo Scientific); 1, DOC01; 2, DOC03; 3, DOC06; 4, DOC09; 5, DOC11; 6, DOC15; 7, DOC16; 8, DOC18; 9, parental strain; 10, non-template negative control.

Almost all *cyaA* and *ptsI* amplicons of the *E. coli* DOC^R mutants have similar size to that of the parental strain, with about 1300 bp for *cyaA* and 1700 bp for *ptsI*, in agreement with point mutations found in these mutants. The mutant DOC02 was an exception in which its *cyaA* amplicon was ~2100 bp in length, indicating the presence of an 800-nucleotide insertion in the *cyaA* gene. This fragment was identified to be an IS*1* sequence inserted at one nucleotide upstream of the *cyaA* open reading frame.

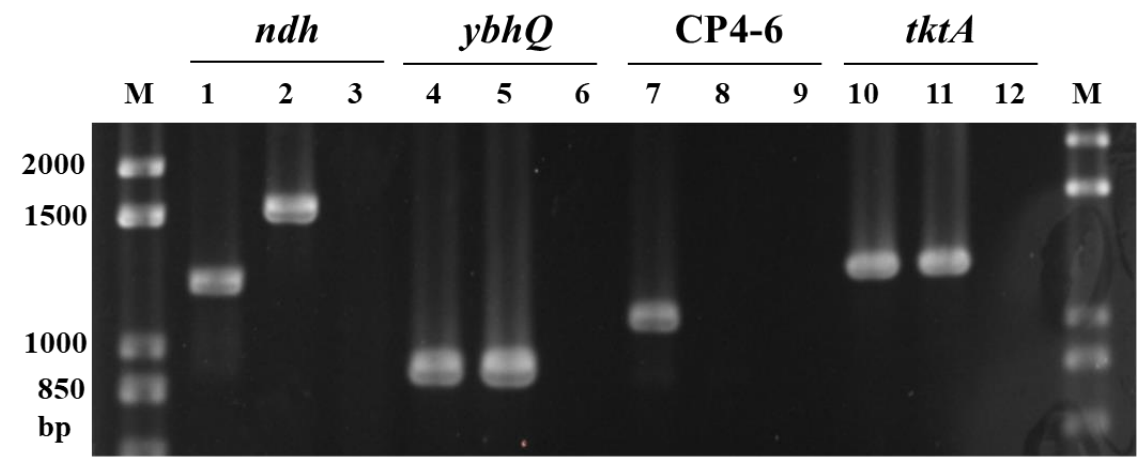

Figure S3: The PCR products of the genes *ndh*, *ybhQ*, CP4-6 fragment, and the gene *tktA* derived from the *E. coli* mutants with enhanced DOC resistance. Amplicons are analyzed using agarose gel electrophoresis. Lanes M, 1 kb plus DNA ladder (Thermo Scientific); 1, DOC07; 4, DOC07; 7, DOC13; 10, DOC17; lanes 2, 5, 8 and 11, parental strain BW25113 Δ*tolC*; lanes 3, 6, 9 and 12, non-template negative control.

The mutant DOC07 had a *ndh* amplicon at about 1300 bp that is smaller than that of the parental strain by about 400 bp. This is in agreement with 405-nucleotide deletion in the *ndh* gene found in the mutant DOC07. For the mutant DOC13, a pair of primers were designed to amplify the sequence flanking the deletion around the CP4-6 prophage (lane 7, ~1100 bp), whereas they were too far apart for the PCR reaction to occur in the parental strain (16585 bp).

Table S1: Hypothetical inverted-repeat-mediated inversion events predicted by Repseek v6.6 (repseek -l 500 -c -i). Yellow-highlighted events were tested by PCR amplification of eight *insH1* sites (P1 to P8). The homologous recombination event in the DOC14 mutant was colored blue.

No.	Position of the first copy	Position of the second copy	Length of the first copy	Length of the second copy	Spacers of the repeat	% identity between the two copies
1	19780	1045234	784	784	1024670	98.087
2	19788	3576787	777	777	1073693	99.485
3	19790	4508283	780	780	142196	89.872
4	206166	4346348	2087	2087	489200	68.597
5	219928	2722896	1950	1956	2126545	94.442
6	219954	3417017	5419	5408	1428998	98.708
7	222124	2719418	3249	3239	2130936	99.015
8	259070	2769008	2114	2115	2119416	80.405
9	261267	2763789	1246	1249	2127698	83.2
10	262486	2760967	2288	2288	2130700	85.066
11	266232	4497260	1257	1257	399184	98.886
12	269661	1390301	1200	1200	1119440	99.917
13	269662	3123505	1199	1199	1776427	99.917
14	274873	1045234	769	769	769592	99.48
15	274873	3576788	769	769	1328785	98.83
16	274873	4508285	773	773	397284	90.168
17	278007	4511973	2838	2846	394657	64.556
18	286345	1045225	776	777	758104	99.099
19	286345	3576788	768	768	1340258	98.828
20	286345	4508284	773	773	408757	90.168
21	310940	387165	1255	1255	74970	100
22	310940	1089698	1258	1258	777500	99.921
23	365991	4497255	1244	1244	498961	99.116

24	376714	2062422	1333	1333	1684375	100
25	376716	1462167	1331	1331	1084120	100
26	376716	2989711	1340	1340	2017134	99.776
27	387157	2163650	1268	1268	1775225	99.842
28	387159	562227	1270	1270	173798	99.921
29	476745	3652643	4268	4240	1451331	66.199
30	476760	3408389	3103	3100	1696740	72.353
31	476762	2580954	3098	3089	2101094	67.514
32	562232	1089700	1260	1260	526208	100
33	**570039**	**3123497**	**1211**	**1211**	**2076800**	**99.752**
34	570043	1390293	1207	1207	819043	99.834
35	575739	1630096	1080	1080	1053277	97.13
36	625393	4579903	1145	1145	675814	72.251
37	683302	1390289	1212	1212	705775	99.752
38	683303	3123494	1210	1210	2190068	99.669
39	1041336	4226989	2639	2642	1443174	62.74
40	1089701	2163651	1259	1259	1072691	100
41	1273461	1536949	1330	1327	262158	70.902
42	1275307	1531596	5268	5265	251021	75.654
43	1390293	3645390	1209	1209	2253888	99.752
44	1390297	2059637	1202	1202	668138	99.501
45	1390297	3358906	1208	1208	1967401	99.834
46	1390298	2095218	1210	1210	703710	99.669
47	1390298	2282395	1201	1201	890896	99.833
48	1390301	1421854	1197	1198	30356	91.5
49	1421854	3123505	1198	1197	1700453	91.5
50	1426465	1626783	2563	2563	197755	98.869
51	1462166	3179454	1333	1333	1715955	100
52	1462167	1645100	706	706	182227	100
53	1462167	4487996	1333	1333	1604307	99.925

54	1463529	4497274	1247	1247	1596477	99.198
55	1541641	4074593	4588	4607	2093910	72.382
56	1645100	2062422	706	706	416616	100
57	1645100	2989720	706	706	1343914	100
58	1891190	3251637	1371	1371	1359076	69.6
59	2059637	3123502	1201	1201	1062664	99.5
60	2062397	4487998	1356	1353	2204515	99.336
61	2062421	3179443	1344	1344	1115678	99.554
62	2095226	3123500	1204	1204	1027070	99.917
63	2282392	3123501	1205	1205	839904	99.751
64	2572998	3073006	1983	1983	498025	71.314
65	2601884	2838671	1128	1131	235659	72.591
66	2719385	4199702	3419	3430	1476898	98.542
67	2719390	4030757	3267	3279	1308100	98.537
68	2719411	4156204	5488	5498	1431305	98.636
69	2719418	3936795	3386	3395	1213991	98.527
70	2722906	4028524	1977	1977	1303641	97.674
71	2722908	3934794	1982	1983	1209904	97.781
72	2722908	4197746	1945	1938	1472893	95.536
73	2765362	3642573	1175	1176	876036	77.381
74	2922934	3251654	1356	1356	327364	70.066
75	2989708	3179454	1344	1346	188402	99.629
76	2989720	4487996	1333	1333	1496943	99.925
77	3123499	3358907	1209	1209	234199	99.752
78	3123502	3645390	1204	1204	520684	100
79	3128227	3630917	1589	1589	501101	75.377
80	3416979	4028581	5446	5458	606156	97.732
81	3417017	3936942	3239	3248	516686	99.169
82	3417021	4199849	3235	3245	779593	99.199
83	3417022	4158447	3234	3243	738191	99.291

84	3420512	4156277	1913	1921	733852	95.634
85	3420514	3934858	1911	1919	512433	95.994
86	3420514	4197773	1911	1911	775348	97.701
87	3463502	4165873	1186	1186	701185	98.988

Chapter V

General discussion

Increasing resistance prevalence to existing antibiotics has urged a coordinated action from industrial, academic and legislative sectors in an attempt to introduce novel antimicrobial therapies against infections (196). Unfortunately, conventional research and development of naturally occurring or semi-synthetic antibiotics that had once brought about the majority of scaffolds of currently used antibiotics during the golden age, no longer meets clinical demand due to the rapid emergence and global spread of antibiotic-resistant pathogens (3, 197). In such a dire context, alternative strategies are being explored to provide more therapeutic options for clinicians, including drug repurposing (198), antimicrobial combinations (22), revival of old antibiotics (199), bacteriophage and bacteriophage lysin therapies (200), antimicrobial peptides, antibodies, probiotics and fecal transplant (201).

In this thesis, I have investigated various combinations of DOC and 5-nitrofurans that synergistically act to inhibit the growth of or kill the enterobacterial species *E. coli*, *S. enterica* subsp. *enterica* serovar Typhimurium LT2 and *C. gillennii*. The findings are surprising and unpredictable for two reasons. Firstly, enterobacteria are inherently resistant to DOC, primarily through the activity of the multidrug efflux pump AcrAB-TolC combined with highly impermeable LPS outer membrane (81, 107). DOC antimicrobial activity against enterobacteria is therefore very minimal, as reflected by the high MIC_{DOC} ($\geq$ 40 mg/mL, Chapter 2, Fig. 1). Secondly, it has been reported that exposure of these enterobacterial cells to DOC or bile salt mixtures results in the increased expression of multidrug efflux pumps, down-regulation of outer membrane porins (OmpC, OmpF) and induction of diverse stress responses that render them resistant to DOC itself and antibiotics of different classes (e.g. polymyxin, ciprofloxacin, meropenem, tigecycline, chloramphenicol) (89, 92, 202-205). Based on

these DOC- or bile-induced effects, one may expect that combinations of an antibiotic with DOC would tend to be antagonistic rather than synergistic in inhibiting/killing enterobacteria.

In Chapter 2, we proposed that DOC and FZ, as a model molecule of 5-nitrofurans, act synergistically to inhibit the growth of *E. coli* via FZ-mediated inhibition of TolC-associated efflux pumps. Part of this inhibition activity was attributed to FZ-induced nitric oxide generation that subsequently inhibits the electron transport chain, disrupting the energy supply necessary for the operation of these efflux pumps. The evidence supporting these propositions was obtained from a genetic study. Further investigation into the effect of FZ on the efflux pump activity and the electron transport chain are required to validate the role of FZ as an efflux pump inhibitor (EPI) and clarify its mechanism.

One important mechanism of multidrug resistance in clinical bacterial isolates is expulsion of xenobiotics from the cells by efflux pumps with broad specificity (*e.g.* AcrAB-TolC) and mutations leading to increased expression of those efflux pumps (206, 207). There is no doubt that the development of an EPI could sensitize resistant clinical isolates to a wide range of antibiotics, making untreatable infections treatable. However, while an impressive number of EPI candidates have been reported *in vitro*, not a single one has entered clinical trials for various reasons such as low stability, narrow spectrum, high cytotoxicity and potentially undesirable pharmacokinetics (23, 208). The discovery of 5-nitrofurans as an EPI is very tempting since they are already approved drugs and thereby can be readily used as an EPI in at least three sites of infection: FZ in the intestine, NIT in the urinary tract and NFZ on the skin. Nevertheless, it is important to inspect, in advance, the pairwise interaction between 5-

nitrofuran drugs and other antibiotics that are substrates of the AcrAB-TolC efflux pump.

Another interesting finding is that simultaneous deletion of *nfsA* and *nfsB*, despite increasing the MIC for FZ, did not remove the synergy between DOC and FZ (Chapter 2, Fig. 6). This suggests a novel mechanism of FZ action that is independent of the two nitroreductases NfsA and NfsB and is responsible for the FZ-induced efflux pump inhibition. To discover the additional mechanism of FZ, we selected for FZ-resistant mutants arising from the Δ*nfsA* Δ*nfsB* strain and employed whole genome sequence analyses to identify mutations in these resistant mutants (Chapter 4). Interestingly, all detected mutations were located in the *ahpF* gene. Using 5-nitrofuran susceptibility assay for the *ahpF* deletion and overexpression strains and nitroreductase enzymatic assays with purified AhpF protein, we reported a novel activity of the AhpF enzyme to activate nitrofurans in a manner different from that of the established nitroreductase enzyme NfsB. An intriguing question is whether this enzyme is involved in the DOC/FZ synergy. Growth inhibition checkerboard assays for the Δ*ahpF* and Δ*nfsA* Δ*nfsB* Δ*ahpF* triple mutants created from the *E. coli* wildtype strain K1508 showed that deletion of the *ahpF* gene, regardless of the wildtype or *nfsA nfsB* null background, did not interfere with the DOC/FZ synergy (Chapter 5, Fig. 1). These results suggested that the mechanism of DOC/FZ synergy or, more specifically, the FZ-mediated efflux pump inhibition is also independent of the newly discovered nitroreductase AhpF. The original question remains to be answered in future studies: there are other unknown nitroreductase(s) in *E. coli* and/or antibacterial activity associated with the unreduced 5-nitrofuran “pro-drugs”. Stepwise selection for FZ resistance-conferring mutations from the Δ*nfsA* Δ*nfsB* Δ*ahpF* triple mutant followed by examination of the DOC/FZ synergy

in the resistant strains may cast more light on the mechanism of DOC/FZ interaction as well as 5-nitrofurans.

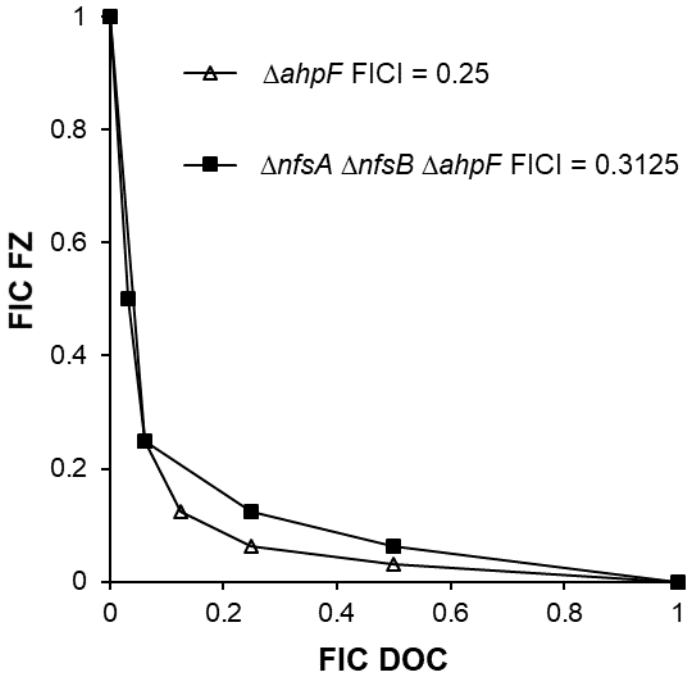

Figure 1: Effect of *ahpF* deletion on FZ-DOC synergy. Isobologram of FZ-DOC interactions in growth inhibition of the Δ*ahpF* mutant (K2504) and the Δ*nfsA* Δ*nfsB* Δ*ahpF* mutant (K2505). The knock-out mutants were created from the wildtype strain K1508. Each data point corresponds to the FIC (ratios of the 50 % growth inhibition concentrations in combination vs. alone) for FZ (y axis) and DOC (x axis).

A *tolC* knock-out was shown to cause a complete loss of DOC/5-nitrofuran synergy (Chapter 2, Fig. 3). However, this deletion also decreased the MIC for DOC by 256-fold (from 40000 µg/mL to 156.25 µg/mL). Therefore, removal of the DOC/5-nitrofuran synergy due to deletion of *tolC* would not influence the antibacterial efficacy of the combinatorial therapy. What is concerning is whether potential mutations would arise to restore DOC resistance once the TolC-associated pumps were inactivated. To answer that question, we selected mutants resistant to DOC from a Δ*tolC* strain, as described in Chapter 5. Mutants with low-level increased DOC resistance in comparison with the parental strain carried mutations in the *cyaA*, *ptsI*, *tktA*, or *ndh* genes. High-level DOC

resistance causing mutations were not identified. This observation supports the use of DOC/5-nitrofuran combinations given that it is rare, if any, to gain a high-level resistance to such combinations.

Overall, this thesis provided proof-of-concept evidence for the synergy between DOC and 5-nitrofurans in inhibiting/killing enterobacteria. Future work is warranted to expand the checkerboard assay towards a broader set of clinically relevant enterobacterial isolates, that is important to evaluate the coverage of the DOC/5-nitrofuran synergy and thereby, the clinical utility of the combination. Also, *in vitro* toxicology profiling and examination of the drug combination safety and efficacy in animal models are prerequisites to advance the combination along the development pathway.

Conclusion

This thesis has presented *in vitro* evidence of the synergy between DOC and 5-nitrofurans in eliminating enterobacterial species and proposed an underlying mechanism for that interaction. Combinations of DOC and 5-nitrofurans are promising additions to the therapeutic antimicrobial pipeline, although additional data, including *in vitro* toxicology and safety and efficacy in animal models are required before advancing to clinical trials.

A novel 5-nitrofuran activation enzyme, AhpF, was reported and its overexpression was capable of increasing nitrofuran sensitivity of the Δ*nfsA* Δ*nfsB* Δ*ahpF* strain to the same level as the wildtype strain. This discovery opens new avenues to counteract nitrofuran-resistant clinical isolates that, in most cases, have mutations in *nfsA* and *nfsB*, by screening for molecules that upregulate AhpF expression or catalytic activity, or designing nitrofuran analogues with high efficacy when activated by the AhpF enzyme.

This thesis also describes possible mutations that cause low-level DOC resistance in the *E. coli* strain deficient in TolC-dependent efflux pumps. These mutations are associated with decreased growth rate and fitness. Singe-step high-level DOC-resistance conferring mutations were not identified in the mutant screen, which supports investigating the use of DOC/nitrofuran combinations in clinical trials because of the scarcity of DOC resistance emergence when efflux pumps are inactivated by 5-nitrofurans.

Bibliography

1. O'Neill J. 2014. Antimicrobial Resistance: Tackling a crisis for the health and wealth of nations. The Review on Antimicrobial Resistance. https://amr-review.org/sites/default/files/AMR%20Review%20Paper%20-%20Tackling%20a%20crisis%20for%20the%20health%20and%20wealth%20of%20nations_1.pdf. Accessed 05-12-2019.
2. O'Neill J. 2015. Securing new drugs for future generations: The pipeline of antibiotics. The Review on Antimicrobial Resistance. https://amr-review.org/sites/default/files/SECURING%20NEW%20DRUGS%20FOR%20FUTURE%20GENERATIONS%20FINAL%20WEB_0.pdf. Accessed 05-12-2019.
3. Farrell LJ, Lo R, Wanford JJ, Jenkins A, Maxwell A, Piddock LJV. 2018. Revitalizing the drug pipeline: AntibioticDB, an open access database to aid antibacterial research and development. J Antimicrob Chemother 73:2284-2297.
4. Dam S, Pages JM, Masi M. 2018. Stress responses, outer membrane permeability control and antimicrobial resistance in *Enterobacteriaceae*. Microbiology 164:260-267.
5. Masi M, Refregiers M, Pos KM, Pages JM. 2017. Mechanisms of envelope permeability and antibiotic influx and efflux in Gram-negative bacteria. Nat Microbiol 2:17001.
6. Zgurskaya HI, Lopez CA, Gnanakaran S. 2015. Permeability barrier of Gram-negative cell envelopes and approaches to bypass It. ACS Infect Dis 1:512-522.
7. Li XZ, Plesiat P, Nikaido H. 2015. The challenge of efflux-mediated antibiotic resistance in Gram-negative bacteria. Clin Microbiol Rev 28:337-418.
8. Silver LL. 2016. A Gestalt approach to Gram-negative entry. Bioorg Med Chem 24:6379-6389.

9. Tacconelli E, Carrara E, Savoldi A, Harbarth S, Mendelson M, Monnet DL, Pulcini C, Kahlmeter G, Kluytmans J, Carmeli Y, Ouellette M, Outterson K, Patel J, Cavaleri M, Cox EM, Houchens CR, Grayson ML, Hansen P, Singh N, Theuretzbacher U, Magrini N, Group WHOPPLW. 2018. Discovery, research, and development of new antibiotics: the WHO priority list of antibiotic-resistant bacteria and tuberculosis. Lancet Infect Dis 18:318-327.

10. The-Pew-Charitable-Trusts. 2019. Antibiotics currently in global clinical development. https://www.pewtrusts.org/en/research-and-analysis/data-visualizations/2014/antibiotics-currently-in-clinical-development. Accessed 06/06/2019.

11. Bliss CI. 1939. The toxicity of poisons applied jointly. Annals of Applied Biology 26:585-615.

12. Loewe S, Muischnek H. 1926. Combinated effects I Announcement - Implements to the problem. Naunyn-Schmiedebergs Archiv Fur Experimentelle Pathologie Und Pharmakologie 114:313-326.

13. Foucquier J, Guedj M. 2015. Analysis of drug combinations: current methodological landscape. Pharmacol Res Perspect 3:e00149.

14. Yeh PJ, Hegreness MJ, Aiden AP, Kishony R. 2009. Drug interactions and the evolution of antibiotic resistance. Nat Rev Microbiol 7:460-466.

15. Odds FC. 2003. Synergy, antagonism, and what the chequerboard puts between them. J Antimicrob Chemother 52:1-1.

16. White RL, Burgess DS, Manduru M, Bosso JA. 1996. Comparison of three different *in vitro* methods of detecting synergy: time-kill, checkerboard, and E test. Antimicrob Agents Chemother 40:1914-1918.

17. Geary N. 2013. Understanding synergy. Am J Physiol Endocrinol Metab 304:E237-253.

18. Gomara M, Ramon-Garcia S. 2019. The FICI paradigm: Correcting flaws in antimicrobial in vitro synergy screens at their inception. Biochem Pharmacol 163:299-307.

19. Doern CD. 2014. When does 2 plus 2 equal 5? A review of antimicrobial synergy testing. J Clin Microbiol 52:4124-4128.

20. Bollenbach T. 2015. Antimicrobial interactions: mechanisms and implications for drug discovery and resistance evolution. Curr Opin Microbiol 27:1-9.

21. Taneja N, Kaur H. 2016. Insights into newer antimicrobial agents against Gram-negative bacteria. Microbiol Insights 9:9-19.

22. Bush K. 2017. Synergistic antibiotic combinations, p 69-88. *In* Fisher J.F. MS, Miller M.J. (ed), Antibacterials, vol I. Springer, Cham.

23. Tyers M, Wright GD. 2019. Drug combinations: a strategy to extend the life of antibiotics in the 21st century. Nat Rev Microbiol 17:141-155.

24. Mohammadi M, Attaran B, Malekzadeh R, Graham DY. 2017. Furazolidone, an underutilized drug for *H. pylori* eradication: Lessons from Iran. Dig Dis Sci 62:1890-1896.

25. Chen L, He J, Wang L, Ge Q, Chu H, Chen Y, Chen X, Long Y, Deng Y, He H, Li A, Chen S. 2018. Efficacies of different proton pump inhibitor-based 14-day bismuth-furazolidone quadruple regimens for the initial eradication of *Helicobacter pylori* in the southeast coastal region of China: an open-label, randomized clinical trial. Clin Exp Med 18:569-576.

26. Zhuge L, Wang Y, Wu S, Zhao RL, Li Z, Xie Y. 2018. Furazolidone treatment for *Helicobacter Pylori* infection: A systematic review and meta-analysis. Helicobacter 23:e12468.

27. Xie Y, Zhang Z, Hong J, Liu W, Lu H, Du Y, Wang W, Xu J, Wang X, Huo L, Zhang G, Lan C, Li X, Li Y, Wang H, Zhang G, Zhu Y, Shu X, Chen Y, Wang J, Lu N, Chinese Society of Gastroenterology Chinese Study Group on Helicobacter p. 2018. Furazolidone-containing triple and quadruple eradication therapy for initial treatment for *Helicobacter pylori* infection: A multicenter randomized controlled trial in China. Helicobacter 23:e12496.

28. Carter ER, Nabarro LE, Hedley L, Chiodini PL. 2018. Nitroimidazole-refractory giardiasis: a growing problem requiring rational solutions. Clin Microbiol Infect 24:37-42.

29. Goldman LM, Upcroft JA, Workowski K, Rapkin A. 2009. Treatment of metronidazole-resistant *Trichomonas vaginalis*. Sex Health 6:345-347.

30. Medina AM, Rivera FP, Pons MJ, Riveros M, Gomes C, Bernal M, Meza R, Maves RC, Huicho L, Chea-Woo E, Lanata CF, Gil AI, Ochoa TJ, Ruiz J. 2015. Comparative analysis of antimicrobial resistance in enterotoxigenic *Escherichia coli* isolates from two paediatric cohort studies in Lima, Peru. Trans R Soc Trop Med Hyg 109:493-502.

31. Martinez-Puchol S, Gomes C, Pons MJ, Ruiz-Roldan L, Torrents de la Pena A, Ochoa TJ, Ruiz J. 2015. Development and analysis of furazolidone-resistant *Escherichia coli* mutants. APMIS 123:676-681.

32. Passos SR, Rodrigues Tde A, Madureira AP, Giunchetti RC, Zanini MS. 2014. Clinical treatment of cutaneous leishmaniasis in dogs with furazolidone and domperidone. Int J Antimicrob Agents 44:463-465.

33. Concia E, Bragantini D, Mazzaferri F. 2017. Clinical evaluation of guidelines and therapeutic approaches in multi drug-resistant urinary tract infections. J Chemother 29:19-28.

34. Huttner A, Verhaegh EM, Harbarth S, Muller AE, Theuretzbacher U, Mouton JW. 2015. Nitrofurantoin revisited: a systematic review and meta-analysis of controlled trials. J Antimicrob Chemother 70:2456-2464.

35. Huttner A, Kowalczyk A, Turjeman A, Babich T, Brossier C, Eliakim-Raz N, Kosiek K, Martinez de Tejada B, Roux X, Shiber S, Theuretzbacher U, von Dach E, Yahav D, Leibovici L, Godycki-Cwirko M, Mouton JW, Harbarth S. 2018. Effect of 5-Day nitrofurantoin vs single-dose fosfomycin on clinical resolution of uncomplicated lower urinary tract infection in women: A randomized clinical trial. JAMA 319:1781-1789.

36. Price JR, Guran LA, Gregory WT, McDonagh MS. 2016. Nitrofurantoin vs other prophylactic agents in reducing recurrent urinary tract infections in adult women: a systematic review and meta-analysis. Am J Obstet Gynecol 215:548-560.

37. Muller AE, Verhaegh EM, Harbarth S, Mouton JW, Huttner A. 2017. Nitrofurantoin's efficacy and safety as prophylaxis for urinary tract infections: a systematic review of the literature and meta-analysis of controlled trials. Clin Microbiol Infect 23:355-362.

38. Chamberlain RE. 1976. Chemotherapeutic properties of prominent nitrofurans. J Antimicrob Chemother 2:325-336.

39. Hooper G, Covarrubias J. 1983. Clinical use and efficacy of furacin - a historical perspective. J Int Med Res 11:289-293.

40. Vass M, Hruska K, Franek M. 2008. Nitrofuran antibiotics: a review on the application, prohibition and residual analysis. Veterinarni Medicina 53:469-500.

41. Allen VL. 2018. Nitrofurazone 0.02% Nasal Solution/Spray. US Parmacist 43:2.

42. Balcao VM, Santos MG, Martins PR, Chaud MV, Oliveira Junior JM, Tubino M, Vila MM. 2014. Development and characterization of a gel formulation integrating microencapsulated nitrofurazone. Curr Pharm Biotechnol 14:1036-1047.

43. Vila MM, Coelho SL, Chaud MV, Tubino M, Oliveira JM, Jr., Balcao VM. 2014. Development and characterization of a hydrogel containing nitrofurazone for antimicrobial topical applications. Curr Pharm Biotechnol 15:182-190.

44. Shen CY, Shen BD, Liu X, Yuan HL. 2018. Nanosuspensions based gel as delivery system of nitrofurazone for enhanced dermal bioavailability. J Drug Deliv Sci Technol 43:1-11.

45. Liu X, Shen BD, Shen CY, Zhong RN, Wang XH, Yuan HL. 2018. Nanoparticle-loaded gels for topical delivery of nitrofurazone: Effect of particle size on skin permeation and retention. J Drug Deliv Sci Technol 45:367-372.

46. Johnson JR, Berggren T, Conway AJ. 1993. Activity of a nitrofurazone matrix urinary catheter against catheter-associated uropathogens. Antimicrob Agents Chemother 37:2033-2036.

47. Johnson JR, Delavari P, Azar M. 1999. Activities of a nitrofurazone-containing urinary catheter and a silver hydrogel catheter against multidrug-resistant bacteria characteristic of catheter-associated urinary tract infection. Antimicrob Agents Chemother 43:2990-2995.

48. Johnson JR, Johnston BD, Kuskowski MA, Pitout J. 2010. *In vitro* activity of available antimicrobial coated Foley catheters against *Escherichia coli*,

including strains resistant to extended spectrum cephalosporins. J Urol 184:2572-2577.

49. Regev-Shoshani G, Ko M, Crowe A, Av-Gay Y. 2011. Comparative efficacy of commercially available and emerging antimicrobial urinary catheters against bacteriuria caused by *E. coli in vitro*. Urology 78:334-339.

50. Johnson JR, Johnston B, Kuskowski MA. 2012. *In vitro* comparison of nitrofurazone- and silver alloy-coated foley catheters for contact-dependent and diffusible inhibition of urinary tract infection-associated microorganisms. Antimicrob Agents Chemother 56:4969-4972.

51. Pickard R, Lam T, MacLennan G, Starr K, Kilonzo M, McPherson G, Gillies K, McDonald A, Walton K, Buckley B, Glazener C, Boachie C, Burr J, Norrie J, Vale L, Grant A, N'Dow J. 2012. Antimicrobial catheters for reduction of symptomatic urinary tract infection in adults requiring short-term catheterisation in hospital: a multicentre randomised controlled trial. Lancet 380:1927-1935.

52. Menezes FG, Correa L, Medina-Pestana JO, Aguiar WF, Camargo LFA. 2018. A randomized clinical trial comparing Nitrofurazone-coated and uncoated urinary catheters in kidney transplant recipients: Results from a pilot study. Transpl Infect Dis 21:e13031.

53. Palma N, Pons MJ, Gomes C, Mateu J, Riveros M, Garcia W, Jacobs J, Garcia C, Ochoa TJ, Ruiz J. 2017. Resistance to quinolones, cephalosporins and macrolides in *Escherichia coli* causing bacteraemia in Peruvian children. J Glob Antimicrob Resist 11:28-33.

54. Lagunas-Rangel FA. 2018. Antimicrobial susceptibility profiles of bacteria causing urinary tract infections in Mexico: Single-centre experience with 10 years of results. J Glob Antimicrob Resist 14:90-94.

55. Bryce A, Costelloe C, Wootton M, Butler CC, Hay AD. 2018. Comparison of risk factors for, and prevalence of, antibiotic resistance in contaminating and pathogenic urinary *Escherichia coli* in children in primary care: prospective cohort study. J Antimicrob Chemother 73:1359-1367.

56. Cordoba G, Holm A, Hansen F, Hammerum AM, Bjerrum L. 2017. Prevalence of antimicrobial resistant *Escherichia coli* from patients with suspected urinary tract infection in primary care, Denmark. BMC Infect Dis 17:670.

57. Hitzenbichler F, Simon M, Holzmann T, Iberer M, Zimmermann M, Salzberger B, Hanses F. 2018. Antibiotic resistance in *E. coli* isolates from patients with urinary tract infections presenting to the emergency department. Infection 46:325-331.

58. Bouxom H, Fournier D, Bouiller K, Hocquet D, Bertrand X. 2018. Which non-carbapenem antibiotics are active against extended-spectrum beta-lactamase-producing *Enterobacteriaceae*? Int J Antimicrob Agents 52:100-103.

59. Shahbazi S, Asadi Karam MR, Habibi M, Talebi A, Bouzari S. 2018. Distribution of extended-spectrum beta-lactam, quinolone and carbapenem resistance genes, and genetic diversity among uropathogenic *Escherichia coli* isolates in Tehran, Iran. J Glob Antimicrob Resist 14:118-125.

60. Zhang X, Zhang Y, Wang F, Wang C, Chen L, Liu H, Lu H, Wen H, Zhou T. 2018. Unravelling mechanisms of nitrofurantoin resistance and epidemiological characteristics among *Escherichia coli* clinical isolates. Int J Antimicrob Agents 52:226-232.

61. McCalla DR, Kaiser C, Green MH. 1978. Genetics of nitrofurazone resistance in *Escherichia coli*. J Bacteriol 133:10-16.

62. Whiteway J, Koziarz P, Veall J, Sandhu N, Kumar P, Hoecher B, Lambert IB. 1998. Oxygen-insensitive nitroreductases: analysis of the roles of *nfsA* and *nfsB* in development of resistance to 5-nitrofuran derivatives in *Escherichia coli*. J Bacteriol 180:5529-5539.

63. Sandegren L, Lindqvist A, Kahlmeter G, Andersson DI. 2008. Nitrofurantoin resistance mechanism and fitness cost in *Escherichia coli*. J Antimicrob Chemother 62:495-503.

64. Zenno S, Koike H, Tanokura M, Saigo K. 1996. Gene cloning, purification, and characterization of NfsB, a minor oxygen-insensitive nitroreductase from *Escherichia coli*, similar in biochemical properties to FRase I, the major flavin reductase in *Vibrio fischeri*. J Biochem 120:736-744.

65. Zenno S, Koike H, Kumar AN, Jayaraman R, Tanokura M, Saigo K. 1996. Biochemical characterization of NfsA, the *Escherichia coli* major nitroreductase exhibiting a high amino acid sequence homology to Frp, a *Vibrio harveyi* flavin oxidoreductase. J Bacteriol 178:4508-4514.

66. Race PR, Lovering AL, Green RM, Ossor A, White SA, Searle PF, Wrighton CJ, Hyde EI. 2005. Structural and mechanistic studies of *Escherichia coli* nitroreductase with the antibiotic nitrofurazone. Reversed binding orientations in different redox states of the enzyme. J Biol Chem 280:13256-13264.

67. Roldan MD, Perez-Reinado E, Castillo F, Moreno-Vivian C. 2008. Reduction of polynitroaromatic compounds: the bacterial nitroreductases. FEMS Microbiol Rev 32:474-500.

68. Hall BS, Bot C, Wilkinson SR. 2011. Nifurtimox activation by trypanosomal type I nitroreductases generates cytotoxic nitrile metabolites. J Biol Chem 286:13088-13095.

69. McCalla DR. 1979. Nitrofurans, p 176-213. *In* Hahn FE (ed), Mechanism of action of antibacterial agents; Antibiotics, vol 5 / 1. Springer Berlin Heidelberg, Germany.

70. McOsker CC, Fitzpatrick PM. 1994. Nitrofurantoin: mechanism of action and implications for resistance development in common uropathogens. J Antimicrob Chemother 33 Suppl A:23-30.

71. Bertenyi KK, Lambert IB. 1996. The mutational specificity of furazolidone in the *lacI* gene of *Escherichia coli*. Mutat Res 357:199-208.

72. Ona KR, Courcelle CT, Courcelle J. 2009. Nucleotide excision repair is a predominant mechanism for processing nitrofurazone-induced DNA damage in *Escherichia coli*. J Bacteriol 191:4959-4965.

73. Mitosch K, Rieckh G, Bollenbach T. 2019. Temporal order and precision of complex stress responses in individual bacteria. Mol Syst Biol 15:e8470.

74. Peterson FJ, Mason RP, Hovsepian J, Holtzman JL. 1979. Oxygen-sensitive and -insensitive nitroreduction by *Escherichia coli* and rat hepatic microsomes. J Biol Chem 254:4009-4014.

75. Patterson S, Wyllie S. 2014. Nitro drugs for the treatment of trypanosomatid diseases: past, present, and future prospects. Trends Parasitol 30:289-298.

76. Begley M, Gahan CG, Hill C. 2005. The interaction between bacteria and bile. FEMS Microbiol Rev 29:625-651.

77. Wahlstrom A, Sayin SI, Marschall HU, Backhed F. 2016. Intestinal crosstalk between bile acids and microbiota and its impact on host metabolism. Cell Metabolism 24:41-50.

78. Ridlon JM, Bajaj JS. 2015. The human gut sterolbiome: bile acid-microbiome endocrine aspects and therapeutics. Acta Pharm Sin B 5:99-105.

79. Theriot CM, Bowman AA, Young VB. 2016. Antibiotic-induced alterations of the gut microbiota alter secondary bile acid production and allow for *Clostridium difficile* spore germination and outgrowth in the large intestine. mSphere 1:e00045-15.

80. Enright EF, Griffin BT, Gahan CGM, Joyce SA. 2018. Microbiome-mediated bile acid modification: Role in intestinal drug absorption and metabolism. Pharmacol Res 133:170-186.

81. Sistrunk JR, Nickerson KP, Chanin RB, Rasko DA, Faherty CS. 2016. Survival of the fittest: how bacterial pathogens utilize bile to enhance infection. Clin Microbiol Rev 29:819-836.

82. Xue Y, Tu F, Shi M, Wu CQ, Ren G, Wang X, Fang W, Song H, Yang M. 2016. Redox pathway sensing bile salts activates virulence gene expression in *Vibrio cholerae*. Mol Microbiol 102:909-924.

83. Delmas J, Gibold L, Fais T, Batista S, Leremboure M, Sinel C, Vazeille E, Cattoir V, Buisson A, Barnich N, Dalmasso G, Bonnet R. 2019. Metabolic adaptation of adherent-invasive *Escherichia coli* to exposure to bile salts. Sci Rep 9:2175.

84. Dubois T, Tremblay YDN, Hamiot A, Martin-Verstraete I, Deschamps J, Monot M, Briandet R, Dupuy B. 2019. A microbiota-generated bile salt induces biofilm formation in *Clostridium difficile*. NPJ Biofilms and Microbiomes 5:14.

85. Koseoglu VK, Hall CP, Rodriguez-Lopez EM, Agaisse H. 2019. The autotransporter IcsA promotes *Shigella flexneri* biofilm formation in the presence of bile salts. Infect Immun 87:e00861-18.

86. Nishino K, Yamaguchi A. 2001. Analysis of a complete library of putative drug transporter genes in *Escherichia coli*. J Bacteriol 183:5803-5812.

87. Paul S, Alegre KO, Holdsworth SR, Rice M, Brown JA, McVeigh P, Kelly SM, Law CJ. 2014. A single-component multidrug transporter of the major facilitator superfamily is part of a network that protects *Escherichia coli* from bile salt stress. Mol Microbiol 92:872-884.

88. Bina XR, Provenzano D, Nguyen N, Bina JE. 2008. *Vibrio cholerae* RND family efflux systems are required for antimicrobial resistance, optimal virulence factor production, and colonization of the infant mouse small intestine. Infect Immun 76:3595-3605.

89. Urdaneta V, Casadesus J. 2018. Adaptation of *Salmonella enterica* to bile: essential role of AcrAB-mediated efflux. Environ Microbiol 20:1405-1418.

90. Kwan BW, Lord DM, Peti W, Page R, Benedik MJ, Wood TK. 2015. The MqsR/MqsA toxin/antitoxin system protects *Escherichia coli* during bile acid stress. Environ Microbiol 17:3168-3181.

91. Prieto AI, Ramos-Morales F, Casadesus J. 2006. Repair of DNA damage induced by bile salts in *Salmonella enterica*. Genetics 174:575-584.

92. Hernandez SB, Cota I, Ducret A, Aussel L, Casadesus J. 2012. Adaptation and preadaptation of *Salmonella enterica* to Bile. PLoS Genet 8:e1002459.

93. Gourley CR, Negretti NM, Konkel ME. 2017. The food-borne pathogen *Campylobacter jejuni* depends on the AddAB DNA repair system to defend against bile in the intestinal environment. Sci Rep 7:14777.

94. Urdaneta V, Hernandez SB, Casadesus J. 2019. Mutational and non mutational adaptation of *Salmonella enterica* to the gall bladder. Sci Rep 9:5203.

95. Hernandez SB, Ayala JA, Rico-Perez G, Garcia-del Portillo F, Casadesus J. 2013. Increased bile resistance in *Salmonella enterica* mutants lacking Prc periplasmic protease. Int Microbiol 16:87-92.

96. Hernandez SB, Cava F, Pucciarelli MG, Garcia-Del Portillo F, de Pedro MA, Casadesus J. 2015. Bile-induced peptidoglycan remodelling in *Salmonella enterica*. Environ Microbiol 17:1081-1089.

97. Merritt ME, Donaldson JR. 2009. Effect of bile salts on the DNA and membrane integrity of enteric bacteria. J Med Microbiol 58:1533-1541.

98. Cremers CM, Knoefler D, Vitvitsky V, Banerjee R, Jakob U. 2014. Bile salts act as effective protein-unfolding agents and instigators of disulfide stress *in vivo*. Proc Natl Acad Sci U S A 111:E1610-E1619.

99. Sannasiddappa TH, Lund PA, Clarke SR. 2017. *In vitro* antibacterial activity of unconjugated and conjugated bile salts on *Staphylococcus aureus*. Front Microbiol 8:1581.

100. Negretti NM, Gourley CR, Clair G, Adkins JN, Konkel ME. 2017. The food-borne pathogen *Campylobacter jejuni* responds to the bile salt deoxycholate with countermeasures to reactive oxygen species. Sci Rep 7:15455.

101. Kumar M, Adhikari S, Hurdle JG. 2014. Action of nitroheterocyclic drugs against *Clostridium difficile*. Int J Antimicrob Agents 44:314-319.

102. Vumma R, Bang CS, Kruse R, Johansson K, Persson K. 2016. Antibacterial effects of nitric oxide on uropathogenic *Escherichia coli* during bladder epithelial cell colonization--a comparison with nitrofurantoin. J Antibiot (Tokyo) 69:183-186.

103. Voak AA, Gobalakrishnapillai V, Seifert K, Balczo E, Hu L, Hall BS, Wilkinson SR. 2013. An essential type I nitroreductase from *Leishmania major* can be used to activate leishmanicidal prodrugs. J Biol Chem 288:28466-28476.

104. Holm R, Mullertz A, Mu HL. 2013. Bile salts and their importance for drug absorption. Int J Pharm 453:44-55.

105. Forrester MT, Foster MW. 2012. Protection from nitrosative stress: a central role for microbial flavohemoglobin. Free Radic Biol Med 52:1620-1633.

106. McCollister BD, Hoffman M, Husain M, Vazquez-Torres A. 2011. Nitric oxide protects bacteria from aminoglycosides by blocking the energy-dependent phases of drug uptake. Antimicrob Agents Chemother 55:2189-2196.

107. Urdaneta V, Casadesus J. 2017. Interactions between bacteria and bile salts in the gastrointestinal and hepatobiliary tracts. Front Med 4:163.

108. Dunican KC, Patel DK. 2016. Deoxycholic Acid (ATX-101) for Reduction of Submental Fat. Ann Pharmacother 50:855-861.

109. Valenta C, Nowack E, Bernkop-Schnurch A. 1999. Deoxycholate-hydrogels: novel drug carrier systems for topical use. Int J Pharm 185:103-111.

110. Senyigit T, Tekmen I, Sonmez U, Santi P, Ozer O. 2011. Deoxycholate hydrogels of betamethasone-17-valerate intended for topical use: *In vitro* and *in vivo* evaluation. Int J Pharm 403:123-129.

111. Darkoh C, Lichtenberger LM, Ajami N, Dial EJ, Jiang ZD, DuPont HL. 2010. Bile acids improve the antimicrobial effect of rifaximin. Antimicrob Agents Chemother 54:3618-3624.

112. LaRusso NF, Szczepanik PA, Hofmann AF. 1977. Effect of deoxycholic acid ingestion on bile acid metabolism and biliary lipid secretion in normal subjects. Gastroenterology 72:132-140.

113. Anes J, McCusker MP, Fanning S, Martins M. 2015. The ins and outs of RND efflux pumps in *Escherichia coli*. Front Microbiol 6:587.

114. Chen MT, Lo CJ. 2016. Using biophysics to monitor the essential proton motive force in bacteria. Adv Exp Med Biol 915:69-79.

115. Baba T, Ara T, Hasegawa M, Takai Y, Okumura Y, Baba M, Datsenko KA, Tomita M, Wanner BL, Mori H. 2006. Construction of *Escherichia coli* K-12 in-frame, single-gene knockout mutants: the Keio collection. Mol Syst Biol 2:2006.0008.

116. Thomason LC, Costantino N, Court DL. 2007. *E. coli* genome manipulation by P1 transduction. Curr Protoc Mol Biol 79:1.17.1-1.17.8.

117. Datsenko KA, Wanner BL. 2000. One-step inactivation of chromosomal genes in *Escherichia coli* K-12 using PCR products. Proc Natl Acad Sci U S A 97:6640-6645.

118. Kitagawa M, Ara T, Arifuzzaman M, Ioka-Nakamichi T, Inamoto E, Toyonaga H, Mori H. 2005. Complete set of ORF clones of *Escherichia coli* ASKA library (a complete set of *E. coli* K-12 ORF archive): unique resources for biological research. DNA Res 12:291-299.

119. Green R, Rogers EJ. 2013. Transformation of chemically competent *E. coli*. Methods Enzymol 529:329-336.

120. Le VVH, Bruce I, Biggs PJ, Rakonjac J. 2019. Draft genome sequence of a canine uropathogenic *Escherichia coli* strain isolated in New Zealand. Microbiol Resour Announc 8:e01665-18.

121. Spagnuolo J, Opalka N, Wen WX, Gagic D, Chabaud E, Bellini P, Bennett MD, Norris GE, Darst SA, Russel M, Rakonjac J. 2010. Identification of the gate regions in the primary structure of the secretin pIV. Mol Microbiol 76:133-150.

122. Cherepanov PP, Wackernagel W. 1995. Gene disruption in *Escherichia coli*: TcR and KmR cassettes with the option of Flp-catalyzed excision of the antibiotic-resistance determinant. Gene 158:9-14.

123. Campbell J. 2010. High-throughput assessment of bacterial growth inhibition by optical density measurements. Curr Protoc Chem Biol 2:195-208.

124. Iredell J, Brown J, Tagg K. 2016. Antibiotic resistance in *Enterobacteriaceae:* mechanisms and clinical implications. BMJ 352:h6420.

125. Theuretzbacher U. 2017. Global antimicrobial resistance in Gram-negative pathogens and clinical need. Curr Opin Microbiol 39:106-112.

126. Ashkenazy H, Abadi S, Martz E, Chay O, Mayrose I, Pupko T, Ben-Tal N. 2016. ConSurf 2016: an improved methodology to estimate and visualize evolutionary conservation in macromolecules. Nucleic Acids Res 44:W344-350.

127. Sim NL, Kumar P, Hu J, Henikoff S, Schneider G, Ng PC. 2012. SIFT web server: predicting effects of amino acid substitutions on proteins. Nucleic Acids Res 40:W452-457.

128. Ng PC, Henikoff S. 2003. SIFT: Predicting amino acid changes that affect protein function. Nucleic Acids Res 31:3812-3814.

129. Kamariah N, Nartey W, Eisenhaber B, Eisenhaber F, Gruber G. 2016. Low resolution solution structure of an enzymatic active AhpC10:AhpF2 ensemble of the *Escherichia coli* Alkyl hydroperoxide Reductase. J Struct Biol 193:13-22.

130. Dip PV, Kamariah N, Nartey W, Beushausen C, Kostyuchenko VA, Ng TS, Lok SM, Saw WG, Eisenhaber F, Eisenhaber B, Gruber G. 2014. Key roles of the *Escherichia coli* AhpC C-terminus in assembly and catalysis of alkylhydroperoxide reductase, an enzyme essential for the alleviation of oxidative stress. Biochim Biophys Acta 1837:1932-1943.

131. Poole LB, Ellis HR. 1996. Flavin-dependent alkyl hydroperoxide reductase from *Salmonella typhimurium*. 1. Purification and enzymatic activities of overexpressed AhpF and AhpC proteins. Biochemistry 35:56-64.

132. Grosdidier A, Zoete V, Michielin O. 2011. SwissDock, a protein-small molecule docking web service based on EADock DSS. Nucleic Acids Res 39:W270-277.

133. Trott O, Olson AJ. 2010. AutoDock Vina: Improving the speed and accuracy of docking with a new scoring function, efficient optimization, and multithreading. J Comput Chem 31:455-461.

134. Jubb HC, Higueruelo AP, Ochoa-Montano B, Pitt WR, Ascher DB, Blundell TL. 2017. Arpeggio: A web server for calculating and visualising interatomic interactions in protein structures. J Mol Biol 429:365-371.

135. Dip PV, Kamariah N, Subramanian Manimekalai MS, Nartey W, Balakrishna AM, Eisenhaber F, Eisenhaber B, Gruber G. 2014. Structure, mechanism and ensemble formation of the alkylhydroperoxide reductase subunits AhpC and AhpF from *Escherichia coli*. Acta Crystallogr D Biol Crystallogr 70:2848-2862.

136. Vervoort J, Xavier BB, Stewardson A, Coenen S, Godycki-Cwirko M, Adriaenssens N, Kowalczyk A, Lammens C, Harbarth S, Goossens H, Malhotra-Kumar S. 2014. An *in vitro* deletion in *ribE* encoding lumazine synthase contributes to nitrofurantoin resistance in *Escherichia coli*. Antimicrob Agents Chemother 58:7225-7233.

137. Lazar V, Nagy I, Spohn R, Csorgo B, Gyorkei A, Nyerges A, Horvath B, Voros A, Busa-Fekete R, Hrtyan M, Bogos B, Mehi O, Fekete G, Szappanos B, Kegl B, Papp B, Pal C. 2014. Genome-wide analysis captures the determinants of the antibiotic cross-resistance interaction network. Nat Commun 5:4352.

138. Chevereau G, Dravecka M, Batur T, Guvenek A, Ayhan DH, Toprak E, Bollenbach T. 2015. Quantifying the determinants of evolutionary dynamics leading to drug resistance. PLoS Biol 13:e1002299.

139. Kamariah N, Manimekalai MS, Nartey W, Eisenhaber F, Eisenhaber B, Gruber G. 2015. Crystallographic and solution studies of NAD(+)- and NADH-bound alkylhydroperoxide reductase subunit F (AhpF) from *Escherichia coli* provide insight into sequential enzymatic steps. Biochim Biophys Acta 1847:1139-1152.

140. Kamariah N, Eisenhaber B, Eisenhaber F, Gruber G. 2017. Essential role of the flexible linker on the conformational equilibrium of bacterial peroxiredoxin reductase for effective regeneration of peroxiredoxin. J Biol Chem 292:6667-6679.

141. Ling JQ, Cho C, Guo LT, Aerni HR, Rinehart J, Soll D. 2012. Protein Aggregation Caused by Aminoglycoside Action Is Prevented by a Hydrogen Peroxide Scavenger. Molecular Cell 48:713-722.

142. Dwyer DJ, Belenky PA, Yang JH, MacDonald IC, Martell JD, Takahashi N, Chan CTY, Lobritz MA, Braff D, Schwarz EG, Ye JD, Pati M, Vercruysse M, Ralifo PS, Allison KR, Khalil AS, Ting AY, Walker GC, Collins JJ. 2014. Antibiotics induce redox-related physiological alterations as part of their lethality. Proc Natl Acad Sci U S A 111:E2100-E2109.

143. Gordon GC, Cameron JC, Pfleger BF. 2017. RNA sequencing identifies new RNase III cleavage sites in *Escherichia coli* and reveals increased regulation of mRNA. MBio 8:e00128-17.

144. Zheng Q. 2017. rSalvador: an R package for the fluctuation experiment. G3 (Bethesda) 7:3849-3856.

145. R-Core-Team. 2018. R: A language and environment for statistical computing, R Foundation for Statistical Computing, Vienna, Austria, https://www.R-project.org/.

146. Cox MP, Peterson DA, Biggs PJ. 2010. SolexaQA: At-a-glance quality assessment of Illumina second-generation sequencing data. BMC Bioinformatics 11:485.

147. Kersey PJ, Allen JE, Allot A, Barba M, Boddu S, Bolt BJ, Carvalho-Silva D, Christensen M, Davis P, Grabmueller C, Kumar N, Liu Z, Maurel T, Moore B, McDowall MD, Maheswari U, Naamati G, Newman V, Ong CK, Paulini M, Pedro H, Perry E, Russell M, Sparrow H, Tapanari E, Taylor K, Vullo A, Williams G, Zadissia A, Olson A, Stein J, Wei S, Tello-Ruiz M, Ware D, Luciani A, Potter S, Finn RD, Urban M, Hammond-Kosack KE, Bolser DM, De Silva N, Howe KL, Langridge N, Maslen G, Staines DM, Yates A. 2018. Ensembl Genomes 2018: an integrated omics infrastructure for non-vertebrate species. Nucleic Acids Res 46:D802-D808.

148. Langmead B, Salzberg SL. 2012. Fast gapped-read alignment with Bowtie 2. Nat Methods 9:357-359.

149. Li H, Handsaker B, Wysoker A, Fennell T, Ruan J, Homer N, Marth G, Abecasis G, Durbin R, Genome Project Data Processing S. 2009. The Sequence Alignment/Map format and SAMtools. Bioinformatics 25:2078-2079.

150. Garrison E, Marth G. 2012. Haplotype-based variant detection from short-read sequencing. arXiv:arXiv:1207.3907. [q-bio.GN].

151. Cingolani P, Platts A, Wang le L, Coon M, Nguyen T, Wang L, Land SJ, Lu X, Ruden DM. 2012. A program for annotating and predicting the effects of single nucleotide polymorphisms, SnpEff: SNPs in the genome of *Drosophila melanogaster* strain w1118; iso-2; iso-3. Fly (Austin) 6:80-92.

152. Ren J, Wen L, Gao X, Jin C, Xue Y, Yao X. 2009. DOG 1.0: illustrator of protein domain structures. Cell Res 19:271-273.

153. Bankevich A, Nurk S, Antipov D, Gurevich AA, Dvorkin M, Kulikov AS, Lesin VM, Nikolenko SI, Pham S, Prjibelski AD, Pyshkin AV, Sirotkin AV, Vyahhi N, Tesler G, Alekseyev MA, Pevzner PA. 2012. SPAdes: a new genome assembly algorithm and its applications to single-cell sequencing. J Comput Biol 19:455-477.

154. Grenier F, Matteau D, Baby V, Rodrigue S. 2014. Complete Genome Sequence of *Escherichia coli* BW25113. Genome Announc 2:e01038-14.

155. Altschul SF, Madden TL, Schaffer AA, Zhang J, Zhang Z, Miller W, Lipman DJ. 1997. Gapped BLAST and PSI-BLAST: a new generation of protein database search programs. Nucleic Acids Res 25:3389-3402.

156. Dashti AA, Jadaon MM, Abdulsamad AM, Dashti HM. 2009. Heat treatment of bacteria: A simple method of DNA extraction for molecular techniques. Kuwait Med J 41:117-122.

157. Koontz L. 2013. Agarose gel electrophoresis. Methods Enzymol 529:35-45.

158. Wiegand I, Hilpert K, Hancock RE. 2008. Agar and broth dilution methods to determine the minimal inhibitory concentration (MIC) of antimicrobial substances. Nat Protoc 3:163-175.

159. Brunelle JL, Green R. 2014. Coomassie blue staining. Methods Enzymol 541:161-167.

160. Brunelle JL, Green R. 2014. One-dimensional SDS-polyacrylamide gel electrophoresis (1D SDS-PAGE). Methods Enzymol 541:151-159.

161. Schneider CA, Rasband WS, Eliceiri KW. 2012. NIH Image to ImageJ: 25 years of image analysis. Nat Methods 9:671-675.

162. Lenth R. 2019. emmeans: Estimated marginal means, aka least-squares means, v1.3.3. https://CRAN.R-project.org/package=emmeans.

163. Grosdidier A, Zoete V, Michielin O. 2011. Fast docking using the CHARMM force field with EADock DSS. J Comput Chem 32:2149-2159.

164. Irwin JJ, Sterling T, Mysinger MM, Bolstad ES, Coleman RG. 2012. ZINC: a free tool to discover chemistry for biology. J Chem Inf Model 52:1757-1768.

165. Pettersen EF, Goddard TD, Huang CC, Couch GS, Greenblatt DM, Meng EC, Ferrin TE. 2004. UCSF chimera - A visualization system for exploratory research and analysis. J Comput Chem 25:1605-1612.

166. Forli S, Huey R, Pique ME, Sanner MF, Goodsell DS, Olson AJ. 2016. Computational protein-ligand docking and virtual drug screening with the AutoDock suite. Nat Protoc 11:905-919.

167. Hassan NM, Alhossary AA, Mu Y, Kwoh CK. 2017. Protein-ligand blind docking using QuickVina-W with inter-process spatio-temporal integration. Sci Rep 7:15451.

168. Schrodinger, LLC. 2015. The PyMOL Molecular Graphics System, v1.8. https://github.com/schrodinger/pymol-open-source.

169. Faustino C, Serafim C, Rijo P, Reis CP. 2016. Bile acids and bile acid derivatives: use in drug delivery systems and as therapeutic agents. Expert Opin Drug Deliv 13:1133-1148.

170. Reen FJ, Flynn S, Woods DF, Dunphy N, Chroinin MN, Mullane D, Stick S, Adams C, O'Gara F. 2016. Bile signalling promotes chronic respiratory infections and antibiotic tolerance. Sci Rep 6:29768.

171. Ridlon JM, Harris SC, Bhowmik S, Kang DJ, Hylemon PB. 2016. Consequences of bile salt biotransformations by intestinal bacteria. Gut Microbes 7:22-39.

172. Shimada T, Fujita N, Yamamoto K, Ishihama A. 2011. Novel roles of cAMP receptor protein (CRP) in regulation of transport and metabolism of carbon sources. PLoS One 6:e20081.

173. Linder JU. 2008. Structure-function relationships in *Escherichia coli* adenylate cyclase. Biochem J 415:449-454.

174. Teplyakov A, Lim K, Zhu PP, Kapadia G, Chen CCH, Schwartz J, Howard A, Reddy PT, Peterkofsky A, Herzberg O. 2006. Structure of phosphorylated enzyme I, the phosphoenolpyruvate : sugar phosphotransferase system sugar translocation signal protein. Proc Natl Acad Sci U S A 103:16218-16223.

175. Melo AM, Bandeiras TM, Teixeira M. 2004. New insights into type II NAD(P)H:quinone oxidoreductases. Microbiol Mol Biol Rev 68:603-616.

176. Vimala A, Harinarayanan R. 2016. Transketolase activity modulates glycerol-3-phosphate levels in *Escherichia coli*. Mol Microbiol 100:263-277.

177. Skovgaard O, Bak M, Lobner-Olesen A, Tommerup N. 2011. Genome-wide detection of chromosomal rearrangements, indels, and mutations in circular chromosomes by short read sequencing. Genome Res 21:1388-1393.

178. Achaz G, Boyer F, Rocha EP, Viari A, Coissac E. 2007. Repseek, a tool to retrieve approximate repeats from large DNA sequences. Bioinformatics 23:119-121.

179. Potapov V, Ong JL. 2017. Examining sources of error in PCR by single-molecule sequencing. PLoS One 12:e0169774.

180. Siebold C, Flukiger K, Beutler R, Erni B. 2001. Carbohydrate transporters of the bacterial phosphoenolpyruvate: sugar phosphotransferase system (PTS). FEBS Lett 504:104-111.

181. Tsuruoka T, Miyata A, Yamada Y. 1978. Two kinds of mutants defective in multiple carbohydrate utilization isolated from in vitro fosfomycin-resistant strains of *Escherichia coli* K-12. J Antibiot (Tokyo) 31:192-201.

182. Tran QH, Bongaerts J, Vlad D, Unden G. 1997. Requirement for the proton-pumping NADH dehydrogenase I of *Escherichia coli* in respiration of NADH to fumarate and its bioenergetic implications. Eur J Biochem 244:155-160.

183. Lobritz MA, Belenky P, Porter CBM, Gutierrez A, Yang JH, Schwarz EG, Dwyer DJ, Khalil AS, Collins JJ. 2015. Antibiotic efficacy is linked to bacterial cellular respiration. Proc Natl Acad Sci U S A 112:8173-8180.

184. Dwyer DJ, Collins JJ, Walker GC. 2015. Unraveling the physiological complexities of antibiotic lethality. Annu Rev Pharmacol Toxicol 55:313-332.

185. Bernstein C, Bernstein H, Payne CM, Beard SE, Schneider J. 1999. Bile salt activation of stress response promoters in *Escherichia coli*. Curr Microbiol 39:68-72.

186. Girgis HS, Harris K, Tavazoie S. 2012. Large mutational target size for rapid emergence of bacterial persistence. Proc Natl Acad Sci U S A 109:12740-12745.

187. Maduike NZ, Tehranchi AK, Wang JD, Kreuzer KN. 2014. Replication of the *Escherichia coli* chromosome in RNase HI-deficient cells: multiple initiation regions and fork dynamics. Mol Microbiol 91:39-56.

188. Rudolph CJ, Upton AL, Stockum A, Nieduszynski CA, Lloyd RG. 2013. Avoiding chromosome pathology when replication forks collide. Nature 500:608-611.

189. Robinson JT, Thorvaldsdottir H, Winckler W, Guttman M, Lander ES, Getz G, Mesirov JP. 2011. Integrative genomics viewer. Nat Biotechnol 29:24-26.

190. UniProt-Consortium. 2019. UniProt: a worldwide hub of protein knowledge. Nucleic Acids Res 47:D506-D515.

191. Quinlan AR, Hall IM. 2010. BEDTools: a flexible suite of utilities for comparing genomic features. Bioinformatics 26:841-842.

192. Carver T, Thomson N, Bleasby A, Berriman M, Parkhill J. 2009. DNAPlotter: circular and linear interactive genome visualization. Bioinformatics 25:119-120.

193. Ye J, Coulouris G, Zaretskaya I, Cutcutache I, Rozen S, Madden TL. 2012. Primer-BLAST: a tool to design target-specific primers for polymerase chain reaction. BMC Bioinformatics 13:134.

194. Hall BG, Acar H, Nandipati A, Barlow M. 2014. Growth Rates Made Easy. Mol Biol Evol 31:232-238.

195. Wickham H. 2016. ggplot2: Elegant Graphics for Data Analysis. Springer-Verlag New York.

196. van Hengel AJ, Marin L. 2019. Research, Innovation, and Policy: An Alliance Combating Antimicrobial Resistance. Trends Microbiol 27:287-289.

197. Brown ED, Wright GD. 2016. Antibacterial drug discovery in the resistance era. Nature 529:336-343.

198. Farha MA, Brown ED. 2019. Drug repurposing for antimicrobial discovery. Nat Microbiol 4:565-577.

199. Zayyad H, Eliakim-Raz N, Leibovici L, Paul M. 2017. Revival of old antibiotics: needs, the state of evidence and expectations. Int J Antimicrob Agents 49:536-541.

200. Rios AC, Moutinho CG, Pinto FC, Del Fiol FS, Jozala A, Chaud MV, Vila MM, Teixeira JA, Balcao VM. 2016. Alternatives to overcoming bacterial resistances: State-of-the-art. Microbiol Res 191:51-80.

201. Ghosh C, Sarkar P, Issa R, Haldar J. 2019. Alternatives to conventional antibiotics in the era of antimicrobial resistance. Trends Microbiol 27:323-338.

202. Rosenberg EY, Bertenthal D, Nilles ML, Bertrand KP, Nikaido H. 2003. Bile salts and fatty acids induce the expression of *Escherichia coli* AcrAB multidrug efflux pump through their interaction with Rob regulatory protein. Mol Microbiol 48:1609-1619.

203. Kus JV, Gebremedhin A, Dang V, Tran SL, Serbanescu A, Barnett Foster D. 2011. Bile salts induce resistance to polymyxin in enterohemorrhagic *Escherichia coli* O157:H7. J Bacteriol 193:4509-4515.

204. Wulkersdorfer B, Jaros D, Eberl S, Poschner S, Jager W, Cosentini E, Zeitlinger M, Schwameis R. 2017. Human bile reduces antimicrobial activity of selected antibiotics against *Enterococcus faecalis* and *Escherichia coli* in vitro. Antimicrob Agents Chemother 61:e00527-17.

205. Prouty AM, Brodsky IE, Falkow S, Gunn JS. 2004. Bile-salt-mediated induction of antimicrobial and bile resistance in *Salmonella typhimurium*. Microbiology 150:775-783.

206. Nikaido H, Pages JM. 2012. Broad-specificity efflux pumps and their role in multidrug resistance of Gram-negative bacteria. FEMS Microbiol Rev 36:340-363.

207. Blair JM, Webber MA, Baylay AJ, Ogbolu DO, Piddock LJ. 2015. Molecular mechanisms of antibiotic resistance. Nat Rev Microbiol 13:42-51.

208. Blanco P, Sanz-Garcia F, Hernando-Amado S, Martinez JL, Alcalde-Rico M. 2018. The development of efflux pump inhibitors to treat Gram-negative infections. Expert Opin Drug Discov 13:919-931.

Appendix

MASSEY UNIVERSITY
GRADUATE RESEARCH SCHOOL

STATEMENT OF CONTRIBUTION
DOCTORATE WITH PUBLICATIONS/MANUSCRIPTS

We, the candidate and the candidate's Primary Supervisor, certify that all co-authors have consented to their work being included in the thesis and they have accepted the candidate's contribution as indicated below in the *Statement of Originality*.

Name of candidate:	Van Hung Vuong Le
Name/title of Primary Supervisor:	Prof Jasna Rakonjac
Name of Research Output and full reference:	
In vitro synergy between sodium deoxycholate and furazolidone against enterobacteria	
In which Chapter is the Manuscript /Published work:	Chapter 2
Please indicate:	
• The percentage of the manuscript/Published Work that was contributed by the candidate:	70 %
and	
• Describe the contribution that the candidate has made to the Manuscript/Published Work:	
The candidate has performed checkerboard and time kill assays for Escherichia coli, created deletion and complemented strains and written the manuscript.	
For manuscripts intended for publication please indicate target journal:	
BMC Microbiology	
Candidate's Signature:	Van Hung Vuong Le Digitally signed by Van Hung Vuong Le Date: 2019.08.29 16:24:28 +12'00'
Date:	29/Aug/2019
Primary Supervisor's Signature:	Jasna Rakonjac Digitally signed by Jasna Rakonjac Date: 2019.08.29 18:29:53 +12'00'
Date:	29/08/2019

(This form should appear at the end of each thesis chapter/section/appendix submitted as a manuscript/ publication or collected as an appendix at the end of the thesis)

MASSEY UNIVERSITY
GRADUATE RESEARCH SCHOOL

STATEMENT OF CONTRIBUTION
DOCTORATE WITH PUBLICATIONS/MANUSCRIPTS

We, the candidate and the candidate's Primary Supervisor, certify that all co-authors have consented to their work being included in the thesis and they have accepted the candidate's contribution as indicated below in the *Statement of Originality*.

Name of candidate:	Van Hung Vuong Le
Name/title of Primary Supervisor:	Prof Jasna Rakonjac
Name of Research Output and full reference:	
Novel 5-nitrofuran-activating reductase in Escherichia coli	
In which Chapter is the Manuscript /Published work:	Chapter 3
Please indicate:	
• The percentage of the manuscript/Published Work that was contributed by the candidate:	95%
and	
• Describe the contribution that the candidate has made to the Manuscript/Published Work:	
The candidate has performed resistance-causing-mutation selection, extracted bacterial genomes, analyzed sequencing data, engineered bacterial genome, performed drug susceptibility assay, purified enzymes, performed enzymatic	
For manuscripts intended for publication please indicate target journal:	
Antimicrobial Agents and Chemotherapy	
Candidate's Signature:	Van Hung Vuong Le Digitally signed by Van Hung Vuong Le Date: 2019.08.29 16:30:25 +12'00'
Date:	29/Aug/2019
Primary Supervisor's Signature:	Jasna Rakonjac Digitally signed by Jasna Rakonjac Date: 2019.08.29 18:27:16 +12'00'
Date:	29/08/2019

(This form should appear at the end of each thesis chapter/section/appendix submitted as a manuscript/ publication or collected as an appendix at the end of the thesis)

MASSEY UNIVERSITY
GRADUATE RESEARCH SCHOOL

STATEMENT OF CONTRIBUTION
DOCTORATE WITH PUBLICATIONS/MANUSCRIPTS

We, the candidate and the candidate's Primary Supervisor, certify that all co-authors have consented to their work being included in the thesis and they have accepted the candidate's contribution as indicated below in the *Statement of Originality*.

Name of candidate:	Van Hung Vuong Le
Name/title of Primary Supervisor:	Prof Jasna Rakonjac
Name of Research Output and full reference:	
Comparative genomic analysis of Escherichia coli mutants with decreased bile salt sensitivity	
In which Chapter is the Manuscript /Published work:	Chapter 4
Please indicate:	
• The percentage of the manuscript/Published Work that was contributed by the candidate:	95 %
and	
• Describe the contribution that the candidate has made to the Manuscript/Published Work:	
The candidate has performed resistance-causing-mutation selection, extracted bacterial genomes, analyzed genome sequences, engineered bacterial genomes, performed drug susceptibility assays, determined growth rate, elucidated genome	
For manuscripts intended for publication please indicate target journal:	
Journal of Bacteriology	
Candidate's Signature:	Van Hung Vuong Le Digitally signed by Van Hung Vuong Le Date: 2019.08.29 16:34:41 +12'00'
Date:	29/Aug/2019
Primary Supervisor's Signature:	Jasna Rakonjac Digitally signed by Jasna Rakonjac Date: 2019.08.29 18:27:58 +12'00'
Date:	29/08/2019

(This form should appear at the end of each thesis chapter/section/appendix submitted as a manuscript/ publication or collected as an appendix at the end of the thesis)